UNIVERSITY OF CALIFORNIA

Santa Barbara

# Building biosensors for Neuropsychopharmacology

A dissertation submitted in partial satisfaction of the

requirements for the degree Doctor of Philosophy

in Psychological & Brain Sciences

by

Julian Oscar Gerson

Committee in charge:

Professor Tod Kippin, Chair

Professor Kevin Plaxco

Professor Karen Szumlinski

Professor Ron Keiflin

March 2022

The dissertation of Julian Oscar Gerson is approved.

_____
Kevin Plaxco

_____
Ron Keiflin

_____
Karen Szumlinski

_____
Tod Kippin, Committee Chair

March 2022

Building biosensors for Neuropsychopharmacology



by

Julian Oscar Gerson

ACKNOWLEDGEMENTS

I would not have been able to complete this milestone by myself. First of all I wish to thank my advisor, Dr Tod Kippin. Your unwavering support and guidance have taught me lessons that extend far beyond my research. I also wish to thank Dr Kevin Plaxco for his persistent mentorship throughout the years of my development. You have pushed me grow in ways I had not imagined possible, and I will be forever grateful for the impact you have had on me.

For Dr Andrea Idili I reserve the highest of praise. Your guidance in my early years here at UCSB was the foundation on which I built my sense of self in the world of science. You taught me many things, but above all you taught me confidence. You have become like an older brother to me, and I will always consider you part of my family. Know that I am forever in your debt on both a human, and a professional level.

I wish to thank all the members of the Kippin and Plaxco labs throughout the years I have been here. There is nothing I will miss more about this place than the immensely thought-provoking discussions that occurred with such frequency in this environment.

I must also thank Dr Alicia Izquierdo at UCLA for taking a chance on me and giving my first start in the field of research. In addition, I must thank Andrew Thompson and Evan Hart for placing their trust in me as a young researcher.

To Courtney Kenyon, I am so grateful for your presence in my life. Your support has been immense, and you showed me aspects of life I didn't know existed. For my parents, there are no words that can explain how grateful I am. I am who I am today because of you both. My gratitude is infinite and will never wain.

VITA OF JULIAN OSCAR GERSON
March 2022

EDUCATION

University of California, Santa Barbara 2022
Doctor of Philosophy in Psychological and Brain Sciences
Emphasis in Bioengineering

University of California, Los Angeles 2016
Bachelor of Science in Neuroscience
Bachelor of Science in Psychobiology

PROFESSIONAL EMPLOYMENT

Department of Psychological and Brain Sciences, University of California, Santa Barbara
Graduate Student Researcher and Teaching Assistant 2017 – 2022

University of California, Los Angeles
Lab Technician, Dr. Alicia Izquierdo 2015 – 2017

PUBLICATIONS

Downs, Alex; **Gerson, Julian**; Leung, Kaylyn; Honeywell, Kevin; Kippin, Tod; Plaxco, Kevin (2021). “"Nanoporous Gold for the Miniaturization of In-Vivo Electrochemical Aptamer-Based Sensors". *Acs Sensors*

Downs, Alex; **Gerson, Julian**; Hossain, M. Nur; Ploense, Kyle; Pham, Michael; Kraatz, Heinz-Bernhard; Kippin, Tod; Plaxco, Kevin (2021). “"Nanoporous Gold for the Miniaturization of In-Vivo Electrochemical Aptamer-Based Sensors". *Acs Sensors*

Andrea Idili, **Julian Gerson (co-first author)**, Tod Kippin, Kevin Plaxco (2021). “Seconds-Resolved, In Situ Measurements of Plasma Phenylalanine Disposition Kinetics in Living Rats”. *Analytical Chemistry*

Alex M Downs, **Julian Gerson**, Kyle Ploense, Kevin W Plaxco, Philippe Dauphin-Ducharme (2020). “Subsecond-Resolved Molecular Measurements Using Elcetrochemical Phase Interrogation of Aptamer-Based Sensors”. *Analytical Chemistry*

Philippe Dauphin-Ducharme, Kyungae Yang, Netzahualcóyotl Arroyo-Currás, Kyle Ploense, Yameng Zhang, **Julian Gerson**, Martin Kurnik, Tod E. Kippin, Milan Stojanovic, Kevin W. Plaxco (2019). "Electrochemical Aptamer-Based Sensors for Improved Therapeutic Drug Monitoring and High-Precision, Feedback-Controlled Drug Delivery". *ACS sensors*

Idili A, **Gerson J**, Parolo C, Kippin T, Plaxco KW (2019). "An electrochemical aptamer-based sensor for the rapid and convenient measurement of L-Tryptophan". *Analytical and Bioanalytical Chemistry (paper in forefront)*

Hart EE, **Gerson JO**, Azquierdo A (2018). "Persistent effect of withdrawal from intravenous methamphetamine self-administration on brain activation and behavioral economic indices involving an effort cost". *Neuropharmacology*

Hart EE, **Gerson JO**, Zoken Y, Garcia M, Izquierdo A (2017). "Anterior cingulate cortex supports effort allocation towards a qualitatively preferred option". *European Journal of Neuroscience*

Thompson AB, **Gerson J**, Stolyarova A, Bugarin A, Hart EE, Jentsch JD, Izquierdo A (2017). "Steep effort discounting of a preferred reward over a freely-available option in prolonged methamphetamine withdrawal in male rats". *Psychopharmacology*

ABSTRACT

Building biosensors for Neuropsychopharmacology

by

Julian Oscar Gerson

Our understanding of the brain's beautiful and complex machinery is largely driven by our ability to measure the chemical and electrical signals that govern its convoluted circuitry. As such, our knowledge is only as good as the tools we have at our disposal. The study of neurochemistry and neuropharmacology research has largely been driven by the use of microdialysis and electrochemical methods to measure targets of interest in the brain. While these techniques are powerful and have contributed immensely to our conceptualization of brain activity, they are not without their limitations. Briefly, microdialysis suffers from poor temporal resolution and lacks the potential for real-time data delivery, while previous electrochemical methods suffer from debatable specificity and limited generalizability for the detection of many critical targets. In response to these limitations, I have applied electrochemical aptamer-based (E-AB) sensors to the field of in-brain molecular sensing. The modular E-AB platform does not rely on the reactivity of its intended target, is generalizable to the detection of a wide range of analytes and has been shown to support real-time detection of small molecules directly in the living body. By modifying the existing E-AB

platform, which has demonstrated success for peripheral measurements in blood, I have developed a novel E-AB sensor platform for making in-brain measurements of small molecules. In-brain E-AB sensing opens a path towards measuring a wide range of targets in the brain. To showcase this, I have applied this platform to model drug transport (using simultaneous measurements in blood and CSF), as well as study neuropsychopharmacology (using simultaneous measurements of a psychoactive drug and on-going behavior). Together these studies lay the foundation for a powerful new tool with which to study neurochemistry and neuropharmacology.

TABLE OF CONTENTS

# Chapter 1:

# General Introduction

## 1.1 Overview

The ability to measure the levels of endogenously produced small molecules, such as neurotransmitters, or exogenously administered agents, such as drugs, in situ in the brain in real time and on the behaviorally relevant, few-seconds time scale would powerfully impact both neuroscience research and our ability to monitor and treat neurological diseases. Specifically, by doing what they cannot, such a technology would greatly augment microdialysis and voltammetry, the currently dominant methods for monitoring changes in neurochemistry and neuropharmacology and their relationships to behavior. Thus motivated, the focus of my thesis work has been the development and implementation of a novel tool — electrochemical aptamer-bases biosensors — for measuring molecules in the brain.

To support continuous seconds/sub-seconds resolved in situ chemical measurements of endogenous and exogenous targets in the brain, an ideal, real-time sensing technology must satisfy four core attributes. First the sensor platform must be *generalizable*. The brain contains a plethora of different signaling molecules that give rise to its complex electrical and chemical communication mechanisms. To fully understand the neuroarchitecture of the brain we must have the ability to reliably measure each of these molecules with sufficiently (scientific and physiologically) relevant accuracy and precision. However, in addition to being able to measure the concentrations of range of molecules in the brain, a sensor must also be able to reliably distinguish between them, such that sensor output is reliably attributable to the target molecule of interest. As such the second attribute is *specificity*. Third, a

functional sensor must have clinically and physiologically relevant *sensitivity*. That is the sensor must be capable of detecting, and resolving changes in the concentration of, these targets at physiologically relevant levels. Finally, the platform must achieve the *temporal resolution* required to measure these analytes on the time scale relevant to their biological activities.

To place my work in context, here I first review the current state of the art technologies for monitoring molecules in the brain that have shaped our modern conception of brain chemistry over the last 40 years. Using the four core attributes described above as a guide, I highlight the strengths and weaknesses of these techniques. While these techniques have paved the way for our understanding of the brain and its incredibly complex circuitry, I suggest that they may not have the characteristics required to address several key questions going forward. I then introduce the emerging field of electrochemical aptamer-based (E-AB) sensors. This is a platform technology that combines the superior time resolution and real-time output of the best resolved prior methods with the ability to monitor molecules irrespective of their redox or enzymatic reactivity. Finally, I present the adaptation and progressive applications of E-AB platform from an ex-vivo diagnostic tool all the way to awake, *in*-brain measurements this thesis seeks to showcase the ability of this platform to address each of these attributes of an ideal, real-time *in-brain* sensor simultaneously. While significant work and improvement remains to be done, it is my belief that E-AB sensors have the potential to immensely impact our understanding of neuroscience.

## 1.2 Microdialysis

Microdialysis, which, since its inception, has been the gold standard for measuring the concentration of most molecules of interest in the brain, is also the most abundantly employed technique in neuroscience for determining the presence and concentration of specific molecules in the brain. This approach, which has propelled the field of neurochemistry and neuropharmacology for many years(Anderzhanova & Wotjak, 2013; Chefer et al., 2009; Saylor & Lunte, 2015), employs diffusion-based extraction of extracellular chemicals across the membrane of a dialysis probe that can be implanted into specific brain regions of interest for later, ex-vivo analysis. The diffusion of small molecules is driven by the flow of a buffer solution through the inner cavity of the dialysis probe which is collected ex vivo to be analyzed roughly at time of collection (i.e. online MD) or, more commonly, is stored and analyzed at a later time. The temporal resolution of the approach is defined by the length of time required in order to collect sufficient volume of sufficiently high concentration dialysate samples.

The major strength of microdialysis stems from its reliance on ex vivo detection. While far from trivial to perform, the technique is enabled, in essence, simply through the removal of fluid samples from the body. And, once out of the body, these samples can be characterized using any of a wide range of extraordinarily sensitive and versatile benchtop analytical approaches. Because of this, microdialysis is generalizable to the measurement of virtually any desired molecule -or even multiple molecules from a single sample- in the rich, complex environment that is the brain. Conversely, however, microdialysis is not real time, even when microdialysis is coupled with online capillary electrophoresis, due to the lag time

associated with transport to the analytical device introduces a significant (multi-minute) time lag, which precludes, for example, the adaptation of microdialysis in feedback control experiments in which real-time information on, for example, in-vivo drug or neurochemical levels, could be used to drive other experimental parameters. The time resolution of microdialysis is also generally poor; although a few highly skilled researchers have demonstrated measurements on the order of seconds (Kennedy et al., n.d.; Lada et al., 1997; M. Wang et al., 2011)), this is far from turnkey, and time resolution of tens of minutes is standard (H. Yang et al., 2013).This fact is highlighted by a survey of microdialysis literature showing a trend of increasing sampling rates over the past 40 years, with over 82% employing times of 20 minutes or more (H. Yang et al., 2013). Measurements of this time scale do not match well with the neurobiological processes that take place in the brain and thus are not well placed to study critical processes in the brain such as neurotransmission, neuromodulation or even the pharmacokinetics of drugs in the brain. In addition, microdialysis suffers from spatial limitations (dialysis probes are typically 200 μM in diameter). The issues stemming from these relatively large dimensions are two-fold. First, the insertion of a probe of this diameter can alter the environment in which it is intended to measure due to the inflammatory response. Second, the length of the probe limits spatial resolution, precluding the use of this technique in the study of localized neurotransmission.

### 1.3 Direct electrochemistry and enzymatic sensors

Prior use of electrochemistry for in brain analyte detection involves the use of redox chemistry to detect molecules of interest. In direct electrochemical approaches, this is done

by directly reducing/oxidizing the target of interest (e.g., dopamine). In the case of analytes that are not redox active enzymatic sensors can be used that indirect detect the target by producing a related/secondary redox species in the presence of target. In the case of direct measurements, an electrode is placed into the brain and the potential at which the electrode is scanned is managed (Bard & Faulkner, 2002). The resulting current output of these electrode scans can be analyzed for their magnitude, shape, and position relative to a reference electrode to inform the identity of molecules present (Bard & Faulkner, 2002). As such, these scans can provide abundant information about the surrounding environment of the electrode. Indirect electrochemical methods measure non-redox-active species by using an enzyme that converts the target of interest into an electrochemically detectable molecule (e.g., hydrogen peroxide) that can then be measured by the electrode.

Electrochemical approaches provide a number of advantages when compared to microdialysis and, as such, have become essential to the field of neuroscience and are exploited by a wide variety of research groups. First, with electrode diameters ranging from hundreds of nanometers to tens of micrometers, electrochemical methods can be considerably less invasive(Burmeister et al., 2000; Ngernsutivorakul et al., 2018b; Seymour et al., 2017). These smaller probes result in less interference with the natural state of brain activity by limiting both damage to the brain and the inflammation that results following probe insertion (Oakes et al., 2018). Likewise, the shorter length of electrodes versus microdialysis probes improves spatial resolution, of allowing for more precise targeting of specific brain regions, or even subregions, of interest. The second, and perhaps more characteristically defining, advantage of electrochemical methods, such as fast scan cyclic

voltammetry (FSCV) and enzymatic biosensors, is their ability to measure analyte levels in real time, and on sub-second timescales (Sarter & Kim, 2015). The significantly superior time resolution of these techniques allows researchers to perform measurements and study processes that are simply out of the reach of microdialysis.

As a result of their superior spatiotemporal resolution, electrochemical approaches have contributed significantly to the field of neuroscience. They have proven invaluable, for example, in the understanding of dopamine's role in the brain. Techniques such as Cyclic voltammetry and chronoamperometry forged our understanding of underlying neural circuitry governing its release and uptake and have elucidated the role of dopamine in the mesocorticolimbic system in driving motivated behaviors by reward-based learning (Ariansen et al., 2012; Carelli, 2004; Owesson-White et al., 2008; Wickham et al., 2013), as well as its apparent essential involvement in the development and manifestation of addiction (Addy et al., 2010; Ehrich et al., 2014; Owesson-White et al., 2009; Pattison et al., 2012; Vander Weele et al., 2014). Dopamine is by far the most studied neurotransmitter to date, using direct electrochemistry, however, this technique has been used to detect several other key players in the brain including serotonin and norepinephrine (Beitollahi et al., 2008; Figueiredo-Filho et al., 2014; J. Park et al., 2009, 2011). In parallel, enzymatic methods have been developed for the detection of glucose (Cordeiro et al., 2018; Kozai et al., 2012), glutamate (HAMDAN & MOHD ZAIN, 2014; Isherwood et al., 2018; G. Xiao et al., 2017), choline, acetylcholine (K. L. Baker et al., 2015; Giuliano et al., 2008; Zhang et al., 2010), pyruvate (Cordeiro et al., 2015; Lin et al., 2014) and lactate (Cordeiro et al., 2015; Lin et al., 2014) in situ in the brain.

While the powerful nature of prior electrochemical approaches is undeniable, they are not without their limitations. First, direct electrochemical approaches and enzymatic sensors suffer from poor generalizability. Specifically, Direct electrochemical measurements are limited to the detection of species that are redox active species, while enzymatic sensors are limited to species that can be enzymatic converted into redox-active species. This precludes the detection of many molecules, including, for example, the majority of pharmaceutical drugs and, save for alcohol (for which an in-vivo enzymatic sensor has recently been demonstrated (Rocchitta et al., 2012)), all drugs of abuse. The lack of generalizability of this platform places obviously limits the potential applications of these techniques.

A second concern about electrochemical approaches is that, in contrast to enzymatic sensors, which are extremely selective due to the specific nature of enzymes, direct electrochemical approaches suffer from a difficulty in differentiating between targets of similar redox chemistry. For example, to distinguish between dopamine and serotonin researchers must employ arduous post-hoc data analysis (Sarter & Kim, 2015) or exceedingly careful background subtraction (Bucher & Wightman, 2015; Dengler & McCarty, 2013; Keithley et al., 2011; Roberts & Sombers, 2018) that can still lead to artifacts in the data. In the case of serotonin (5-HT), however, *in-vivo* voltammetric methods have proved much less effective due to the above-described selectivity issues (Bucher & Wightman, 2015). Recently, researchers have sought to overcome this by targeting areas of the brain with low levels of potentially interfering redox active species or by electrode and waveform modifications (Wei et al., 2018). Nevertheless, although there has been some apparent progress in better

isolating serotonin detection (Dankoski et al., 2014; Hashemi et al., 2009; Wei et al., 2018), direct redox-based voltammetry may not be best suited to the task of characterizing serotonergic circuitry to the degree with which it did for the mesocorticolimbic dopamine system. Conversely, emerging developments in AI have been argued to be capable of potential re-definement of direct redox neurochemistry by increasing the amount of information derived containined in voltagramms by parsing contributions of multiple electroactive molecules via machine learning (Moran et al., 2018). It is unclear, however, how many species can be parsed, nor is this widely accepted. Nonetheless, direct redox is limited to electroactive species and indirect redox is limited to instance of highly specific enzyme catalysis.

### 1.4 Electrochemical Aptamer Based (E-AB) Sensors

E-AB sensors are rapidly emerging as a uniquely powerful sensing platform capable of making specific, high frequency measurements of a broad range of molecular targets at biologically relevant concentrations in the living body. As its foundation, this technique exploits the versatile recogniton properties of DNA aptamers. DNA aptamers are carefully selected oligonucelotide seuqeneces capable of binding molecular targets with a high degree specifictiy and sensitivity.

***1.4.1 Aptamer Selection (SELEX):*** The *in*-vitro process for selecting DNA aptamers, termed SELEX, is well established and has led to the discovery of aptamers that bind a plethora of different analytes ranging from small molecules to proteins and whole cells. Briefly, this process involves incubating the target of interest in a random DNA/RNA library.

Sequences of DNA that bind to the target analyte can be identified, separated and then amplified. Iterations of this process can result in a selection of aptamers that bind the desired target. To improve the selectivity of aptamers, the pool of aptamers that successfully bind the target can be further restricted by incubating with non-target molecules that may be present in the desired sampling medium. Sequences that bind these potential interferents can then be excluded, leaving behind a pool of aptamers that bind their intended target with high affinity and selectivity. Notably, the employment of aptamers extends well beyond incorporation into E-AB sensors as they are being explored in a very wide range of applications, including multiple potential avenues for studying brain chemistry (see for a recent review (Moraldo et al., 2022)); however, description of these alternative approaches is beyond the scope of this review.

***1.4.2 E-AB sensor mechanism:*** Although DNA aptamers do not have an inherent signal transduction mechanism built in to them, they can be rationally reengineered to generate an electrochemical signal upon target binding. Specifcially, by modifying aptamers with a covalently attached redox reporter (typically methylene blue) and attaching them to an electrode surface using thiol chemistry we can exploit the tendency of aptamers to display target binding induced conformational change. This change in conformational state induced by the target can, in turn, be harnessed to alter the proximity of the redox reporter to an electrode surface. This then alters the rate of electron transfer producing an easily measurable signal when the sensor is interrogated, for instance, via square wave voltammetry (SWV) (Arroyo-Currás et al., 2017; Dauphin-Ducharme et al., 2019; Idili, Arroyo-Currás, et al., 2019; Idili et al., 2021; Vieira et al., 2019) or chronoamperometry (Arroyo-

Currás, Dauphin-Ducharme, et al., 2018). And because the electron transfer rate changes monotonically with respect to the target concentration, precise, concentration controlled, *in-vitro* calibrations can be generated. It is precisely because of this unique sensing mechanism that led me to hypothesize that E-AB sensors are able to satisfy the core requriements of an ideal neurochemistry/neuropharmacology sensing technology, and also overcome some of the major limitations of existing platforms.

***1.4.3 Generalizability:*** Unlike prior electrochemical techniques, E-AB sensors are independent of the reactivity of their targets, rendering them general. This generality stems from the the robust nature of aptamer selection strategies, such as SELEX, to generate aptamers exhibiting high affinity to a wide range of target analytes. Since a modified aptamer is a module within the EAB platform, it is facile to replace the recognition element aptamer to produce a novel sensor. That is, the modular nature of EABs along with the ability to determine target analyte interactions based on substitution of the aptamer should enable molecular monitoring of a wide range of targets. In support of this E-AB sensors have successfully targeted antibiotics, chemotherapeutics, amino acids, biomarkers (ngal), the metabolite ATP, and even drugs of abuse.

***1.4.4 Temporal Resolution:*** On par with direct and indirect electrochemical methods, E-AB sensors provide the temporal resolution required to study many analytes on physiologically relevant time scales. Measurements can be made on the order of seconds using SWV (Arroyo-Currás et al., 2017; Dauphin-Ducharme et al., 2019; Idili, Arroyo-Currás, et al., 2019; Idili et al., 2021; Vieira et al., 2019), and hundreds of milliseconds using

chronoamperometry (Arroyo-Currás, Dauphin-Ducharme, et al., 2018). In addition, the signaling mechanism of E-AB sensors allows for real-time, in situ, reversible measurements.

***1.4.5 Sensitivity:*** E-AB sensors employ highly sensitive DNA aptamers as their recognition element. As a result of this, E-AB sensors typically have sufficient affinities to measure biologically relevant concentrations of their targets. To date E-AB sensors have been shown to function well in relevant ranges for several dozen molecular analytes (Lubin & Plaxco, 2010; Schoukroun-Barnes et al., 2016).

***1.4.6 Specificity:*** E-AB sensors are highly specific to their targets and capable to discriminating between molecules with a high degree of structural similarity and perform well when placed in complex, biological media. For example, none of the endogenous compounds found in blood/CSF/urine/tumors cause any significant response in any of the in-vivo E-AB sensors we have characterized. And while E-AB sensors cannot be any more specific than the aptamers they employ, these have proven sufficiently specific to support scientifically meaningful in complex, biological environments that have historically proven challenging for other electrochemical techniques. Direct electrochemistry, for example, is hard pressed to differentiate between dopamine and norepinephrine (Fox & Wightman, 2017; Robinson et al., 2008) due to their standard reduction potentials being so similar. In the case of E-AB sensors, the local (to the electrode) concentration of the tethered methylene blue redox reporter employed on the electrode surface dwarfs the concentration of potential redox interferents and thus, in contrast to those of conventional electrochemical techniques, E-AB output is effectively immune to redox active interferents.

***1.4.7 In-Vivo applications to date:*** The high level of specificity, sensitivity, and selectvity traits listed, coupled with the real-time nature of E-AB sensing lends itself well to *in-vivo* studies of drug pharmacokinetics. Consistent with this, myself and others have previously demonstrated the ability of E-AB sensors to support molecular measurements in situ in the blood streams of live rats.

E-AB sensors deployed in the circulatory system have successfully supported the measurement of chemotherapeutics (doxorubicin (Arroyo-Currás et al., 2017; Ferguson et al., 2013; Mage et al., 2017), and irinotecan (Idili, Arroyo-Currás, et al., 2019), the metabolite ATP (Li et al., 2019), antibiotics (aminoglycosides (Arroyo-Currás, Dauphin-Ducharme, et al., 2018; Arroyo-Currás et al., 2017; Arroyo-Currás, Ortega, et al., 2018) and vancomycin (Dauphin-Ducharme et al., 2019)). Many of the targets listed above are drugs with narrow therapeutic windows (the concentration range between the effective dose and toxic dose of a drug). As such, these drugs require therapeutic drug monitoring (TDM) in which the concentrations of drugs in the plasma are measured and a patient's dosing regimen is adjusted accordingly (Fournier et al., 2018; Papamichael & Cheifetz, 2017; Stott & Hope, 2017). While TDM is the highest standard of care available, it is only as powerful as the sensing technique that is used to perform it. The current "gold standard" method of venous lab draws requires a full lab in order to process samples using HPLC/MS (Farin et al., 1998; Javorska et al., 2016; Jesús Valle et al., 2008; Oyaert et al., 2015) or immunoassays (Farin et al., 1998; Oyaert et al., 2015) and is time consuming, with answers typically arriving in hours to days. Furthermore, the sparce data points obtained may not accurately reflect a person's metabolism (Aucella et al., 2013; Brandhorst et al., 2012; Dasgupta, 2016; Patsalos et al.,

2018). Combined, these limitations do not readily support the implementation of TDM and as a result, TDM is often performed less frequently than is ideal. In contrast, E-AB studies have produced unprecedentedly rich data sets, with hundreds of data points over multiple hours, that support high precision pharmacokinetic estimates for individual subjects (Vieira et al., 2019) that offer to revolutionize TDM by accurately determine individual patient PKs. Beyond simply monitoring concentrations of a drug *in-vivo*, E-AB sensors can be used to actively control drug plasma levels through closed-loop feedback-controlled drug delivery (Arroyo-Currás, Ortega, et al., 2018; Dauphin-Ducharme et al., 2019; Mage et al., 2017). The implementation of such a technology in the clinic would immensely improve the ease, and success with which TDM could be performed.

E-AB sensors can also be used to measure directly in the solid tissues of live animals. Specifically, an E-AB sensor can be inserted directly into the tumor tissue of a rat to assess the penetration of the chemotherapeutic doxorubicin at multiple sites of the tumor tissue (Seo et al., 2022). This recent study from Soh's group shows a significant difference between the pharmacokinetics of the drug in the plasma vs tumor tissue, as well as at different layers of the tumor itself. Current methods for determining the penetration and pharmacokinetics of drugs in a tumor rely on the collection of a biopsy from the tumor site that provides a single time point snapshot. Single biopsies are unlikely to generate accurate pharmacokinetic estimates, and multiple time point biopsies are rarely performed as they risk tumor seeding (Egbers et al., 2015; Pepe & Aragona, 2013; Regev et al., 2002; Shyamala et al., 2014). Differing levels between plasma and tumor concentrations drugs implies that plasma levels

themselves may be misleading when treating patients and highlights the need for in situ measurements of drugs directly at their site of action.

***1.4.8 In-brain applications:*** As evidenced above, the field of E-AB sensing has made significant strides in recent years with respect to peripheral measurements of various target analytes directly *in*-vivo. At the time of writing, however, this platform has not yet been adapted to make in brain measurements in awake, ambulatory animals, capable of performing behavioral tasks. Indeed, I am only aware of only 3 prior reports of drug measurements being performed in situ in the brains of live animals *at all*, all of which required averaging over multiple animals to achieve statistical significance. In the two, Rocchitta et al. employed an enzymatic sensor specific for alcohols to measure ethanol in the brains of awake, behaving rats, albeit with averaging over multiple animals (Rocchitta et al., 2012, 2019) In the third, Taylor et al, employed an aptamer-based sensor similar to that described here to monitor cocaine in the brains of anesthetized rats after 2 mg/kg intravenous dosing (Taylor et al., 2017), but they had to average over four sensors placed in the brains of two animals. For example, the study reports peak in-brain cocaine concentrations of 15 µM, a value exceeding by many-fold the peak levels measured in prior microdialysis studies employing similar drug doses (S. H. Ahmed et al., 2003; Bradberry et al., 1993; Hurd et al., 1988; Minogianis et al., 2019; H.-T. Pan et al., 1991; W. H. T. Pan et al., 1994; Pettit & Pettit, 1994; Rocchitta et al., 2019; Taylor et al., 2017). Thus, although the potential exists, to date, there is very limited employment of biosensors to measure drugs in brain.

Another significant hurdle to using E-AB sensors for neuroscience and behavior is the detection of endogenous targets. Exogenous drug targets can be administered after sensor insertion meaning that an accurate baseline can be generated with ease as the experimenter knows, with confidence, that there is a true zero concentration of the desired target during baseline acquisition. A reliable baseline is essential to making real-time, *in*-vivo measurements because concentration estimates are made from *relative* signal change generated by the sensor. Because endogenous targets, such as neurotransmitters or amino acids, are already present at the time of sensor insertion it is critical that the experimenter has a method of determining the initial concentration of target. Beyond allowing the experimenter to measure the basal levels of their target prior to manipulation, the initial concentration is crucial as it determines where on your calibration curve that signal gain is occurring and calibration curves are not always linear (or have a constant mathematical function) across all of the concentrations relevant to measurements. Inaccurate estimates of basal concentrations will lead to inaccurate target concentration estimates and thus incorrect PK estimates. Unfortunately, to date, no E-AB sensor has been successfully deployed *in-vivo* that detects an endogenous target. Despite their limitations, both microdialysis and voltammetry are capable of measuring endogenous targets, such as dopamine, in the brain. If E-AB sensors are to reach their full potential as a tool for neuroscience research, the platform must be capable of measuring targets that are produced in the brain.

**1.5 Aims**

In response to these challenges, this thesis presents four studies that seek to show that E-AB sensors have all the necessary attributes for serving the neuroscience community's needs. Together the first two studies show how E-AB sensing can be adapted to make *in-vivo* measurements of endogenous targets. The first shows proof of principle for an *ex-vivo* point of care (POC) diagnostic tool for the measurement of tryptophan (TRP). Here I show that an E-AB sensor can successfully measure clinically relevant concentrations of TRP when challenged in synthetic urine. This sensor is specific to an inorganic receptor, TRP complex. As it is not reagentless, this sensor cannot be successfully implemented *in-vivo*. Building on this the second study removes the need for an inorganic receptor addition. Here I present the development and implementation of the first indwelling E-AB sensor directed against an endogenous target, the aromatic amino acid phenylalanine (PHE). Using a novel sensor calibration technique, the sensor is able to determine basal levels of PHE at the time of insertion as well as measure the metabolic response of animals in response to PHE infusions.

In the final two studies of this thesis, I describe the adaptation of the E-AB platform to the problem of performing seconds-resolved, real-time, multi-hour measurements of drugs in situ in the brains of awake, freely behaving rats. The first of the two studies is a proof-of-principle application of E-AB sensing to monitoring molecules at multiple sites within the body simultaneously. Here I apply E-AB sensing platform to the problem of performing *simultaneous* measurements in the CSF (in the lateral ventricle) and the blood (in the jugular). The resulting two-compartment measurements provide an unprecedented, high-precision picture of intercompartmental molecular transport that allows for the quantitative testing of several of the long-standing assumptions traditionally employed

multi-compartment pharmacokinetic models. In the final study I present the adaptation of the E-AB platform to the problem of molecular monitoring in the brains of freely moving, behaving subjects. This, first of its kind, application shows the *in-brain* E-AB platform is capable of measuring psychoactive drugs in the brains of awake, ambulatory rats, while simultaneously measuring a behavioral output associated with the drug. Specifically, here I perform seconds-resolved, real-time, multi-hour measurements of procaine concentration in situ in the brains of rats while measuring their locomotion behavior.

**Chapter 2:**

# An electrochemical aptamer-based sensor for the rapid and convenient measurement of L-tryptophan

## 2.1 Abstract

The field of precision medicine – the possibility to accurately tailor pharmacological treatments to each specific patient – would be significantly advanced by the ability to rapidly, conveniently, and cost-effectively measure biomarkers directly at the point-of-care. Electrochemical aptamer- based (E-AB) sensors appear a promising approach to this end due to their low cost, ease of use, and good analytical performance in complex clinical samples. Thus motivated, we present here the development of an E-AB sensor for the measurement of the amino acid L-tryptophan, a diagnostic marker indicative of a number of metabolic and mental health disorders, in urine. The sensor employs a previously reported DNA aptamer able to recognize the complex formed between tryptophan and a rhodium-based amino-acid receptor. We adopted the aptamer to the E-AB sensing platform by truncating it, causing it to undergo a binding-induced conformational change, modifying it with a redox-reporting methylene blue, and attaching it to an interrogating electrode. The resulting sensor is able to measure tryptophan concentrations in the micromolar range in minutes and readily discriminates between its target and other aromatic and non-aromatic amino acids. Using it we demonstrate the measurement of clinically relevant tryptophan levels in synthetic urine in a process requiring only a single dilution step. The speed and convenience with which this is achieved suggests that the E-AB platform could significantly improve the ease and frequency with which metabolic diseases are monitored.

**Keywords:** Amino acids detection, Electrochemical aptamer-based biosensor, DNA aptamer, Point of Care device, Metabolic diseases

## 2.2 Introduction

In recent years, the concept of precision medicine is inspiring the development of diagnostic technologies that can be implemented at the point of care or even employed in the home, thus improving the convenience and frequency with which health is monitored (M. U. Ahmed et al., 2014; Schork, 2015). Towards this end, significant effort has been focused on the development of devices able to monitor drugs and biomarkers rapidly and conveniently (M. U. Ahmed et al., 2014; Nayak et al., 2017). Glucometers, for example, allow for the frequent measurement of glucose in finger-prick blood samples (Hoedemaekers et al., 2008; Solnica et al., 2003), thus dramatically improving the management of blood sugar (Clarke & Foster, 2012). To date, however, glucose remains one of only a small number of metabolites for which such "self-test" clinical measurements are possible (M. U. Ahmed et al., 2014; Nayak et al., 2017). Moreover, as is true with most of the single-step molecular measurement technologies reported to date, the glucose sensor is critically reliant on the chemical (in this case, enzymatic) reactivity of its target and thus is not generalizable to other analytes.

In response to the need for platforms supporting the rapid, convenient measurement of specific molecules irrespective of their chemical reactivity we are developing Electrochemical Aptamer-based (E-AB) sensors, an approach that supports such measurements directly in complex clinical samples (Lubin & Plaxco, 2010; Schoukroun-Barnes et al., 2016). In this platform, an aptamer selected to specifically bind the desired target is attached to the surface of a gold electrode via a thiol group and modified with a redox reporter (here methylene blue) to support electrochemical signaling (Fig. 1, left). The

binding of the target induces a conformational change in the aptamer, altering electron transfer from the redox reporter and, ultimately, resulting in a concentration-dependent change in current (Fig. 1, right). Because E-AB signaling is predicated on a binding-induced conformational change (and not simply the adsorption of the target to a surface) the platform is insensitive to the nonspecific binding of interferants and performs well even when challenged directly in, for example, undiluted serum or blood (Lubin & Plaxco, 2010; Schoukroun-Barnes et al., 2016). And because they are electrochemical, they support detection in small volumes using low-cost, hand-held electronics (Lubin & Plaxco, 2010; Schoukroun-Barnes et al., 2016). Finally, because E-AB sensors rely on the binding of aptamers, and not the chemical or enzymatic reactivity of the target, the platform is fairly general, allowing for the detection of targets ranging from proteins (Lai et al., 2007; Y. Xiao, Lubin, et al., 2005) to small molecules (B. Baker et al., 2006; Rowe et al., 2010). Given these attributes, the E-AB platform appears a promising approach to point-of-care molecular measurements (Lubin & Plaxco, 2010; Schoukroun-Barnes et al., 2016). Exploring this idea we describe here the rapid and convenient measurement of the aromatic amino acid L-tryptophan in urine using a newly developed E-AB sensor.

Tryptophan is an essential amino acid in humans is necessary for protein synthesis but also plays key roles in many metabolic functions (Palego et al., 2016).For example, it is a precursor of the neurologically important molecules serotonin and melatonin (Palego et al., 2016). In addition, the level of tryptophan in biological fluids has been proposed as a means of diagnosing and monitoring multiple diseases (Kaluzna-Czaplinska et al., 2019). Among these are numerous inborn metabolic disorders (hypertryptophanemia. tryptophanuria

(MARTIN et al., 1995; SNEDDEN et al., 1983) and Hartnup disease (WILCKEN et al., 1977)]), as well as emotional, cognitive and developmental disorders (Kaluzna-Czaplinska et al., 2010; Lindseth et al., 2015). To treat these clinicians are increasingly turning to tailored dietary therapies or nutritional regimes (Camp et al., 2012; Kaluzna-Czaplinska et al., 2019). The rapid and convenient measurement of urinary tryptophan levels could impact the efficacy of these treatments by supporting the rapid, frequent adjustment of therapy (Camp et al., 2012; Saudubray et al., 2006). Current methods for measuring this amino acid in clinical samples, however, which include chromatography and mass spectrometry, fail to fill this need because they required specialized personnel and expensive instrumentation and are slow (typically days) to return an answer (K.-A. Yang et al., 2014). Here, however, we describe an E-AB sensor able to measure clinical tryptophan levels rapidly and conveniently enough to support point-of-care and even in-home measurements.

## 2.3 Materials and Methods

### Chemical reagents

Reagent-grade chemicals, including sodium hydroxide, sulfuric acid, 6-mercapto-1-hexanol, sodium chloride, ethanol, HEPES (4-(2-Hydroxyethyl)-1-piperazineethanesulfonic acid), tris(2-carboxyethyl)-phosphine (TCEP), hydrochloride tris[hydroxymethyl]-aminomethane hydrochloride, magnesium chloride, ethylenediaminetetraacetic acid (EDTA), potassium chloride, Pentamethylcyclopentadienyl rhodium(III) chloride dimer, L-tryptophan, L-phenylalanine, L-tyrosine, L-glutamine, L-histidine, L-arginine, L-alanine,

sodium phosphate monobasic and artificial urine (Surine™ Negative Urine Control) (all from Sigma-Aldrich, St. Louis, Missouri, USA) were used as received.

HPLC purified oligonucleotide were purchased from Biosearch Technologies (Novato, CA, USA). The aptamer variant was modified with a thiol-$C_6$-SS group at its 3' end, and a methylene blue attached by a six-carbon linker to an amine at its 5' end. The oligonucleotide was dissolved in buffer (100 mM Tris buffer, 10 mM $MgCl_2$, pH 7.8) at a concentration of 100 µM and then aliquot and stored at -20 °C. The final concentration of the oligonucleotide was confirmed using a Beckman Coulter DU 800 UV-Vis Spectrophotometer (Männedorf, Switzerland) using a 100 µL quartz cuvette and measuring the relative absorbance at 260 nm.

The aptamer sequence we employed was a truncated version of a previously reported aptamer against this target (K.-A. Yang et al., 2014):

5'- CGCGGTAGTCTTAACCTAAAGCGGTGTCA -3'

**Sensor Fabrication**

**Electrode Polishing and Cleaning.** The sensors were fabricated using an established approach (Y. Xiao et al., 2007). Briefly, E-AB sensors were fabricated on rod gold disk electrodes (3.0 mm diameter, BAS, West Lafayette, IN, USA). The disk electrodes were prepared by polishing on a microcloth pad soaked before with a 1 µm diamond suspension slurry (MetaDi, Buehler, Lake Bluff, IL, USA) and then with a 0.05 µm alumina powder aqueous suspension. Each polishing step is followed by sonication of the electrodes in a

solution 1:1 water/ethanol for 5 min. The electrodes were then electrochemically cleaned following this procedure: a) The electrodes are placed in a 0.5 M NaOH solution and through cyclic voltammetry (CV) 1000-2000 scans are performed using a potential between −0.4 and −1.35 V versus Ag/AgCl at a scan rate of 2 V $s^{-1}$; b) The electrodes were moved to a 0.5 M $H_2SO_4$ solution and using Chronoamperometry an oxidizing potential of 2 V was applied for 5 s. After a reducing potential of −0.35 V was then applied for 10 s; c) Using CV we cycled the electrodes rapidly (4 V $s^{-1}$) in the same solution between −0.35 and 1.5 V for 10 scans followed by 2 cycles recorded at 0.1 V $s^{-1}$ using the same potential window.

**Electrode functionalization.** We first reduced the probe DNA (100 µM) by treating it for 1 h in a solution of 10 mM tris(2-carboxyethyl)-phosphine hydrochloride (TCEP) in the dark. This was then dissolved in "assembling buffer" (10 mM $Na_2HPO_4$ with 1 M NaCl and 1 mM $MgCl_2$ at pH 7.3) at a final concentration of 500 nM. The electrochemically cleaned gold electrodes were then immersed in 200 µL of this solution for 1 h in the dark. Following this the electrode surface was rinsed with distilled water and incubated overnight at 4°C in assembling buffer containing 2 mM 6-mercaptohexanol, followed by a further rinse with distilled water before use.

**Electrochemical Experiments**

Electrochemical measurements were performed at room temperature using a CHI660D potentiostat with a CHI684 Multiplexer (CH Instruments, Austin, TX) and a standard three-electrode cell containing a platinum counter electrode and a Ag/AgCl (3 M KCl) reference electrode. Square Wave Voltammetry (SWV) was performed using a potential window of -0.1 to -0.4 V, a potential step of 0.001 V and 0.05 V amplitude.

**Titration curves.** Experimental titration curves (Fig. 2b and 3) were performed in 10 mL of working buffer (20 mM HEPES, 1 M NaCl, 10 mM MgCl2, 5 mM KCl, pH 7.5) using three E-AB sensors modified with the oligonucleotide probe and using a SWV frequency of 500 Hz. Initially, in absence of target and rhodium-based receptor, we performed a preliminary treatment by interrogating the electrodes with 60-120 scans until a stable current peaks were obtained. Once the sensor's signal was stable, the desired rhodium-based receptor concentration was added to the solution to reach the final concentration of 100 µM. Then, increasing concentrations of the target was added and the sensors were interrogated after 10 min. Titration curves in Fig. 4 were performed using the same experimental approach but adding the appropriate volume of artificial urine spiked with the target (30 µL and 100 µL) to achieve dilution factors of 1:333 and 1:100.

The peak current was extracted for each sensor by subtracting the baseline current from the peak maxima in absence ($C_0$) and for each concentrations of target ($C_{Target}$). We converted the signal current in signal change % ($C_{\%}$) using the following equation:

$$C_{\%} = \left(\frac{C_{Target} - C_0}{C_0}\right) \cdot 100$$

Where $C_{Target}$ is the current peak in the presence of target and $C_0$ is the current peak in the absence of target. The resultant data were fitted using a Langmuir equation (single-site binding mechanism) in Kaleidagraph (Synergy Software):

$$C_{\%}^{[Target]} = C_{\%}^{0} + \left(\frac{[X](C_{\%}^{X} - C_{\%}^{0})}{[X] + K_D}\right)$$

Where [X] is the target concentration, $C_{\%}^{[Target]}$ is the relative change in signal current in the presence of target, $C_{\%}^{0}$ is the background current seen in the absence of the target, $C_{\%}^{X}$ is the relative signal change seen at saturating target, and $K_D$ *i*s the dissociation constant of the surface-bound aptamer.

**Sensor equilibration time.** We determined the sensor's equilibration time (Fig. 2c) using the above experimental approach and interrogating the sensor every 10 s in working buffer. After we achieved a stable current baseline, in presence (100 μM) or in absence of the rhodium-based receptor, we added to the solution the target and then we monitored the voltammetric signal for over 15 min. The observed signal change was fitted to a single exponential decay in Kaleidagraph (Synergy Software) to obtain the equilibration time constant of the sensor.

**2.4 Results**

We employed a DNA aptamer previously developed by the Stojanovic group (K.-A. Yang et al., 2014), which displays high affinity and good specificity for a supramolecular complex between tryptophan and a amino-acid-binding rhodium-based inorganic receptor, pentamethylcyclopentadienyl rhodium(III) (Fig. 1). In order to adapt this into the E-AB

platform we re-engineered the original, “original” sequence (Fig. 2a) via truncation so that, in absence of the target, the aptamer populates a non-binding, partially unfolded conformation (White et al., 2010). We then modified this with a thiol group on its 5’end (to anchor the aptamer to a gold electrode) and a methylene blue redox reporter on its 3’ end. When interrogated using square wave voltammetry (SWV) the re-engineered aptamer responds as expected to tryptophan (Fig. 1, left). For example, in the presence of the rhodium-based inorganic receptor (at 100 μM) and saturating target (100 μM) the sensor responds with a 25.2 ± 1.1% decrease in its electrochemical signal (Fig. 1, right). (Note: the error bars here and elsewhere in this paper represent standard deviations of multiple, interdependently fabricated devices.). This response is rapid; at 10 μM tryptophan the sensor responds with an equilibration time constant of 2.1 ± 0.1 min (Fig. 2c), a time scale reasonable for point of care applications. Titrating the sensor with increasing concentrations of tryptophan we obtain the expected Langmuir binding curve with a dissociation constant ($K_D$) of 6.2 ± 1.3 μM (Fig. 2b, red curve). Titrations with other amino acids indicate that the sensor’s specificity is sufficient to support clinical measurements. Specifically, when challenge with the amino acids L-phenylalanine, L-tyrosine, or a solution formed by 5 different amino acids (L-glutamine, L-histidine, L-proline, L-arginine, L-alanine) (Fig. 3) we do not observe any significant signal change at concentrations below 30 μM, and thus none are expected to interfere with tryptophan under clinical sample conditions (MARTIN et al., 1995; SNEDDEN et al., 1983; WILCKEN et al., 1977; K.-A. Yang et al., 2014).

Clinically relevant urinary tryptophan ranges in healthy individuals range from 20 to 70 µM. In individuals suffering from a number of inborn metabolic disorders, this rises to 0.1 to 10 mM (MARTIN et al., 1995; SNEDDEN et al., 1983; WILCKEN et al., 1977). The useful dynamic range of our sensor (defined here as the range from 10% to 90% of the maximum signal change), is 0.7 µM to 40 µM, rendering it both lower than and narrower than clinical range seen in the metabolic disorders alone, thus necessitating that we perform sample dilutions (Fig. 4). Specifically, using a dilution of 1:100 we can measure urinary concentrations from 0.1 mM to 1 mM (corresponding to concentrations of 1 to 10 □M in the test solution) and using 1:333 we can measure urinary tryptophan over the range 1 mM to 10 mM (corresponding to concentrations of 3 to 30 □M in the test solution). Using this approach to characterize synthetic urine spiked with known tryptophan concentrations we find that the sensor accurately measures its target with a relevant accuracy of ±20% from 0.2 to 8 mM (Fig. 4).

**2.5 Discussion**

Here we describe an E-AB sensor that can rapidly (<10 min) and conveniently (simply a dilution with buffer containing the inorganic receptor) measure urinary tryptophan in urine. The sensor can measure the entire clinically-relevant range (from 0.1 to 10 mM) achieving an accuracy of 20% across the majority of this range (from 0.2 to 8 mM). Finally, the sensor also efficiently rejects interference by other amino acids that might be present in the clinical samples.

The ability for patients to self-test for metabolite levels in the urine would provide immediate information regarding their metabolic and health status. This, in turn, would open new paths to individualized, patient-centered healthcare. To this end, the miniaturazibility of E-AB sensors and potential cost-effectiveness of E-AB sensors are also significant advantages. For example, exploiting screen-printed electrodes (Grabowska et al., 2018), it could be possible to adapt E-AB sensors on disposable strips read by a small portable potentiostat. At the same time, the development of a user-friendly interface could help patients converting the analytical signal into useful clinical data, for example, creating a specific application for the mobile phone. The resultant convenient measurement of tryptophan levels could support the tailored diets and treatments in a patient specific manner, circumventing the issue presented by individual differences in metabolism and nutrient absorption and correcting for them in real-time. In particular this could significantly impact the health of patients unable to care for themselves, such as children and patient with mental health disorders, whose intake of tryptophan could thus be easily and rapidly monitored.

## 2.6 Figures

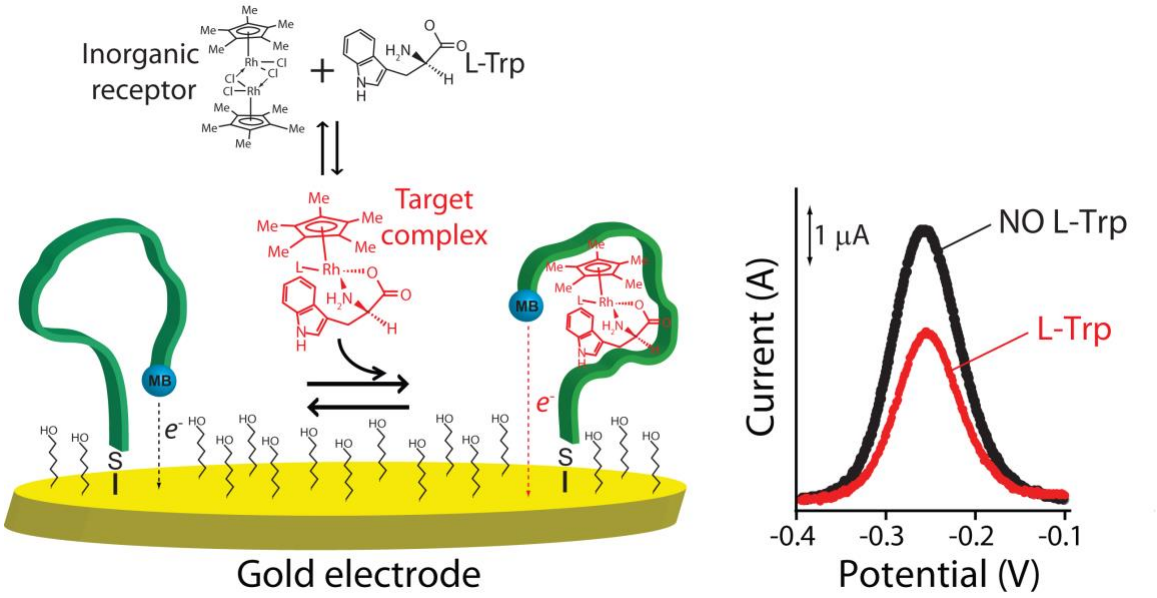


**Fig. 1.** Electrochemical Aptamer-based (E-AB) sensors generate a detectable electrochemical signal via a binding-induced conformational change in a redox-reporter-modified, electrode-bound aptamer. (Left) In the absence of the target, the aptamer is relatively unfolded and extended. Target binding induces a conformational change, leading in turn to a change in the electron transfer rate of the methylene blue reporter. (Right) Binding of the tryptophan /inorganic receptor complex produces decreases the electrochemical signal in a manner quantitatively related to the concentration of tryptophan in the solution.

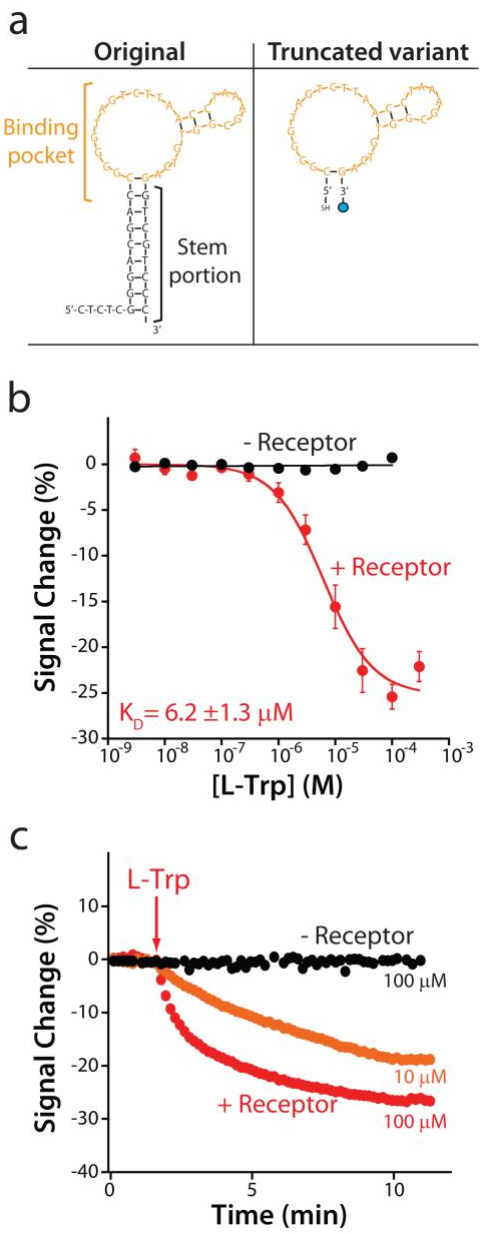


**Fig. 2.** The re-engineered E-AB sensor responds sensitively and rapidly to its target. (a) To ensure that the aptamer undergoes a large-scale conformational change upon target binding we truncated the parent aptamer sequence to better populate the aptamer's unfolded state in the absence of target. (b) A sensor fabricated using this truncated aptamer responds to increasing concentrations of tryptophan only in the presence (red curve) of the rhodium-based inorganic receptor, producing a well-defined Langmuir isotherm with a dissociation constant ($K_D$) of 6.2 ± 1.3 µM. (c) The sensor rapidly responds to the addition of 10 or 100 µM tryptophan.

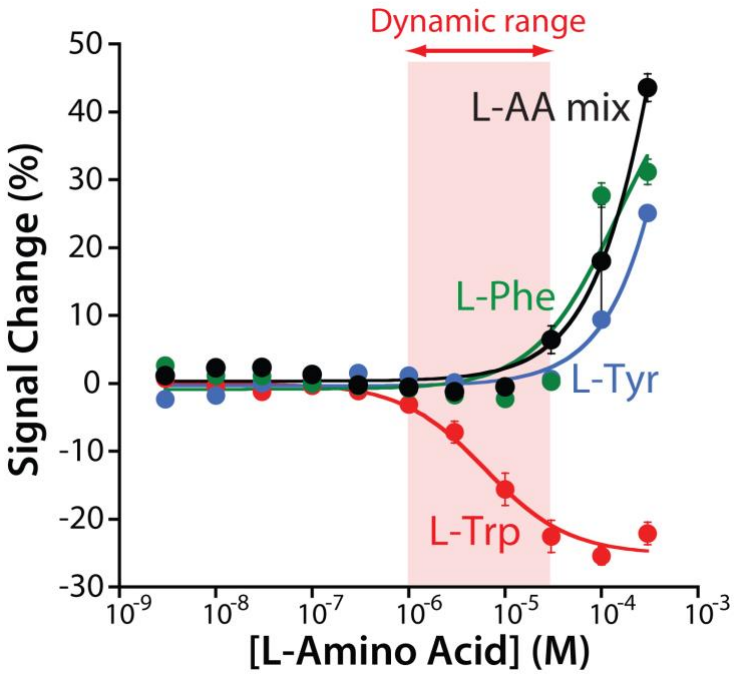


**Fig. 3.** To test sensor specificity we challenged it against the other two aromatic amino acids (L-phenylalanine and L-tyrosine), as well as a mix of five amino acids (L-glutamine, L-histidine, L-proline, L-arginine, L-alanine). None of these potential interferents produces a measurable signal change below 30 µM, suggesting that none of them will interfere under realistic clinical conditions.

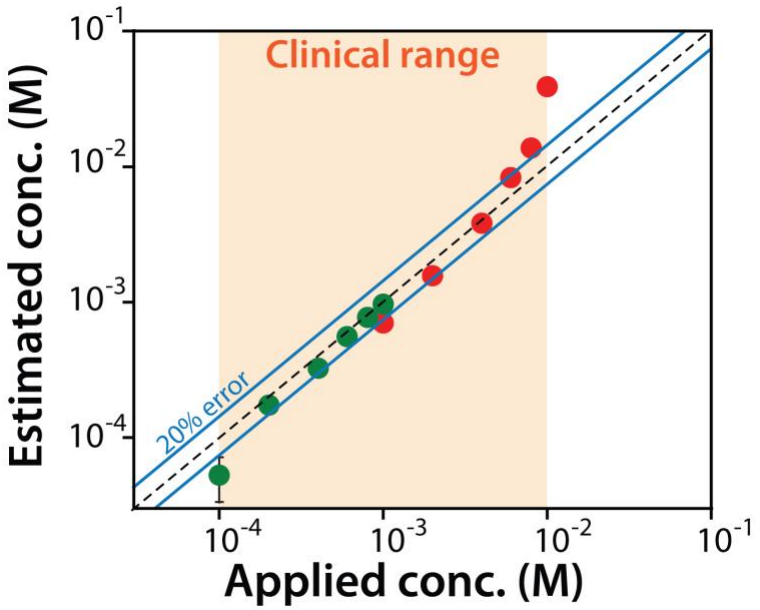


**Fig. 4.** The sensor exhibits clinically relevant accuracy when challenged in synthetic urine. Using two different dilution factors of 1:333 (green) and 1:100 (red) we can detect across the entire clinically relevant range of tryptophan seen for patients with metabolic disorders. Shown are the known (spiked concentration prior to dilution) versus E-AB estimated concentrations (back calculated to correct for the dilution).

# Chapter 3:

# Seconds-resolved, in-situ measurements of plasma phenylalanine disposition kinetics in living rats

**3.1 Abstract**

Current knowledge of the disposition kinetics of endogenous metabolites is founded almost entirely on poorly-time-resolved experiments in which samples are removed from the body for later, bench-top analysis. Here, in contrast, we describe real-time, seconds-resolved measurements of plasma phenylalanine collected in-situ in the body via electrochemical aptamer-based (EAB) sensors, a platform technology that is independent of the reactivity of its targets and thus is generalizable to many. Specifically, using indwelling EAB sensors we have monitored plasma phenylalanine in live rats with few micromolar precision and 12 s temporal resolution, identifying a large-amplitude, few-seconds phase in the animals' metabolic response that had not previously been reported. Using the hundreds of individual measurements that the approach provides from each animal, we also identify inter-subject variability, including statistically significant differences associated with feeding status. These results highlight the power of in vivo EAB measurements, an advance that could dramatically impact our understanding of physiology and provide a valuable new tool for the monitoring and treatment of metabolic disorders.

**Keywords:** Phenylketonuria, PKU, amino acids, metabolism, metabolomics, continuous monitoring, intravenous.

## 3.2 Introduction

The development of a platform technology supporting the seconds-resolved, real-time measurement of small molecules in the body would significantly advance our understanding of metabolism as well as our clinical ability to track it, and when necessary, intervene to alter it. As a research tool, for example, such a technology would vastly improve the precision with which we can measure metabolic fluxes and their regulation (Metallo & Vander Heiden, 2013; Wegner et al., 2015). By providing real-time information regarding therapeutic efficacy, such a technology could, by analogy to how the continuous glucose monitor has impacted the treatment of diabetes (Rodbard, 2016), revolutionize how we monitor and treat a wide range of inborn errors of metabolism (Camp et al., 2012; Goldstein & Vockley, 2017; Walter et al., 2002). To date, however, all prior methods of measuring specific metabolites in situ the body, including current electrochemical approaches for the measurement of glucose, lactate, pyruvate and glutamate (Kucherenko et al., 2019; Rathee et al., 2016; Wilson & Gifford, 2005; Wilson & Hu, 2000; Yoo & Lee, 2010), are “one-offs.” That is, each relies critically on the availability of a highly-selective oxidase enzyme able to convert the target molecule into an electrochemically-detectable product (typically hydrogen peroxide), and thus this approach is not generalizable to the many important targets for which suitable enzymes are not available.

In response to the need for an in-vivo molecular measurement technology that, in contrast to prior approaches, is independent of the enzymatic reactivity of its targets we are developing electrochemical aptamer-based (EAB) sensors (Idili, Gerson, et al., 2019; Idili, Parolo, et al., 2019; Lai et al., 2007; Parolo et al., 2020; Y. Xiao, Lubin, et al., 2005; Y.

Xiao, Piorek, et al., 2005). This reagentless, reversible sensor architecture exploits an electrode-bound, redox-reporter-modified aptamer as its recognition element (Figure 1A). The presence of the specific target induces a conformational change in the aptamer. This, in turn, produces an easily measurable electrochemical output that can be used to measure molecular concentrations with high frequency and in real time (Figure 1B). And because this binding-induced conformational change mechanism is analogous to the conformation-linked signaling employed by nature (Plaxco & Soh, 2011), EAB sensors are selective enough to work in situ in the living body. For example, using indwelling EAB sensors (Figure 1C, left) we have previously performed the real-time, seconds (and even sub-second) resolved measurement of multiple drugs in situ in the veins of live rats (Figure 1C, right) (Arroyo-Currás, Dauphin-Ducharme, et al., 2018; Arroyo-Currás et al., 2017; Dauphin-Ducharme et al., 2019; Idili, Arroyo-Currás, et al., 2019). Expanding on this, here we describe the development and implementation of the first indwelling EAB sensor directed against an endogenous target, the aromatic amino acid phenylalanine. To the best of our knowledge, this is the first electrochemical sensor able to measure this or any metabolite in real time in the living body without relying on the target's redox chemistry, spectroscopic properties, or enzymatic reactivity.

### 3.3 Experimental section

Chemical reagents and materials. Reagent-grade chemicals, including sodium hydroxide (NaOH), hydrochloric acid (HCl), 6-mercapto-1-hexanol, sodium chloride (NaCl), ethanol, potassium chloride (KCl), calcium chloride ($CaCl_2$), dextrose, sodium bicarbonate

($NaHCO_3$), potassium phosphate dibasic ($K_2HPO_4$), sodium phosphate monobasic ($NaH_2PO_4$), tris(2-carboxyethyl)-phosphine hydrochloride (TCEP), tris[hydroxymethyl]-aminomethane hydrochloride (Trizma®), magnesium chloride, bovine serum albumin (BSA), ethylenediaminetetraacetic acid (EDTA), L-phenylalanine, L-tryptophan, L-tyrosine, L-glutamine, L-histidine, L-arginine, L-alanine, L-proline, sodium phenylpyruvate and N-acetyl-L-phenylalanine were obtained from Sigma-Aldrich (St. Louis, MO, USA) and they were used as received. Sulfuric acid ($H_2SO_4$) was obtained from EMD Millipore (Darmstadt, Germany), and fritted Ag|AgCl electrodes and platinum wire were from CH Instruments (Austin, TX, USA). Bovine blood in Heparin (3 IU/ml) was obtained from HemoStat Laboratories (Dixon, CA, USA) and it was used as received.

Catheters (22 G) and 1 mL syringes were purchased from Becton Dickinson (Franklin Lakes, NJ, USA). PTFE-insulated gold, platinum, and silver wires (75 µm diameter) were purchased from A-M systems (Sequim, WA, USA). Bare gold wire (100 µm diameter) for in vitro studies was purchased from Alfa Aesar (Kandel, Germany). Heat-shrink polytetrafluoroethylene insulation (PTFE, HS Sub-Lite-Wall, 0.02, 0.005, 0.003 ± 0.001 in, blackopaque, Lot No. 17747112-3), used to electrically insulate gold, silver, and platinum wires, was purchased from ZEUS (Branchburg Township, CA, USA). Custom-made, open ended, mesh-covered three channel connector cables to fabricate in vivo probes were purchased from PlasticsOne (Roanoke, VA, USA).

Oligonucleotides

RP-HPLC purified oligonucleotide was purchased from Biosearch Technologies (Novato, CA, USA). The aptamer sequence was modified with a thiol-$C_6$-SS group at its 5’

end, and a methylene blue attached by a six-carbon linker to an amine at its 3' end. The oligonucleotide was dissolved in TE buffer (100 mM Tris buffer, 10 mM $MgCl_2$, pH 7.8) at a concentration of 100 µM and then aliquot and stored at -20 °C. The final concentration of the oligonucleotide was confirmed using a Beckman Coulter DU 800 UV-Vis Spectrophotometer (Männedorf, Switzerland) using a 100 µL quartz cuvette and measuring the relative absorbance at 260 nm.

The aptamer sequence we employed in this work it was previously reported (Cheung et al., 2019):

Phenylalanine-binding aptamer:

5'-CGACC-GCGTT-TCCCA-AGAAA-GCAAG-TATTG-GTTGG-TCG-3'

For the sequence above the underlined nucleotides represent the stem portion.

EAB Sensors fabrication for in-vitro experiments

Gold Electrode Fabrication and Electrochemical Cleaning

The EAB sensors employed in our in-vitro characterization (Figure 2, 3A, and S1-3) were fabricated using an established approach. Briefly, segments of bare gold wire (100 µm diameter) were cut (5 cm in length) and the insulated body of the wires was coated using two layers of heat-shrink PTFE tubing. To facilitate connection with the potentiostat, a gold pin was soldered to one end of the electrode and this contact further coated with insulating connector paint (MG Chemicals, Burlington, ON, Canada). Finally, the uninsulated end of the electrodes was cut to a final length of 3 mm prior to electrochemical cleaning with the following protocol: (1) 300 cycles between −1 and −1.6 V in a solution of 0.5 M NaOH at 1 V

$s^{-1}$ to remove any residual thiol/organic contaminants on the electrode surface and (2) pulsed between 0 and 2 V for at least 16,000 cycles with a pulse length of 20 ms (no waiting between pulses) in 0.5 M $H_2SO_4$ to increase the electrode roughness, as previously reported.[2-5]

Electrode functionalization

For the EAB sensors (Figure 2, 3A, and S1-3), we first reduced the thiol-modified DNA probe (100 µM) by treating it for 1 h in a solution of 10 mM tris(2-carboxyethyl)-phosphine hydrochloride (TCEP) at room temperature in the dark. This was then dissolved in "assembling buffer" (10 mM $Na_2HPO_4$ with 1 M NaCl and 1 mM $MgCl_2$ at pH 7.3) at a final concentration of 500 nM. The electrochemically cleaned wire gold electrodes were then immersed in 400 µL of this solution for 1 h in the dark. Following this the electrode surface was rinsed with distilled water and incubated overnight in assembling buffer containing 5 mM 6-mercaptohexanol at room temperature in the dark, followed by a further rinse with distilled water before use. Of note, during the modification steps the solutions have to cover all the area of uninsulated gold electrode.

EAB Sensors fabrication for in-vivo experiments

Electrode fabrication

The EAB sensors employed in-vivo (Figure 3B, 4, 5, S5 and S6) were fabricated as described in previous reports.[19-22] Segments of PTFE-insulated gold (75 µm diameter by 12 cm in length), platinum (75 µm by 11.5 cm), and silver (75 µm by 11 cm) wire, were cut to make sensors. We removed 2 cm of PTFE-insulation layer using a surgical blade from one end to allow electrical contact and ~5 mm from the other. To convert the silver wire into a

reference electrode we immersed the short portion of it in concentrated sodium hypochlorite (commercial bleach) overnight to form a stable silver chloride film. We then placed the gold wire and platinum wires together such that their short, exposed areas were close but not in contact. We applied heat shrinkable tubing around these and used heat to draw them together. Finally, using the same process, we incorporate the silver wire into the bundle using an additional layer of heat-shrink tubing. The resulting, three-layer-thick insulation approach provides mechanical strength to the body of the otherwise malleable probe. Finally, we cut the exposed portion of the gold wire to 3 mm in length. To increase microscopic surface area of the gold, which improves signaling, we roughened them electrochemically via immersion in 0.5 M sulfuric acid followed by stepping the potential between $E_{initial}$ = 0.0 V to $E_{high}$ = 2.0 V versus Ag/AgCl, back and forth, for at least 16,000 pulses.[5] Each potential step was of 20 ms duration with no waiting time in-between pulses.

Electrode functionalization

We first reduced the DNA aptamer (100 µM) by treating it for 1 h in a solution of 10 mM tris(2-carboxyethyl)-phosphine hydrochloride (TCEP) at room temperature in the dark. We then diluted this in “assembling buffer” (10 mM $Na_2HPO_4$ with 1 M NaCl and 1 mM $MgCl_2$ at pH 7.3) to a concentration of 500 nM. We then cleaned an electrochemically roughened gold electrode via rinsing in deionized water and immersed it in 200 µL of this solution for 1 h in the dark. Following this the electrode surface was again rinsed with distilled water, incubated overnight at 25°C in assembling buffer containing 5 mM 6-mercaptohexanol, and rinsed a final time with distilled water before use.

Electrochemical measurements in-vitro

Electrochemical measurements were performed at room temperature using a CHI660D potentiostat with a CHI684 Multiplexer (CH Instruments, Austin, TX, USA) and a standard three-electrode cell containing a platinum counter electrode and a Ag/AgCl (3 M KCl) reference electrode. Square Wave Voltammetry (SWV) was performed using a potential window of -0.1 to -0.4 V, a potential step of 0.001 V and 0.05 V amplitude.

Titration curves

Experimental titration curves were performed in 10 mL of working buffer (137 mM NaCl, 2.7 mM KCl, 10 mM $Na_2HPO_4$, 1.8 mM $KH_2PO_4$ at pH 7.3) (Figure 2A and 2B) or in 10 mL of Ringer's buffer (154 mM NaCl, 5.64 mM KCl, 2.16 mM $CaCl_2$, 11.10 dextrose, 2.38 $NaHCO_3$, 2 mM Trizma® at pH 7.4) (Figure S3), or blood bovine (Figure S2) using at least three EAB sensors modified with the selected aptamer sequence and using a SWV frequency of 10 Hz and 300 Hz. Initially, in absence of phenylalanine, we performed a preliminary treatment by interrogating the sensors with 30-60 scans until stable peak currents were obtained. Once the sensor's signal was stable increasing concentrations of the phenylalanine was added at 5 min intervals and the sensors were interrogated. The electrochemical signal (peak current) of each sensor was plotted in function of phenylalanine concentrations and then it was fitted using a single-site binding mechanism equation[3] in Kaleidagraph (Synergy Software).

Sensor equilibration time

We determined the sensor's equilibration time (Figure 2C) using the above experimental approach and interrogating the sensor every 5 s at 300 Hz in working buffer (137 mM NaCl, 2.7 mM KCl, 10 mM $Na_2HPO_4$, 1.8 mM $KH_2PO_4$ at pH 7.3). After we achieved

a stable current baseline (5 min) we added to the solution the different concentrations of phenylalanine and then we monitored the voltammetric signal for over 15 min.

Calibration curves

Calibration curves (Figure 3A) were obtained using a new approach which requires the use of two calibration solutions: the first is a buffer designed to mimic the relevant properties of whole blood (pH, ionic strength, protein and sugar content) and the second is a whole bovine blood sample with a known exogenous concentration of phenylalanine (here 80 µM). The concentration phenylalanine in the bovine blood calibrant was determined via liquid chromatography–mass spectrometry (Agilent 6470 Triple Quadrupole LC/MS). To mimic the properties of bovine blood we selected as calibration buffer a solution composed by Ringer's buffer (154 mM NaCl, 5.64 mM KCl, 2.16 mM $CaCl_2$, 11.10 dextrose, 2.38 $NaHCO_3$, 2 mM Trizma® at pH 7.4) in presence of BSA (35 mg/mL).[24,25] To determine the lower portion of the calibration curve we placed the sensors in the calibration buffer (20 mL) for 1 h, mixing the solution with a magnetic stirrer. We then interrogated the sensors for 30 to 60 scans at square wave frequencies of 10 and 300 Hz until stable peak currents were obtained. Once the signal was stable, we challenged the sensors with increasing amounts of whole blood of known (80 µM) phenylalanine concentration until we reached 70% (v/v) blood, which corresponds to a total concentration of phenylalanine of 56 µM. To determine the upper portion of the calibration curve we then transferred these sensors into undiluted whole blood (20 mL) and added additional phenylalanine until it reached a final concentration of 1 mM. Adding the two data sets together we obtain the entire Langmuir isotherm for each sensor.

To perform KDM we normalized the raw current observed at each phenylalanine concentration, $I_{Raw}^{[phe]}$, relative to the current seen in the absence of target $I_{Raw}^{0}$:

$$i_{OFF}^{[phe]} = \frac{I_{Raw-10Hz}^{[phe]}}{I_{Raw-10Hz}^{0}} \quad (1)$$

$$i_{ON}^{[phe]} = \frac{I_{Raw-300Hz}^{[phe]}}{I_{Raw-300Hz}^{0}} \quad (2)$$

Using these normalized currents estimated from the previous calibration curves we converted the raw signal current in KDM signal using the following equation:

$$i_{KDM}^{[phe]} = i_{ON}^{[phe]} - i_{OFF}^{[phe]} \quad (3)$$

Finally, we fitted the entire Langmuir isotherm plotted as KDM signal with the following equation:

$$i_{KDM}^{[phe]} = i_{KDM}^{0} + \frac{[\text{phenylalanine}]\left(i_{KDM-MAX}^{[phe]} - i_{KDM}^{0}\right)}{[\text{phenylalanine}] + K_D} \quad (4)$$

where [phenylalanine] is the phenylalanine concentration, $I_{KDM}^{[phe]}$ is KDM signal in the presence of different concentrations of phenylalanine, $I_{KDM}^{0}$ is the background signal seen in the absence of the aromatic amino acid target, $I_{KDM-MAX}^{[phe]}$ is the KDM signal seen at saturating concentrations of phenylalanine, and $K_D$ *i*s the dissociation constant of the aptamer in the context of the sensor.

Square wave voltammetry frequency versus signal change plot

We determined the square-wave frequency dependence of the sensor's gain (Figure S1) in 10 mL of buffered saline (137 mM NaCl, 2.7 mM KCl, 10 mM $Na_2HPO_4$, 1.8 mM $KH_2PO_4$ at pH 7.3). The sensors were interrogated using various frequencies (from 5 Hz to

4000 Hz) in absence and in presence of three different amounts of phenylalanine (100 µM, 300 µM and 1 mM), with a 10 min incubation between phenylalanine additions.

Electrochemical measurements in-vivo

All in vivo measurements were performed using a three-electrode setup in which the reference and counter electrodes were a silver wire coated with a silver chloride film as described above and a platinum wire. The measurements carried out in vivo were recorded using a handheld potentiostat from CH Instruments (Austin, TX, USA - Model 1242 B).

Animals

In vivo measurements were performed in male and female Sprague-Dawley rats (4−5 months old) purchased from Charles River Laboratories (Santa Cruz, CA), weighing between 300 and 500 g. All animals were pair housed in a standard light cycle room (08:00 on, 20:00 off) and allowed ad libitum access to food and water. The experimental protocol (n. 824) was approved by the Institutional Animal Care and Use Committee (IACUC) of the University of California Santa Barbara and adhered to the guidelines given by the NIH Guide for Care and Use of Laboratory Animals (8th edition, National Academy Press, 2011).

Surgery

For in vivo measurements rats were induced under 4% isoflurane anesthesia in a Plexiglas anesthesia chamber. The rats were then maintained on 2−3% isoflurane gas for the duration of the experiment. While anesthetized, an infusion line was inserted into the left jugular vein of the rats and EAB sensors were inserted into the opposite, right vein. Briefly, the area above each jugular vein was shaved and cleaned with betadine and 70% ethanol. A small incision was made above each vein, and then each vein was isolated. A

small hole was cut into each vein with spring-loaded microscissors. Into one we inserted a silastic catheter constructed with a bent steel cannula with a screw-type connector (Plastics One, Roanoke, VA) and silastic tubing (11 cm, i.d. 0.64 mm, o.d. 1.19 mm, Dow Corning, Midland, MI) for infusions. In the other we inserted the EAB sensor. In order to maintain the positional stability of the EAB sensor, two sterile 6–0 silk sutures (Fine Science Tools, Foster City, CA) were used to tie the sensor to the vein and anchor it in place. 30 units of heparin were infused following insertion of the E-AB sensor.

Calibration of in-vivo sensors

Before its use in vivo, the catheter (22 G) encased sensor was calibrated using the procedure described above (Figure 3). The signal collected at 10 Hz and 300 Hz in the absence of phenylalanine ($I_{Raw}^{0}$) was used to convert the raw current collected in vivo ($I_{Raw}^{[phe]}$) to KDM signal (Eq. 1-3).

In-vivo real-time measurements

For the in vivo experiments (Figures 4, 5, and S6) a 20 min sensor baseline was established before the metabolite infusion. A 3 mL syringe filled with the target metabolite was connected to the sensor-free catheter (placed in the jugular opposite that in which the sensor is emplaced) and placed in a motorized syringe pump (KDS 200, KD Scientific Inc., Holliston, MA, USA). After establishing a stable baseline, the target was infused through this catheter at a rate of 1 mL/min. For phenylalanine we used a 15 mg/mL solution, for tyrosine 2 mg/mL, and for tryptophan 8 mg/mL. The real-time plotting and analysis of voltammetric data were carried out with the help of a script written in Python (Curtis et al., 2019).

Pharmacokinetic analysis

Phenylalanine plasma basal levels (Table 1) were estimated fitting the phenylalanine concentration values with a linear fit using a slope fixed to zero. We estimated the pre- and post-challenge baselines using first 20 minutes ($[phe]_{t=0}$ - before the i.v. injection) and last 20 minutes ($[phe]_{t=70}$ – of data before and after the challenge). We fit post-injection plasma phenylalanine concentration time courses (Figure 5, S5 and Table 1) to the biexponential equation appropriate for a two-compartment model (CAMPISTRON et al., 1982; JAGENBURG et al., 1977) (Equation 1 and Scheme 1).

**3.4 Results and Discussion**

EAB sensor development requires an aptamer that: (1) binds the desired target with relevant affinity and specificity and (2) undergoes the binding-induced conformational change required to generate an EAB signal (see e.g., (Arroyo-Currás et al., 2017; Dauphin-Ducharme et al., 2019; Idili, Arroyo-Currás, et al., 2019)). In this work we have employed a phenylalanine-binding aptamer recently reported by Cheung et al. (Cheung et al., 2019), which is thought to transition from a partially unfolded conformation to a folded stem-loop structure upon target binding. To adapt this aptamer into the EAB platform we modified its 3’ end with a methylene blue redox reporter and its 5’ end with a six-carbon thiol for attachment to an interrogating gold electrode.

The resulting sensor supports the measurement of phenylalanine over the 30 µM to 1 mM physiologically relevant range seen across both healthy humans and those who suffer from phenylketonuria (PKU), an inborn metabolic disorder that leads to excessively high

plasma phenylalanine levels (Blau et al., 2010; Cleary et al., 2013; Waisbren et al., 2007). Specifically, the sensor exhibits both “signal-on” (target binding increases signal) and “signal-off” (binding decreases signal) behavior at higher and lower square wave frequencies (Figures 2a and S1), respectively, with signal gain (relative change in signal upon the addition of saturating target) of +46 ± 1% at 300 Hz and -40 ± 1% at 10 Hz (the “error bars” we report for descriptions of sensor performance reflect standard deviations derived using at least three independently fabricated sensors).

The phenylalanine-detecting sensor achieves clinically relevant specificity and speed. For example, even at the upper ends of their physiologically-relevant concentration ranges the sensor does not detectably respond to the aromatic amino acids tryptophan or tyrosine, or the phenylalanine metabolites phenylpyruvate or phenylacetate (Figure 2B). The sensor is likewise quite rapid; at the few tens of micromolar phenylalanine concentrations seen in the body the sensor equilibrates to bidirectional concentration changes within the 5 s required to collect a single square wave voltammogram (Figure 2C). This is orders of magnitude faster than the time resolution typically associated with measurement approaches that require blood draws, and thus is far faster than any timescales previously reported for phenylalanine metabolism (Cleary et al., 2013).

As is generally true for EAB sensors (Arroyo-Currás et al., 2017; Dauphin-Ducharme et al., 2019; Idili, Arroyo-Currás, et al., 2019), the phenylalanine-detecting sensor is stable and accurate when deployed in undiluted whole blood. A complication in such deployment, however, is that endogenous plasma phenylalanine complicates calibration in this sample matrix. Specifically, because the endogenous concentration of the target (which are

generally between 35 and 85 µM) (Cleary et al., 2013) falls within the sensor's useful dynamic range a complete Langmuir calibration curve cannot be obtained using only blood (Figure S2), which was our prior approach to EAB calibration (Arroyo-Currás et al., 2017; Dauphin-Ducharme et al., 2019; Idili, Arroyo-Currás, et al., 2019). To circumvent this, here we demonstrate the use of a simple, buffered calibration solution that mimics the pH, ionic strength, protein and sugar content of whole blood as a blood dilutant and proxy. That is, we determined the lower-concentration portion of the calibration curve by placing sensors in this buffer and then titrated in whole bovine blood of known (80 µM) phenylalanine concentration until we reached 70% (v/v) blood (corresponding to 56 µM phenylalanine). To determine the higher-concentration portion of the calibration curve we then transferred the sensor into undiluted whole blood (i.e., at 80 µM phenylalanine) and titrated additional phenylalanine until we reached a final concentration of 1 mM. Combining the two data sets we obtain the entire Langmuir isotherm for the sensor, producing affinity and signal gain similar those seen in buffered saline (Figures 3A; see also Figure S3). To determine the device-to-device reproducibility of this calibration approach we used it to calibrate four independently fabricated sensors, obtaining a standard deviation of 8 µM at a target concentration of 45 µM (Figure 3B).

To adapt the phenylalanine-detecting sensor to placement in the living body we fabricated indwelling sensors using 75 µm diameter by 3 mm long gold wire electrodes. We matched these with equal diameter platinum counter and chloride-anodized silver reference electrodes (Figure 1C, left) and encased the bundle in a 22-gauge catheter in which slots were cut to provide blood access (Dauphin-Ducharme et al., 2022). The

resulting devices are small enough to be inserted into the jugular veins of anesthetized Sprague-Dawley (Figure 1C, right). Because rats have four jugular veins (left and right interior and exterior pairs), such placements cause only minor changes to blood flow and likely no changes to molecular physiology. When so deployed, EAB sensors often they exhibit significant baseline drift (see e.g., (Arroyo-Currás et al., 2017; Dauphin-Ducharme et al., 2019; Idili, Arroyo-Currás, et al., 2019)). This is due to the chemical degradation of the aptamer and the self-assembled alkanethiol monolayer over the course of electrochemical interrogation (Shaver et al., 2020). To correct this, here we employed "Kinetic Differential Measurements" (KDM), an approach that exploits the fact that the signal-on and signal-off responses of EAB sensors drift in concert (Figure 4A; see also Figures 3A and S2), such that taking the difference between signals measured at 10 and 300 Hz removes this drift and allows for the accurate determination of target concentration (Arroyo-Currás et al., 2017; Ferguson et al., 2013). These differential measurements, which require performing two sequential square wave scans, can be collected every 12 s, providing effectively continuous, real-time information on plasma target levels.

Indwelling EAB sensors support multi-hour measurement of plasma phenylalanine levels. For example, following a series of increasing intravenous phenylalanine challenges we see concomitantly varying peaks in plasma concentration for which we collect hundreds of measurements during the "decay" phase (Figure 4B). As defined by the standard deviations seen for baseline measurements performed prior to dosing the precision of these in-vivo measurements is between 7 and 15 μM across multiple animals. While these values include true measurement precision (which, as noted above, we estimate to be ~8

μM at these target concentrations), it also includes any physiologically driven fluctuations in phenylalanine levels that may have occurred during the measurements. The specificity of the in-vivo EAB sensor likewise remains excellent: control injections of either saline blanks or doses of the aromatic amino acids tyrosine or tryptophan produce no significant response (Figure 4C).

The few-seconds time resolution of the EAB sensor renders it a novel and powerful tool for the study the disposition kinetics of phenylalanine. To illustrate this, we first measured basal phenylalanine levels in two fasted rats (12 h) for 20 min (see Table 1), obtaining values of 27.9 ± 0.6 and 37.0 ± 1.4 μM (the confidence intervals we report for estimates of phenylalanine concentrations and their kinetic parameters are at the 95% confidence level), values consistent with the results of prior, much more poorly time resolved studies employing ex-vivo measurements (BOURGET & CHANG, 1986; Cheung et al., 2019; DUNLOP et al., 1994; HJELLE et al., 1992; TENGAMNUAY et al., 1991) (Figure S4). We next challenged the rats with 100 mg/kg intravenous boluses of phenylalanine over the course of ~1 min (Figure 5A-B). In response, peak plasma concentrations rapidly reached 87 μM and 131 μM in the two, which was followed by a monotonic return to within 20% of the pre-dosing baseline over the course of approximately 20 min (Table 1).

Although the kinetics of phenylalanine metabolism are modestly complex,[45,46] they are often described using a simple two-compartment model (CAMPISTRON et al., 1982; JAGENBURG et al., 1977):

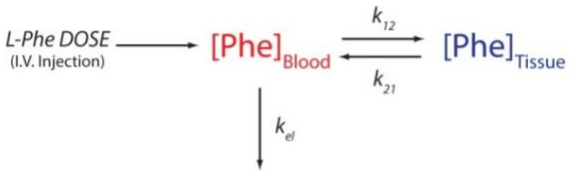


in which $k_{12}$ and $k_{21}$ are the rate constants associated with the transport of phenylalanine into and out of tissue stores and $k_{el}$ is the rate constant for its metabolic degradation. In this model, the time-varying phenylalanine concentration given by the sum of two exponentials:

$$[\text{Phe}]_{\text{Blood}} = Ae^{-\left(\frac{\ln(2)t}{\alpha}\right)} + Be^{-\left(\frac{\ln(2)t}{\beta}\right)} + C$$

where *A* and *B* are the amplitudes of the two phases, *α* and *β* are the half-lives for phenylalanine distribution and elimination, respectively, and *C* is the basal plasma phenylalanine concentration reached after re-equilibration. Fitting our concentration-time profiles to this model, we find that α is 0.4±0.1 min and 0.5±0.2 min and *β* is 8.9±1.8 min and 2.7±0.6 min for the two fasted animals shown (Figure S5; see also Table 1).

The precision with which the large number of measurements we can collect over physiologically relevant timescales *in a single animal* provides an unprecedentedly high-precision window into phenylalanine metabolism. For example, the only prior time-resolved study of phenylalanine disposition kinetics in fasted rats we are aware of collected just 9 samples (for later, ex-vivo analysis) per animal over the course of 2.5 h and then averaged these over multiple animals (Figure S6) (TENGAMNUAY et al., 1991). This was a direct consequence of the study's reliance on blood-draw sampling: the limited blood volume of rats (from 8 to 24 ml) (LEE & BLAUFOX, 1985) restricts the total number of measurements that can be made without unacceptable loss of blood. With so few measurements, this data set cannot meaningfully be fit to the expected two-exponential model (e.g., doing so produces estimates for four of the five parameters that, at the 95% confidence level, overlap with zero). If we instead fit this prior data to a single exponential, which captures only the slower of the two phases, we obtain a half-life of 14±15 min. While the data provided only poorly constrain this value, it is consistent with the slower-phase half-lives we have observed.

The poor fit of the limited prior rat data (TENGAMNUAY et al., 1991) to the two-compartment (dual-exponential) model and its poor ability to constrain even a single-compartment (single-exponential) model stems from three issues that have systematically plagued all prior studies of amino acid disposition kinetics (see e.g., (CHAMI et al., 1978; JAGENBURG et al., 1977, 1977; TESSARI et al., 1994; Tessari et al., 2008; Tugtekin et al., 2002) for studies of phenylalanine disposition kinetics in humans). The first is time resolution that is typically poor relative to the timescales of metabolite disposition. The

earliest samples in the prior rat study (TENGAMNUAY et al., 1991), for example, were collected 6 min after the completion of infusion. This is an order of magnitude slower than the phenylalanine distribution phase we have identified here. A related issue is that, given the noise invariably present in such measurements, dozens or hundreds of measurements are required to constrain multi-exponential models with good statistical significance, and yet prior studies could collect only on the order of a half dozen measurements per subject (CHAMI et al., 1978; JAGENBURG et al., 1977; TENGAMNUAY et al., 1991; Tessari et al., 2008; Tugtekin et al., 2002). Finally, inter-subject differences in physiology likely also contribute to the inability of prior data sets to constrain a two-compartment model. For example, the one prior study of phenylalanine disposition kinetics in the rat (TENGAMNUAY et al., 1991) pooled samples collected from multiple subjects, reducing the validity of disposition/metabolic models. Specifically, the differing half-lives of the same process in different individuals will confound efforts to delineate between the kinetics of two different processes in data that have been averaged over multiple animals.

The hundreds of metabolite level measurements that EAB sensors can provide each for individual animal also provides an unprecedented ability to observe physiological variability between individuals. To illustrate this, we performed phenylalanine challenge experiments on two rats that, in contrast to those employed in the above study, were not food restricted, likely causing their metabolic status to differ (Al Hafid & Christodoulou, 2015; Lutz et al., 2010). Upon intravenous injection of a bolus 100 mg/kg of phenylalanine, the peak plasma concentrations, distribution half-lives and elimination half-lives we determined are similar to those we observed for fasted animals (Figure 5; see also Table 1).

Given that short-term food restriction is not thought to alter the activity or level of phenylalanine hydroylase (CastelS & Shirali, 1971), this is perhaps to be expected. While plasma phenylalanine levels in fasted animals return to close to their pre-challenge baseline values, however, the post-challenge baseline levels seen in freely-fed animals remain elevated by ~50% over the course of our several-hour experiments (Figure 5; see also Table 1). And though it is premature to speculate deeply based on studies performed with just four animals, given the strong statistical significance we observe for these effects in each animal we suspect that this difference is real and arises due to physiological differences between the two sets of animals.

**3.5 Conclusion**

In what we believe is the first seconds-resolved measurements of any endogenous metabolite in vivo using an enzyme-free biosensor, we describe here the real-time monitoring of plasma phenylalanine levels in situ in the veins of live rats with few-micromolar concentration resolution and 12 s temporal resolution. This orders-of-magnitude improved time resolution enables the high-precision determination of physiological phases that are too rapid to capture using traditional approaches. It also produces sufficient numbers and quality of data to characterize the kinetics of individual animals with good statistical significance, thus providing an unprecedented tool with which to study inter-subject disposition kinetics variability.

EAB sensors could also prove valuable in support of personalized medicine. The real-time measurement of phenylalanine, for example, could impact the treatment of PKU, an

important (frequency 1 in 10,000 live births in Europe and 1 in 15,000 in the US) (Blau et al., 2010) inborn metabolic disorder of phenylalanine that is managed via personalized nutritional regimes aimed at maintaining phenylalanine levels above the minimum needed for healthy protein production but below threshold levels that lead to neurotoxicity and mental retardation. Specifically, as a first step EAB sensors would render it possible to estimate the phenylalanine disposition kinetics of individual patients conveniently and with precision. This, in turn, would improve clinical predictions of patient-specific bioavailability and clearance rates of free phenylalanine, improving both diagnosis and treatment (Bik-Multanowski & Pietrzyk, 2011; Kaufman, 1999; Lutz et al., 2010). Looking further forward, the real-time plasma phenylalanine measurements provided by EAB could be used by patients to guide their phenylalanine intake (Al Hafid & Christodoulou, 2015). This might prove of especially significant value in the context of enzyme replacement therapy (Pegvaliase treatment), during which it is currently difficult to ensure that sufficient levels of this critical amino acid are maintained (Blau et al., 2010; Camp et al., 2012; Goldstein & Vockley, 2017). Together, these opportunities suggest that EAB-based metabolic monitoring could significantly impact the quality of life of patients with this common inborn metabolic disorder (Camp et al., 2012; Goldstein & Vockley, 2017; Walter et al., 2002).

Looking beyond phenylalanine and PKU, EAB sensors can be adapted to new targets via the simple expedient of changing their aptamer receptor (see e.g.,(Idili, Gerson, et al., 2019; Idili, Parolo, et al., 2019; Lai et al., 2007; Parolo et al., 2020; Y. Xiao, Lubin, et al., 2005; Y. Xiao, Piorek, et al., 2005)). Given this, we believe the approach may prove of value in the ultra-high-precision determination of disposition kinetics and the real-time

monitoring of a wide range of clinically important metabolites that, currently, can only be measured using blood draws and laboratory analysis.

### 3.6 Figures

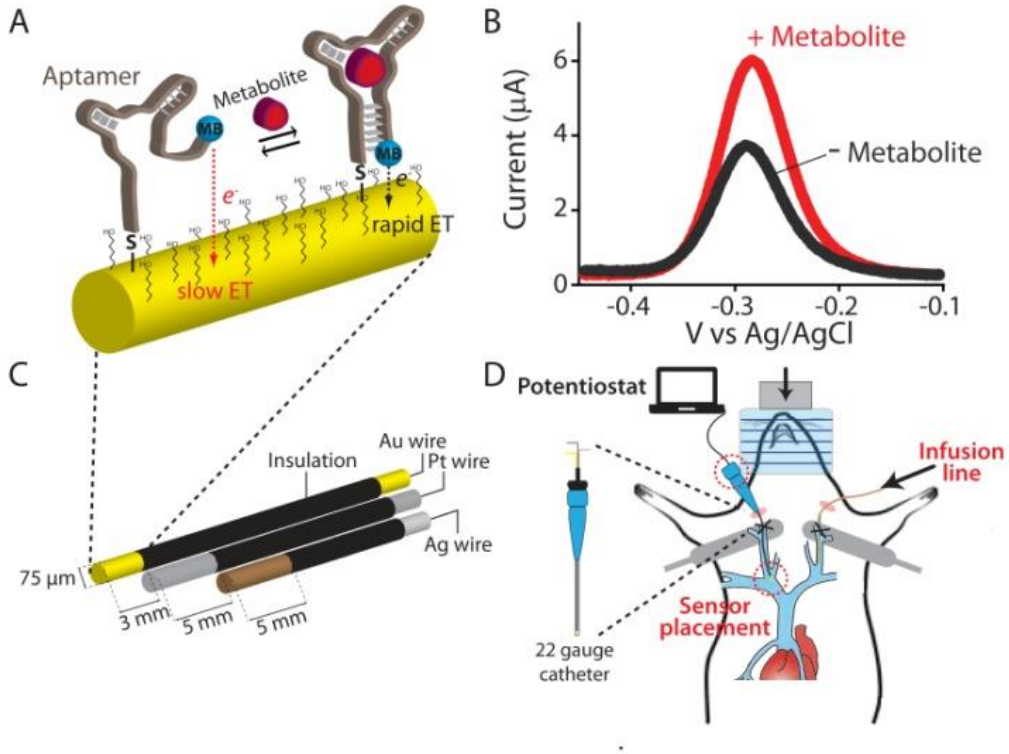


Figure 1. (A) Electrochemical aptamer-based (EAB) sensors exploit the binding-induced folding of a redox-reporter-modified aptamer that is covalently attached to an interrogating electrode via a self-assembled monolayer. (B) Target binding alters the efficiency with which the redox reporter (here methylene blue) approaches the electrode, producing an electrochemical signal easily measured using square wave voltammetry. (C) We fabricate indwelling EAB sensors using a 75 μm-diameter, 3 mm-long gold-wire working electrode bundled with same-diameter platinum counter and silver/silver-chloride reference electrodes. (D) The completed sensor is small enough to be emplaced in the external jugular vein of a rat via a 22-gauge guide catheter.

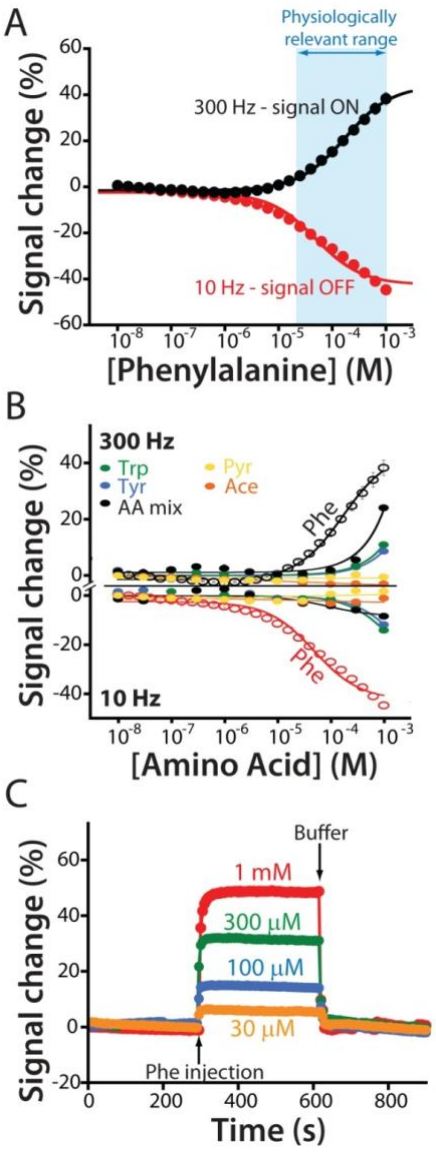


Figure 2. (A) The EAB sensor response to increasing concentrations of phenylalanine produces the expected Langmuir binding curve. As is common for sensors in this class, the device's response is signal on at higher square wave frequencies and signal-off at lower frequencies. The physiologically relevant range of plasma phenylalanine levels in healthy individuals and individuals suffering from PKU is shown in blue.[29-31] (B) To show that the sensor achieves clinically relevant specificity we challenged it with tryptophan (trp), tyrosine (tyr), a mixture of the amino acids glutamine, histidine, proline, arginine, and alanine (AA mix), and the phenylalanine metabolites phenylpyruvate (Pyr) and phenylacetate (Ace). Using the same frequencies as in (A), the sensor does not measurably respond to any of these at concentrations below 300 µM, a level far above those seen physiologically. (C) Finally, the sensor is rapid, responding in just a few seconds to the addition of physiologically relevant target concentrations.

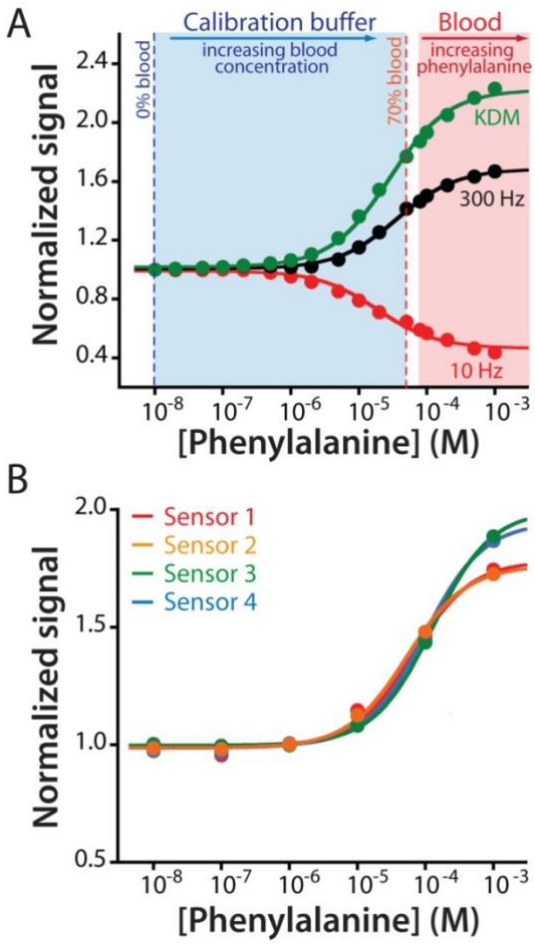


Figure 3. The adaptation of EAB sensors to the measurement of an endogenous component of blood required the development of a new calibration approach suitable for use with endogenous targets (i.e., for which target-free blood is not available). (A) For this we employed a calibration buffer comprised of Ringer's solution and bovine serum albumin (35 mg/mL) that mimics the pH, ionic strength, protein, and sugar content of whole blood. We determined the lower portion of the calibration curve by titrating whole bovine blood of known phenylalanine concentration (80 µM) into this buffer to a final concentration of 70% blood (56 µM). To determine the upper portion of the curve we then moved the sensor into undiluted whole blood (at 80 µM phenylalanine) and adding exogenous phenylalanine until we reached a final concentration of 1 mM. Merging the data sets we can obtain the entire Langmuir isotherm, which produces dissociation constants and signal gains similar those seen in phosphate buffered saline (Figures 3A; see also Figure S3). (B) Using this approach to calibrate EAB sensors prior to deployment in vivo we observe good reproducibility between individually fabricated devices. The mean and standard deviation of the concentration estimates associated with a signal increase of 30% are 45.1 µM and 7.8 µM, respectively

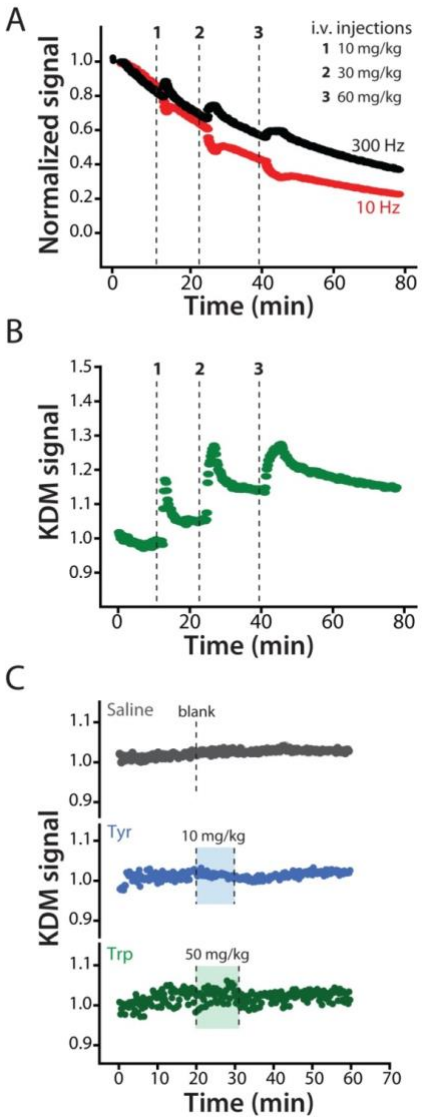


Figure 4. When placed in situ in the body EAB sensors drift (Arroyo-Currás et al., 2017; Dauphin-Ducharme et al., 2019; Idili, Arroyo-Currás, et al., 2019). To correct this, we employed kinetic differential measurements (KDM) (Arroyo-Currás et al., 2017; Ferguson et al., 2013). (A) Normalized signals collected at 300 Hz (black) and 10 Hz (red) square-wave frequencies drift in concert, such that taking their difference via KDM eliminates the drift. (B) Using KDM we can easily see the results of serial increasing intravenous injections of phenylalanine in an anesthetized rat. The 12 s time resolution achieved in these measurements is sufficient to monitor both the injection itself and the subsequent distribution of the metabolite within the body. This reflects a 30-fold improvement over the time resolution of the best prior studies of phenylalanine metabolism kinetics in either rats or humans (CHAMI et al., 1978; JAGENBURG et al., 1977; TENGAMNUAY et al., 1991; TESSARI et al., 1994; Tessari et al., 2008; Tugtekin et al., 2002). (C) As expected, the in-vivo sensor does not respond to intravenous injections of either a saline “blank” or the aromatic amino acids tyrosine or tryptophan at the indicated dosages.

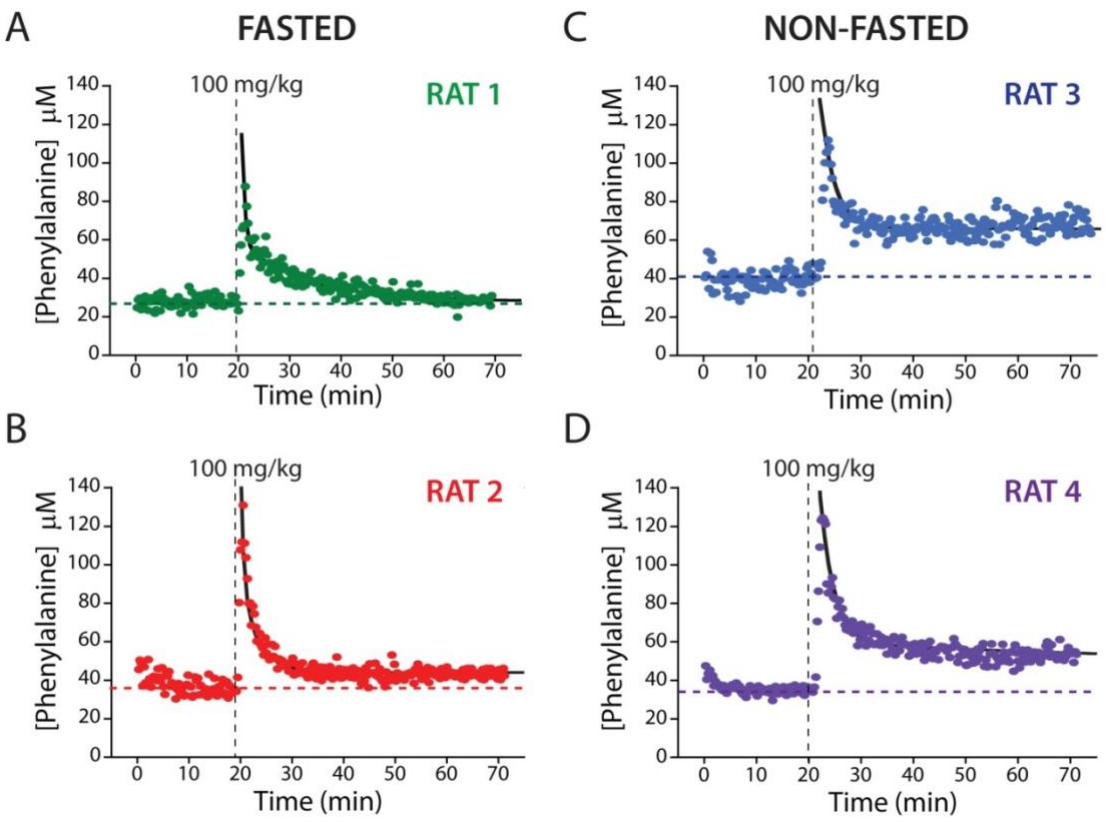


Figure 5. EAB sensors provide an unprecedentedly high-precision view into metabolism and inter-subject metabolic variability. Shown, for example, are plasma phenylalanine levels after a single, 100 mg/kg intravenous injections into four live rats, two of which were fasted for 12 h (A, B) and two of which had free access to food (C, D). These high-precision measurements reveal similar peak concentrations, distribution rates, and elimination rates for all four animals. For the two fasted animals, plasma phenylalanine levels returned to within 20% of the pre-dosing baseline over the course of approximately 20 min. In contrast to the situation with fasted animals, however, the plasma phenylalanine levels in these animals remain elevated by ~50% above pre-challenge baseline levels over the course of our experiments. The black lines represent the fit of each injection dataset to a two-compartment pharmacokinetic model (Eq. 1).

| **Animal** | **Fasted** | **Pre-bolus baseline** (μM)[a] | **Post-bolus baseline** (μM)[b] | **A** (μM)[b] | **α** half life (min)[b] | **B** (μM)[b] | **β** half life (min)[b] | **$R^2$** | **$C_{MAX}$** (μM) |
|---|---|---|---|---|---|---|---|---|---|
| RAT 1 | Yes | 27.9±0.6 | 28.4±1.4 | 53±16 | 0.4±0.1 | 29 ±3 | 8.9±1.8 | 0.898 | 87 |
| RAT 2 | Yes | 37.0±1.4 | 43.3±0.6 | 68±13 | 0.5±0.2 | 43±13 | 2.7±0.6 | 0.944 | 131 |
| RAT 3 | No | 40.8±1.6 | 66.9±0.8 | 34±16 | 0.5±0.4 | 16.2±16.4 | 2.7±2.4 | 0.755 | 112 |
| RAT 4 | No | 34.5±0.9 | 52.5±1.3 | 63±11 | 1.1±0.4 | 26±11 | 6.6±3.0 | 0.916 | 124 |
| Ref. [21][c] | Yes | 72±22 | 109±13 | NA | NA | 72±34 | 14±15 | 0.831 | 154±32 |

[a] The error bars reported here are 95% confidence intervals derived from standard deviations. [b] The error bars reported here are 95% confidence intervals based on estimated standard errors of the fits. [c] Values obtained using a single exponential fit.

Table 1. Kinetic parameters corresponding to a single i.v. injection of phenylalanine in four Sprague– Dawley rats

# Chapter 4

## A high-precision view of intercompartmental drug transport via simultaneous, seconds-resolved measurements in situ in the vein and brain

## 4.1 Abstract

The ability to measure specific molecules at multiple sites within the body simultaneously and with seconds time resolution could greatly advance our understanding of drug transport, metabolism, and elimination. As a proof-of-principle demonstration of this, here we describe the use of electrochemical aptamer-based (EAB) sensors to measure transport of the antibiotic vancomycin from the plasma (in the jugular) to the cerebrospinal fluid (in the lateral ventricle) of live rats with few seconds temporal resolution. In our first effort we made measurements solely in the ventricles of awake ambulatory animals. Doing so we find that, although the collection of hundreds of concentration values over a single drug lifetime enables high-precision estimates of the parameters describing intracranial transport, due to a mathematical equivalence the data produce two divergent descriptions of the drug's pharmacokinetics that fit the data equally well. The simultaneous collection of intravenous measurements, however, resolves this ambiguity, enabling high-precision (±5 to ±20% at the 95% confidence level) estimates of the key pharmacokinetic parameters describing transport from the blood to the cerebrospinal fluid in individual animals. The availability of such simultaneous, high-density "in-vein" (plasma) and "in-brain" (cerebrospinal fluid) measurements also provides an opportunity to explore the assumptions almost universally employed in prior compartmental models of drug transport, allowing us to quantitatively address (rather than simply assume), for example, whether the targeted drug is subject to bulk transport out of the central nervous system via the lymphatic system.

## 4.2 Introduction

The ability to measure specific molecules a high temporal resolution and at multiple sites within the body simultaneously could significantly impact both scientific research and clinical practice. Such an ability could, for example, vastly improve our understanding of the blood-brain and blood-cerebral spinal fluid barriers that protect the central nervous system by regulating the transfer of molecules to and from these central compartments. This, in turn, could lead to new therapies as these barriers often limit the transport of drugs into the brain, creating enormous obstacles for the pharmacological treatment of diseases of the central nervous system. However, while the *in vitro* characterization of the blood-brain and blood-cerebral spinal fluid barriers have seen significant recent progress in generating translational organoids (Cakir et al., 2019) or even "barrier-on-a-chip" devices (Motallebnejad et al., 2019; T.-E. Park et al., 2019; Vatine et al., 2019), the precision with which we can measure transport across them in live animals has historically been poor. As a result, serious limitations remain regarding our understanding of molecular transport from circulation into the central nervous system and, more generally, between any two body compartments.

Conventional approaches (Cornford et al., 1992; Uitert et al., 1981; Zlokovic et al., 1986) to measuring molecular transport between bodily compartments are limited on many axes. The earliest pharmacokinetic methods, for example, utilized systemic injections of radiolabeled drugs followed by sacrificing the animal, thus allowing only a single time point per subject with enormous limitations for accurately tracking molecular concentrations over

time with any real precision and an inability to investigate single-subject pharmacokinetics. More recent studies, in contrast, have employed microdialysis to collect multiple, time-stamped samples (EC et al., 1999) for after-the-fact, bench-top analysis. The time resolution of this approach, however, is generally poor: with only rare, far-from-turn-key exceptions (Kennedy et al., 2002; Lada et al., 1997; Quintero et al., 2007; M. Wang et al., 2011), microdialysis typically employs tens of minute collection times (H. Yang et al., 2013). More recently, non-invasive imaging techniques such as PET and NMR have been introduced into. Use of the former, however, has been limited by its need to rapidly radiolabel the compound of interest with (invariably short-lived) positron-emitting radionucleotides (Elsinga et al., 2004; Miranda, 2019). MRI (R. Wang et al., 2007) likewise suffers from a lack of sensitivity, limiting the range of molecules it can detect (Brunner & Langer, 2006). Finally, PET and, to a lesser extent NMR, have difficulty distinguishing between the target of interest and its metabolites, and are limited by high cost, significant technical complexity (Nicolazzo et al., 2006; Yuan et al., 2009), and poor absolute quantativity.

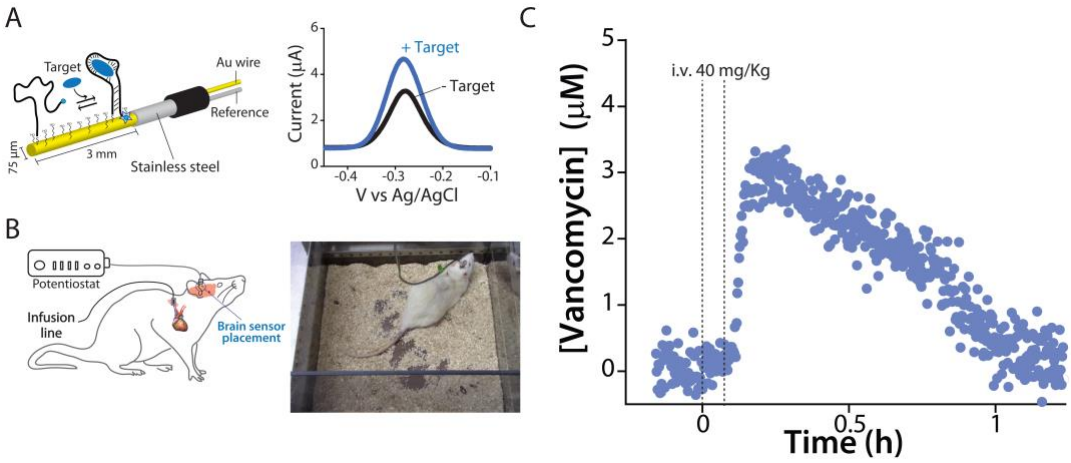


**Figure 1. Cartoon image of in brain E-AB biosensors function, platform and *in-vivo* implementation along with awake, ambulatory measurement of vancomycin.**

**A)** The specialized platform developed for in-brain detection. The setup utilizes a two-electrode system of a gold working electrode and stainless-steel pseudo counter/reference electrode. Aptamers are attached via a 3' thiol group to the gold working electrode. Electrochemical aptamer-based (E-AB) sensors generate a detectable electrochemical signal via a binding-induced conformational change in a redox-reporter-modified (methylene blue), electrode-bound aptamer. In the absence of the target, the aptamer is relatively unfolded and extended. Target binding induces a conformational change, leading in turn to a change in the electron transfer rate of the methylene blue reporter which increases the electrochemical signal in a manner quantitatively related to the concentration of target in the solution. **B)** Cartoon and live image of experimental setup for awake measurements. An infusion line is attached to a chronic, indwelling catheter for drug infusion. The E-AB sensor is inserted through a 19G cannula and is attached to a potentiostat while real-time concentration levels can be visualized on a computer screen. **C)** Real time output of the sensor *in-vivo* following a 40 mg/kg IV dose of vancomycin. The platform is capable of tracking, in real-time, the levels of vancomycin present in the CSF by translating the current output of the sensor into concentration using the *in-vitro* calibration curve in CSF.

In response to the limitations of existing methods for measuring molecular disposition kinetics in the living body, we describe here a novel approach based on electrochemical aptamer-based (EAB) sensors, an in-vivo molecular measurement platform that achieves low-seconds time resolution and that, because it is independent of the chemical reactivity of its targets, is generalizable to targets across a broad range of molecular classes [23]. EAB sensors are comprised of a target-recognizing aptamer re-engineered to undergo binding-induced folding. This is modified with a redox reporter (here methylene blue) and site-specifically attached to a 75 mm diameter, 3 mm long gold electrode (Fig. 1A). When interrogated electrochemically (e.g., via square wave voltammetry (White & Plaxco, 2010), the resulting signal (Fig. 1B) is monotonically and reversibly related to the concentration of the sensor's target, providing a means of monitoring rising and falling molecular concentrations in vivo. Using this approach, we have previously used EAB sensors to perform real-time measurements of plasma drug and metabolite levels in situ in the veins of live rats (Arroyo-Currás et al., 2017; Dauphin-Ducharme et al., 2019; Idili, Arroyo-Currás, et al., 2019; Idili et al., 2021). Building on this, here we have adapted the EAB platform to the problem of performing *simultaneous* measurements in the cerebrospinal fluid (CSF) of the lateral ventricle and the venous blood of the jugular vein. The resulting measurements provide an unprecedented, high-precision picture of intercompartmental molecular transport that allows for the quantitative testing of several of the long-standing assumptions traditionally employed multi-compartment pharmacokinetic models.

**4.3 Methods**

*Reagents and Materials for sensor fabrication and testing*

All materials purchased were used as received. Sodium phosphate monobasic, sodium chloride, sodium hydroxide, potassium chloride and potassium phosphate dibasic were acquired from Fischer Scientific (Waltham, MA). 6-mercapto-1-hexanol, phosphate buffered saline (1X PBS, pH = 7.4) and tris(2-carboxyethyl)phosphine hydrochloride (TCEP) were obtained from Sigma Aldrich (St. Louis, MO). Sulfuric acid was obtained from EMD (Burlington, MA) and vancomycin hydrochloride (USP grade) was purchased from Gold BioTechnology, Inc. (St. Louis, MO).

Bovine cerebral spinal fluid (CSF) was purchased from BioIVT. Catheters (22G) and 1 mL syringes were acquired from Becton Dickinson (Franklin Lakes, NJ). Channel connector cables for in vivo probe fabrication were obtained from PlasticsOne (Roanoke, VA). Polytetrafluoroethylene (PTFE) insulated gold, platinum and silver wires (75 µm diameter, 64 µm insulation thickness) were purchased from A-M Systems (Sequim, WA) and were further insulated using a heat-shrink PTFE insulation (PTFE, HS Sub-Lite-Wall, 0.02 in, black-opaque, Lot #17747112-3) from ZEUS (Branchburg Township, CA). We also acquired fritted Ag|AgCl reference and platinum counter electrodes from CH Instruments (Austin, TX) and used those in a three-electrode setup.

*In vein electrode fabrication and electrochemical cleaning*

7.75 cm segments of gold, platinum, and silver wires were cut and a number 11 scalpel was used to remove the insulating coating from either end. Wires were then

assembled together with heat shrinking PTFE tubing using a heat gun. 5mm of exposed wire was left at the end where aptamer was to be deposited. Wires were staggered with a physical gap between each to avoid shorts. Lastly, the gold wire was trimmed to a final length of 3mm.

Electrode assembly was followed by implementation of our established E-AB sensor functionalization protocol (Arroyo-Currás et al., 2017). In summary the electrode is electrochemically cleaned by cycling the potential 300 times between -1 and -1.6 V in a solution of 0.5 M NaOH at 1 $Vs^{-1}$ to remove any potential contaminants from the electrodes surface. This is immediately followed by electrochemical roughening to increase the surface area of the gold electrode in order to allow more of the aptamer to deposit on the surface and ultimately increase the baseline current output of the sensor. This is achieved by pulsing between 0 and 2 V for 16,000 cycles with a pulse length of 0.02 s in 0.5 M H2SO4. Finally, the clean, pulsed electrodes are functionalized with the aptamer. A DNA stock solution (2 µL of 100 µM) of the desired construct was reduced using a 1000x molar excess of aqueous TCEP solution (10 mM) at room temperature and in the dark for 1h. Concentration of the reduced DNA was then altered to 500 nM (diluting in 1X PBS) based on its UV-VIS adsorption at 260 nm.

To deposit the aptamer, the gold wire portion of the probe was submerged in this solution for 1h at room temperature. Following this, the gold wire is rinsed in 1X PBS and only the gold wire submerged in 10 mM 6-mercapto-1- hexanethiol overnight. In order to

generate the Ag|Cl reference electrode, the silver wire was immersed, separately, overnight in a concentrated hypochlorite solution.

*In brain electrode fabrication and electrochemical cleaning*

In order to adapt the previously reported E-AB sensor platform to make in brain measurements our group designed a custom intracranial system that was then fabricated externally (Plastics1, Roanoke, VA). The in-brain probes consist of two crucial elements, a two-electrode gold/stainless steel in brain probe (Insert Fig), and an electrode leash (insert Fig) to facilitate connection to a potentiostat. For the in-brain probe, the gold wire serves as the working electrode and the stainless-steel portion of the probe serves as a pseudo counter/reference. The in-brain probe has two pin ports (one for the working and one for the counter/reference electrode) for connection to the electrode leash. The electrode leash is 50 cm long and consists of two copper wires encased in a protective, braided stainless-steel mesh leash. Each end of the wire has two copper pins (1 mm apart), for connection to the probe and to the potentiostat, and a plastic casing and screw collar to secure the leash in place. The electrochemical cleaning parameters for the in-brain probes were identical to those for the in-vein E-AB sensors reported above. Following cleaning, the aptamer was deposited onto the gold working electrode surface by immersing it in a 500 nM solution of the reduced DNA aptamer solution for 1h at room temperature and then in a 10 mM 6-mercapto-1- hexanethiol overnight.

*Sensor construct.*

SH-$(CH2)_6$ - CGAGG GTACC GCAAT AGTAC TTATT GTTCG CCTAT TGTGG GTCGG - O-CH2-CHCH2OH-(CH2)4-NH-CO-(CH2)2-MB). Where MB represents Methylene Blue.

*In vitro sensor characterization*

Characterization and optimization of the E-AB sensor in whole blood has been previously reported by our group (Dauphin-Ducharme et al., 2019) and the parameters were unchanged for all of the experiments performed in this paper. In brain sensors were submerged in bovine cerebral spinal fluid (CSF) and known quantities of vancomycin (also dissolved in CSF) were titrated in to generate a full binding curve (insert figure). This binding curve serves as a calibration curve from which we are able to estimate the concentration of vancomycin directly in vivo and also to generate the KD value, observed signal gain and $\gamma$.

*Animal Housing and Care*

Sprague-Dawley rats weighing 300-500g were pair-housed in a standard light cycle room (8:00 on, 20:00 off). All animals had ad-libitum access to food and water throughout the duration of the study. Guidelines imposed by the "Guide for the Care and Use of Laboratory Rats, 8$^{th}$ edition" were adhered to for the duration of the study. Furthermore, all experimental protocol was approved by the Institutional Animal Care and Use Committee (IACUC) of the University of California at Santa Barbara.

*Surgical procedure parameters*

Anesthesia was induced prior to surgery by administering 4% isoflurane gas (Medline, Northfield, IL) and was maintained with 2-3% for the rest of surgery. During surgical

procedures temperature, heart rate, SPO2 (specific peripheral oxygen concentration), and breathing rate were monitored, recorded, and kept within the veterinary recommended boundaries.

*Intracranial surgical procedure*

After inducing anesthesia, the rat's heads were shaved above the skull. Rats were then mounted in a Stoelting stereotaxic apparatus equipped with a nose cone for isofluorane delivery in order to maintain anesthesia. The shaved area was then disinfected by rotating 10% betadine and 70% isopropanol solutions, applied using sterile cotton gauze, three times. To prevent desiccation of the eyes, we applied proparacaine hydrochloride ophthalmic solution (0.5%, Henry Schein Veterinary, Dublin, OH). An incision was then made on the skin above the skull at 1 mm anterior to the eyes to 1 mm posterior to the ears. To expose the skull the fascia was scraped and held in place using bulldog clips. The surface of the skull was cleaned of blood and dried using sterile cotton swabs and bregma was marked. To target the lateral ventricle, we drilled a hole in the skull utilizing a microdrill (Braintree Scientific, Braintree, MA) fitted with a 1.4 mm micro-burr drill bit at the coordinates AP: Bregma – 0.50 mm; ML: Bregma + 1.25 mm. To provide structural support for the head cap bone screws were inserted into four holes drilled using a 0.9 mm microburr drill bit in the four corners of the skull. An 18-gauge, 14 mm long cannula was lowered DV: Bregma – 1mm ventral. To make the head cap, methyl methacrylate dental cement was mixed into Teets cold cure liquid (Pearson Dental Supply, Sylmar, CA) and applied to the surface of the skull with a stainless-steel spatula. The rat was then removed from the stereotax following the cement drying and a 22-gauge stainless steel obdurator was inserted into the cannula. Rats were

given subcutaneous Buprenorphine injections (0.05 mg/kg) and then placed on a heating pad to recover from anesthesia. Intracranial cannula were emplaced at least 7 days prior to performing sensor recordings in order to minimize potential tissue trauma at the time of drug measurement.

*Drift correction*

To correct for the drift inevitably seen in in-vivo placements we used sequential measurements performed at 25 and 300 Hz to achieve "kinetic differential measurement" drift correction (KDM). To convert KDM signals into drug concentrations we fit the in-vitro titration data to the equation: $y = B_{MAX} \times \frac{[target]}{K_D + [target]}$, where y is the KDM signal, $B_{MAX}$ is the signal change seen at saturating target concentrations, [target] is drug concentration, and $K_D$ is the dissociation constant of the aptamer.

*In vivo testing and animal procedures (two-compartment)*

For in vein measurements, the three electrode sensors were sheathed in a protective 22G catheter and implanted into the right jugular vein as previously reported (Dauphin-Ducharme et al., 2019). After inducing anesthesia, the area of skin on the chest above the jugular veins was shaved and sterilized with 10% betadine and 70% isopropanol solutions. A small incision in the skin was made above each jugular vein and the jugular veins were both isolated using sharp surgical scissors, #7 Dumont forceps, and a stainless-steel spatula. A small, lateral, incision was then made in each jugular vein into which the silastic catheter (left vein) and E-AB sensor (right vein) were inserted rostrally. Both veins were then secured and tied off using sterile 6-0 silk suture (Fine Science Tools, Foster City, CA). An infusion line

was then connected to the top of the catheter for vancomycin delivery as has been previously described. Silastic catheters were constructed in house using a bent steel cannula with a screw-type connector (Plastics One, Roanoke, VA) and silastic tubing (11 cm, 0.64 mm, i.d. 1.19 mm o.d, Dow Corning, Midland, MI).

In order to insert the in-brain E-AB sensor, the rats were then, delicately flipped onto their dorsal side and the in-brain probe was passed inserted through the chronic, stainless-steel cannula and screwed into place. 30 units of heparin were administered prior to commencing recordings and minimal 20-minute baseline of the sensor was recorded prior to drug infusion. Sensor output and response was visualized in real-time using a python program developed by our group and previously reported (cite SAM). In short, this program allows extraction of peak current in real-time and directly derives the kinetic differential measurement required for monitoring vancomycin directly in vivo.

*Model Selection Metrics*

We provide two metrics in tables showing our results. The first one is the Bayesian Information Criterion (BIC). This criterion is obtained by adding two distinct terms together, one measuring how well the data fit is, and an additive cost punishing additional model complexities (Schwarz, 1978). Therefore, BIC is not a measure of wellness of data fit but, rather, it is a metric to determine the best model among a given family of models. The smallest BIC is the one favored the most for this criterion, but as a rule of thumb, a difference below 2 between two models means that they are indistinguishable by BIC (Fabozzi, 2014).

The other metric we calculate to help us understand the model-fits better is Root Mean Square (RMS) values for the residual deviations of the data from the given fit. This metric is a measure of how well the data fit is for the estimated model. It corresponds to the sample standard deviation of the residuals and, therefore, a smaller value indicates a better fit. We provide RMS values for both measurements given the model-fit we have.

**4.4 Results**

As our test bed we have employed studies of the transport of vancomycin from the blood into the ventricular CSF (Beach et al., 2017). We have done so by building on our previous demonstration of intravenous sensors for the antibiotic (Dauphin-Ducharme et al., 2019), which we have adapted here to the goal of also performing seconds-resolved intracranial measurements (Fig. 1). For this we employed an intracranial probe directed to the lateral ventricle (Fig 1C). This consists of a two-electrode set up employing a stainless-steel counter/pseudo-reference electrode and a gold working electrode on which the aptamer is deposited (Fig. 1A). For measurements performed only in the ventricles we employed awake animals (Fig. 1D). To perform simultaneous measurements in the ventricle and the jugular vein we employed anesthetized animals.

Upon bolus intravenous vancomycin challenge, vancomycin levels in the lateral ventricle of an awake animal exhibit biphasic kinetics in which drug levels rapidly rise before then slowly falling (Fig. 2A). For example, when we dosed an awake, ambulatory rat at 40 mg/kg (delivered over 89 s) via intravenous infusion, the drug was first detectable (defined as the first measurement after which the concentration consistently remained more than 2-

standard deviations above zero) in the CSF 1.1 min after the initiation of this infusion, after which it rose to peak concentrations of about 20 μM over the course of 9.8 min before then falling again towards zero.

The disposition of drugs within the body is often approximated using compartment models in which the body is approximated as a series of discrete, homogeneous compartments, which can be thought of as groups of different tissues/organs with similar drug penetration. The few-second (here 11.1 s) time resolution of EAB measurements renders it possible to collect hundreds of data points in a single animal over the pharmacokinetic lifetime of a single drug challenge. This, in turn, provides an opportunity to constrain compartmental models of drug disposition kinetics with unprecedented precision. In the simplest of these, the one-compartment model, the drug is assumed to equilibrate instantaneously between the blood and the solid tissues, and to be eliminated from this equilibrating pool via single exponential kinetics driven by metabolism or excretion. Given that we are performing simultaneous dual-compartment measurements, this model is presumably too simplistic to account for our observations. Thus, here we explore two- and three-compartment models in which, in addition to the "central" compartment (i.e., the blood plus any solid tissues that rapidly equilibrate with it) we model the brain and the rest of the body (tissues that equilibrate slowly relative to the rate of elimination of the drug from the body) as two additional compartments, maintaining the assumption that transport between the latter two compartments occurs only via their respective equilibration with the blood.

The amount of drug transported from one compartment to another per unit time is proportional to the difference in the drug concentrations, $C_i$, found in the two compartments with the proportionality constant being a rate constant of units L/min. This rate constant, which is called the clearance rate, is denoted by $CL$ with subscripts describing between which compartments the transfer is occurring.

$$\frac{dD_0(t)}{dt} = \sum_{i=1}^{m} CL_{i0}\big(C_i(t) - C_0(t)\big) - CL_{E_0}C_0(t) + u(t) \tag{1}$$

Here $\frac{dD_0(t)}{dt}$ denotes the change in the amount of drug in compartment 0 (the central compartment) in mol/min, as a function of the differences in concentration between that compartment and neighboring compartments, $C_i(t) - C_0(t)$, in mol/L; $CL_{i0}$ the clearance rate constant in L/min for transport between compartments 0 and $i$; $CL_{E_0}$ the clearance rate constant in L/min with which the drug is excreted or otherwise removed from the body via compartment 0; and $u(t)$, the rate with which the drug is originally delivered to compartment 0 by injection in mol/min.

Measurements of drug concentration alone will not uniquely define the coefficients in equation (1). This is because the left-hand side of the equation, $\frac{dD_0(t)}{dt}$, has units of mol/min, not mol/L/min, and thus relating it to concentrations requires knowledge of the distribution volume (the effective volume) of compartment 0, $V_{Dis_0}$, in liters. Given this, we prefer to work with equations employing solely concentrations. We achieve this by normalizing the equation by the distribution volume.

$$\frac{dC_0(t)}{dt} = \sum_{i=1}^{m} \frac{CL_{i0}}{V_{Dis_0}} \left( C_{D_i}(t) - C_0(t) \right) - \frac{CL_{E_0}}{V_{Dis_0}} C_0(t) + \frac{1}{V_{Dis_0}} u(t)$$

(2)

$$= \sum_{i=1}^{m} k_{i_0} \left( C_i(t) - C_0(t) \right) - k_{E_0} C_0(t) + \frac{1}{V_{Dis_0}} u(t)$$

Note that the clearance rates, $CL_{i0}$, in equation (1) were reciprocal, in other words, the same rate would determine the change in the amount of drug both in compartment $0$ and compartment $i$, only the directions would have been different. We lose this symmetry, however, when we convert to the rate constants, $k_{i_0}$, used in equation (2), which are in units of $min^{-1}$. That is, while the rate of change of the absolute amount of the drug (in mol/min) in a compartment does not depend on the distribution volume contained within the compartment, the rate of change of the concentration of the drug (in mol/L/min) does depend on this volume.

We start by defining dynamical equations on the two compartments of primary interest to us: the "brain" (i.e., the CSF of the ventricles) and the "vein" (i.e., the blood in the circulatory system plus the interstitial fluid in any rapidly perfusing tissues), which is consistent with the way vancomycin pharmacokinetics have historically been modeled in the literature (Matzke et al., 1986).

$$\frac{dC_V(t)}{dt} = \frac{1}{V_{Dis}} u(t) + \mathrm{k_{B_V}} \left( C_B(t) - C_V(t) \right) - k_{E_V} \mathrm{C_V}(t) \quad (3)$$

$$\frac{dC_B(t)}{dt} = k_{V_B}\big(C_V(t) - C_B(t)\big) - k_{E_B}C_B(t) \quad (4)$$

where $V_{Dis}$ is the distribution volume associated with the vein (in L), $u(t)$ is the (experimentally-defined) rate with which the drug is injected into the vein (mol/min), $C_B(t)$ and $C_V(t)$ are the time-varying concentrations (in mol/L) of the drug in the brain (in the CSF) and in the vein (in plasma), $k_{B_V}$ is the rate constant for transport from the brain into the vein, $k_{V_B}$ is the rate constant of transport from the vein into the brain, $k_{E_V}$ is the rate constant for elimination of the drug from the body via the veins (i.e., here via renal excretion), and $k_{E_B}$ is the rate constant for degradation of the drug (if any) in the brain, with all of the rate constants having units of $min^{-1}$.

Typical pharmacokinetic measurements are insufficient to constrain (i.e., uniquely identify) assumption-free pharmacokinetic models. For example, a fundamental problem of observing only in the compartment that is not receiving the initial injection (here the brain) to estimate the rate constants in the two-compartment model (Eq. 3, 4) is that, given only the measurements, $C_B(t)$, and the experimentally defined injection rate, $u(t)$, the model allows for only 3 parameters to be estimated (see proof in SI). Equations 3 and 4, however, include many more than 3 parameters and thus, in order to fit data collected only in the brain to a multi-compartment model (i.e., to fit $C_B(t)$ while simultaneously estimating $C_V(t)$ we must apply some simplifying assumptions. As our initial approach, we have employed two such assumptions, both of which have seen near universal employment in the prior

literature, before exploring each the assumptions (and a third assumption) later in this paper.

**Assumption 1.** The rate constant for elimination within the brain, $k_{E_B}$, is zero. That is, drug is only removed from the brain via passive diffusion into the blood.

**Assumption 2.** The volume of the vein compartment (which is defined here as the circulatory system plus any rapidly perfusing tissues) is so dominant that the transport of drug to or from any other tissue (including the brain) has a negligible impact on the concentration in the vein.

The first assumption can be justified by noting that vancomycin is excreted unmetabolized via the kidneys and is not known to undergo biotransformation in brain tissue (Matzke et al., 1986). Our second assumption implies that the time-varying concentration of vancomycin in the blood can be approximated as a single-exponential process. This is equivalent to assuming that drug transport into most tissues is rapid, and that the total distribution volume of any tissues for which such transport is slow (e.g., the brain) is small such that their contributions to drug distribution can be neglected. With these assumptions in place, equations 3 and 4 are transformed into:

$$\frac{dC_V(t)}{dt} = \frac{1}{V_{Dis}} u(\mathrm{t}) - k_{E_V} C_V(t) \tag{5}$$

$$\frac{dC_B(t)}{dt} = k_{V_B}\big(C_V(t) - C_B(t)\big) \tag{6}$$

Together these equations include only 3 parameters, and thus it is possible to constrain them using observations limited to measurements performed in a single compartment.

**Table 1. parameters derived using only in-brain data**

| Parameters | Solution 1 | Solution 2 |
|---|---|---|
| $V_{Dis}$ (L) | $0.53^{+0.02}_{-0.03}$ | $0.07 \pm 0.01$ |
| $k_{E_V}$ (min$^{-1}$) | 0.030±0.002 | $0.24^{+0.03}_{-0.04}$ |
| $k_{V_B}$ (min$^{-1}$) | $0.24^{+0.03}_{-0.04}$ | 0.030±0.002 |
| rms residuals (mM) | 2.14 | 2.14 |

Error bars are 95% confidence intervals derived analytically.

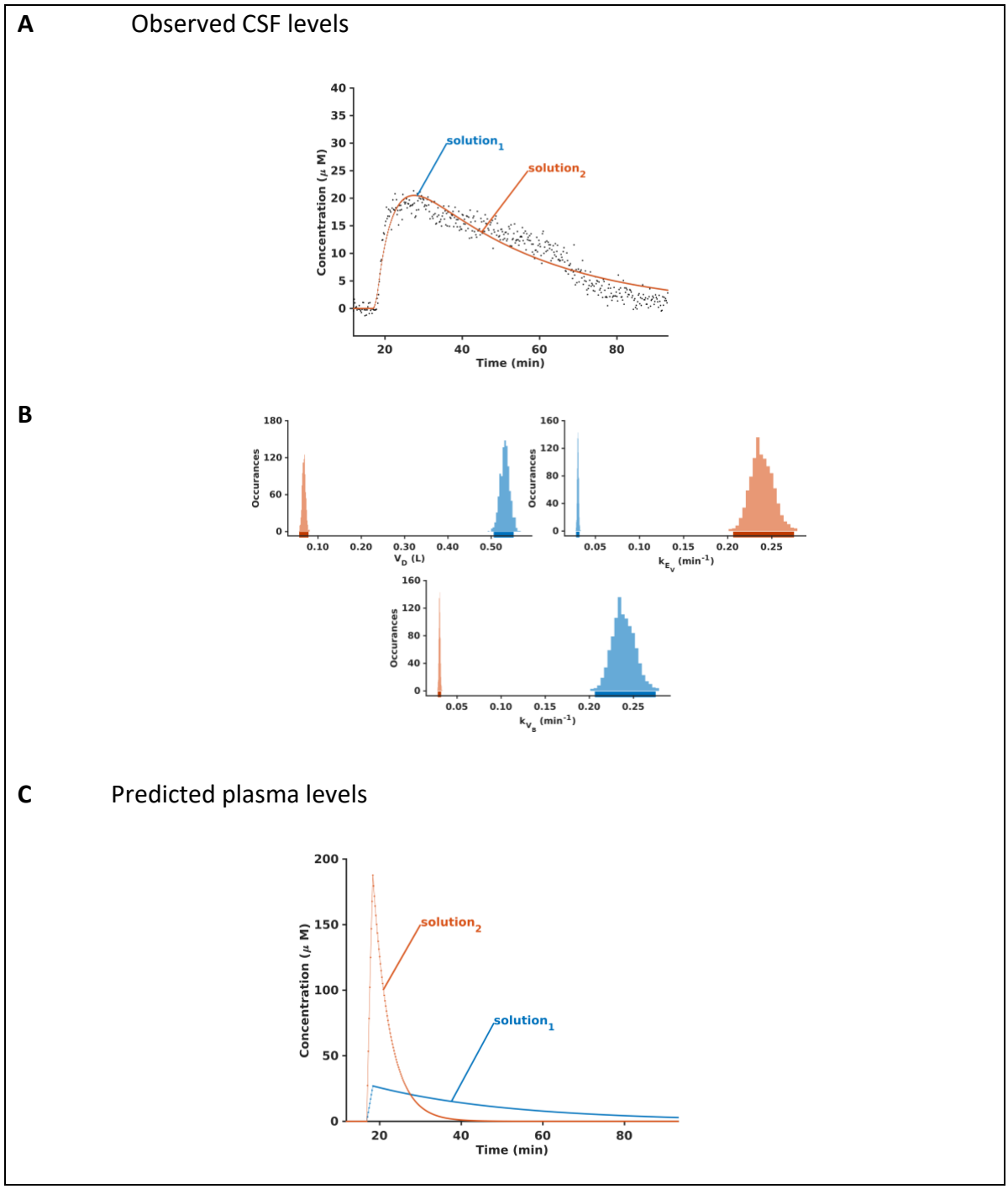


**Figure 2**. (**A**) Intraventricular vancomycin levels after the indicated intravenous dosing of the drug exhibit a biphasic rise and fall that are well-fitted to a simple, two-compartment model. Fitting only in-brain data to this model, however, suffers from a significant ambiguity: due to the model's inability to distinguish between effects driven by the rate constant for transfer into and out of the brain, $k_{V_B}$, and those driven by the rate constant for elimination from the vein, $k_{E_V}$, two mathematically equivalent "solutions" (sets of parameters) fit the data identically well. (**B**) Simulations indicate that the three parameters that define each of the two equivalently good solutions are all reasonably well-constrained by the in-brain data. (**C**) The two solutions, however, predict quite distinct plasma drug profiles, which cannot be distinguished by employing only data collected in the brain

As expected, concentration measurements performed in the brain fit to equations 5 and 6 reasonably well (Fig. 2A). Unfortunately, however, this fitting does not constrain the relevant pharmacokinetic parameters. This is due to a second, fundamental problem associated with applying the two-compartment model to measurements obtained in the brain compartment alone: due to a mathematical dependence between the rate constants for elimination, $k_{E_V}$, and transport, $k_{V_B}$, measurements performed only in the brain do not unambiguously constrain equations 5 and 6. Specifically, two sets of numerically equivalent solutions, in which $k_{E_V}$ and $k_{V_B}$ swap values and $V_{Dis}$ changes by the ratio of the two, will always fit the data equivalently (see proof in SI). Consistent with this, two non-overlapping parameter sets fit our data equally well. Thus, although our estimates of values of each of the parameters in the two parameter sets are well constrained (Table 1), ambiguity over which of the two parameter sets represents the true description of the system greatly broadens our confidence intervals, as these must simultaneously encompass both parameter sets (Fig. 2B).

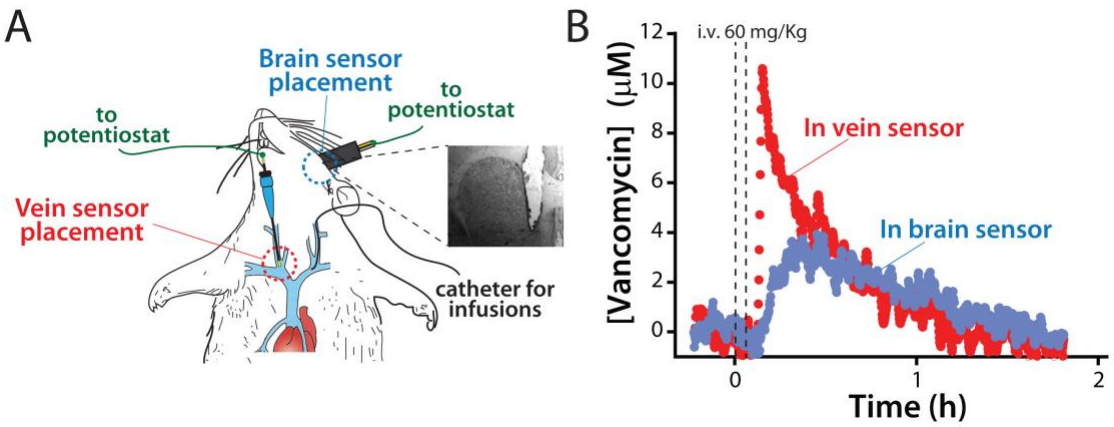


**Figure 3.** The convenience of EAB sensors renders it relatively easy to collect data simultaneously in the two compartments. (**A**) Here we have used this to simultaneously collect data in the left ventricle and the right external jugular of anesthetized rats. (**B**) Upon intravenous challenge with the drug (here 40 and 60 mg/kg over 1.35 and 1.28 min), we see a rapid increase in plasma drug levels followed by their slow decline. In the CSF, in contrast, the initial rise is much slower, and the subsequent decline slightly lags that seen in the vein

One could attempt to distinguish between the two mathematically equivalent models of in-brain pharmacokinetics based on their "physiological plausibility," but this is not without serious difficulties. For example, while the two model fits predict distribution volumes of 530 mL and 70 mL (Table 1), each of these are physiologically plausible. Specifically, the first value approximates the total body volume of the >450 g rats we have employed in our study, and thus cannot be discounted (distribution volumes can be larger than true volumes if, for example, protein binding reduces the concentration of free drug in the compartment (Albrecht et al., 1991)). The second value, however, is also physiologically plausible as it is within a factor of two of the 25-30 mL blood volume of a rat of this size. Given these observations, neither of the two mathematically equivalent models can be rejected solely on physiological grounds.

**Table 2. Simultaneous in-brain and in-vein pharmacokinetics**

| | | In-brain data only | | Simultaneous in-vein and in-brain data |
|---|---|---|---|---|
| | | Solution 1 | Solution 2 | |
| **Animal 1** | $V_{Dis}$ (L) | $0.089^{+0.117}_{-0.04}$ | $0.376^{+0.086}_{-0.169}$ | $0.155^{+0.010}_{-0.009}$ |
| | $k_{E_V}$ (min$^{-1}$) | $0.118^{+0.044}_{-0.06}$ | $0.028^{+0.033}_{-0.011}$ | $0.091 \pm 0.007$ |
| | $k_{VB}$ (min$^{-1}$) | $0.028^{+0.033}_{-0.011}$ | $0.118^{+0.044}_{-0.06}$ | $0.05 \pm 0.003$ |
| | Brain RMS residuals (mM) | 3.02 | 3.02 | 3.15 |
| | Vein RMS residuals (mM) | 16.45 | 14.28 | 8.66 |
| | | | | |
| **Animal 2** | $V_{Dis}$ (L) | $0.036^{+0.016}_{-0.009}$ | $0.227^{+0.023}_{-0.031}$ | $0.132^{+0.008}_{-0.007}$ |
| | $k_{E_V}$ (min$^{-1}$) | $0.1^{+0.025}_{-0.026}$ | $0.018^{+0.004}_{-0.003}$ | $0.039 \pm 0.003$ |
| | $k_{VB}$ (min$^{-1}$) | $0.018^{+0.004}_{-0.003}$ | $0.1^{+0.025}_{-0.026}$ | $0.049 \pm 0.005$ |
| | Brain RMS residuals (mM) | 10.57 | 10.57 | 10.78 |
| | Vein RMS residuals (mM) | 48.35 | 20.73 | 17.34 |
| | | | | |
| **Animal 3** | $V_{Dis}$ (L) | $0.12^{+0.022}_{-0.007}$ | $0.871^{+0.093}_{-0.05}$ | $0.091^{+0.05}_{-0.04}$ |
| | $k_{E_V}$ (min$^{-1}$) | $0.048 \pm 0.005$ | $0.007 \pm 0.001$ | $0.057 \pm 0.002$ |
| | $k_{VB}$ (min$^{-1}$) | $0.007 \pm 0.001$ | $0.048 \pm 0.005$ | $0.006 \pm 0.001$ |
| | Brain RMS residuals (mM) | 0.84 | 0.84 | 0.85 |
| | Vein RMS residuals (mM) | 9.95 | 18.50 | 9.14 |

A more rigorous solution to the problem of discriminating between the two parameter sets is suggested by the fact that, although the two solutions fit the in-brain data equally well, they produce quite divergent estimates of the plasma vancomycin levels that are driving transport into and out of the brain (Fig. 2C). That is, by performing in-vein measurements simultaneously with our in-brain measurements we can unambiguously discriminate between the two solutions, producing high-precision estimates of the kinetics with which the drug crosses into the compartment. Conveniently, EAB sensors render the performance of such simultaneous measurements relatively straightforward (Fig. 3). Using the above-described intercranial sensors and previously described intravenous sensors (Dauphin-Ducharme et al., 2019) we have taken this approach (Fig. 4). Doing so we obtained unambiguous estimates for the relevant pharmacokinetic rate constants that are typically constrained to within rather better than 10% (Table 2), a level of precision that is significantly better than any prior measurements of intercranial pharmacokinetics we are aware of. Consistent with this, the simultaneous fitting matches the observed plasma drug levels quite well without significantly altering the goodness of fit of the observed CSF drug levels. For example, in moving from fitting only in-brain data to simultaneously fitting in-brain and in-vein data the root-mean-squared residuals for the fits to the in-brain data increase by 3% or less (Table 2).

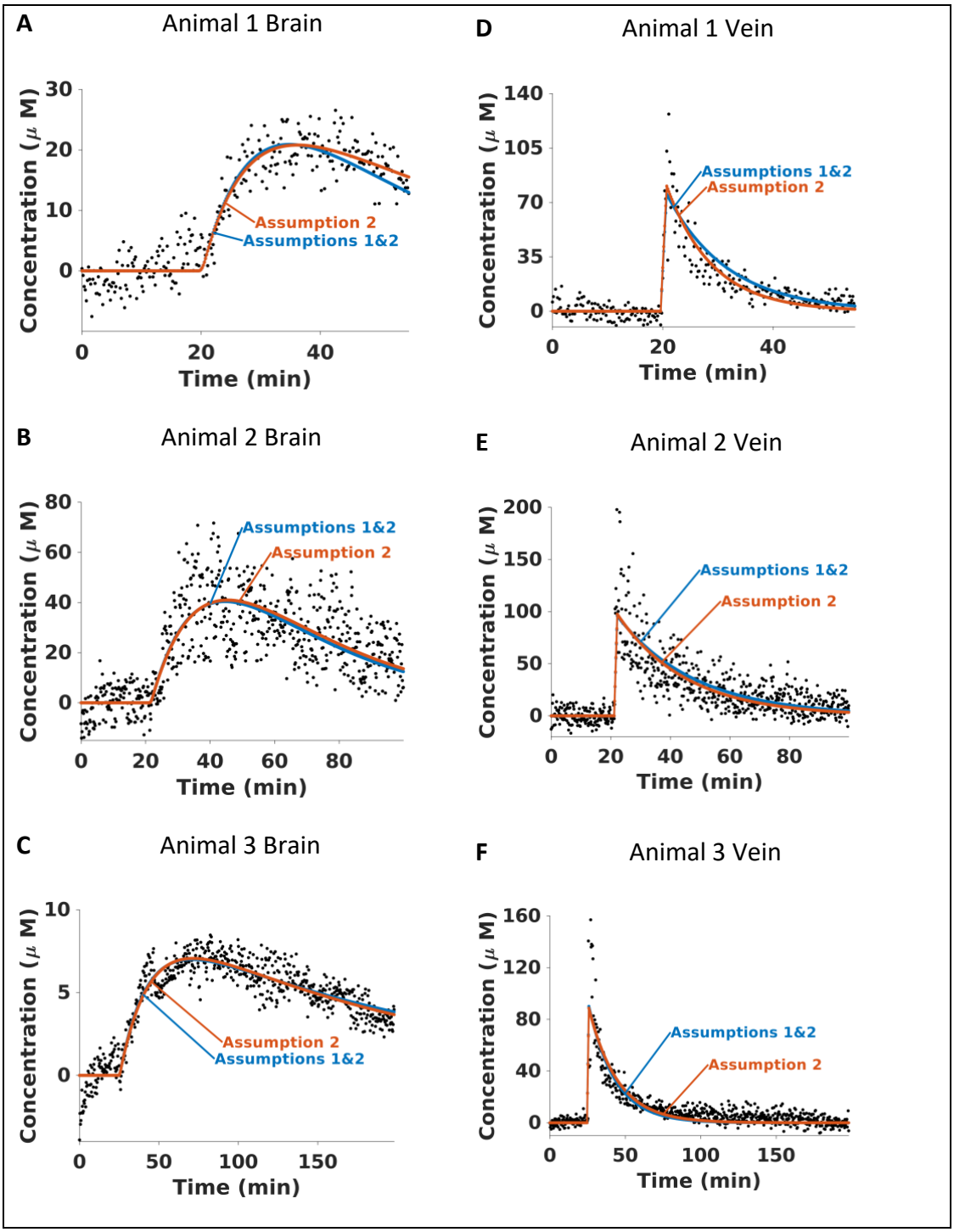


**Figure 4.** Simultaneous fits of both in-brain and in-vein vancomycin levels provide a high-resolution picture of the drug's transport across the blood-CSF barrier. Specifically, the addition of in-vein data helps to discriminate between the redundant, numerically equivalent descriptions that plague fits constrained only by in-brain data. The intravenous doses employed were 40 mg/kg and 60 mg/kg over a minute s for the two animals, respectively. The blue lines indicate the best fits to a 2-compartment model that includes both assumptions 1 and 2, and the orange lines indicate the best fits to a 2-compartment model that relaxes assumption 1 and thus includes only assumption 2

**Table 3. Relaxing assumptions with simultaneous in-brain and in-vein data**

| | Assumptions applied | 1, 2 and 3 | 2 and 3 | 1, and 3 | 3 |
|---|---|---|---|---|---|
| | Compartments | Two | | Three | |
| | Plasma pharmacokinetics | Mono-exponential | | Bi-exponential | |
| **Animal 1** | $V_{Dis}$ (L) | $0.155^{+0.01}_{-0.009}$ | $0.143^{+0.009}_{-0.008}$ | $0.118^{+0.011}_{-0.009}$ | $0.119^{+0.001}_{-0.009}$ |
| | $k_{E_V}$ (min$^{-1}$) | $0.091 \pm 0.007$ | $0.121 \pm 0.011$ | $0.108 \pm 0.001$ | $0.13 \pm 0.02$ |
| | $k_{VB}$ (min$^{-1}$) | $0.05 \pm 0.003$ | $0.045 \pm 0.003$ | $0.053 \pm 0.004$ | $0.048 \pm 0.003$ |
| | $k_{E_B}$ (min$^{-1}$) | N/A | $-0.018 \pm 0.004$ | N/A | $-0.014 \pm 0.004$ |
| | $k_{DV}$ (min$^{-1}$) | N/A | N/A | $0.125 \pm 0.05$ | $0.1 \pm 0.4$ |
| | $k_{VD}$ (min$^{-1}$) | N/A | N/A | $0.185 \pm 0.081$ | $0.2 \pm 0.1$ |
| | BIC | 3703 | 3637 | 3644 | 3601 |
| | Brain RMS residuals (mM) | 3.15 | 3.02 | 3.13 | 3.03 |
| | Vein RMS residuals (mM) | 8.66 | 8.01 | 7.71 | 7.35 |
| | | | | | |
| **Animal 2** | $V_{Dis}$ (L) | $0.132^{+0.008}_{-0.007}$ | $0.130^{+0.008}_{-0.007}$ | $0.094^{+0.012}_{-0.009}$ | $0.096^{+0.011}_{-0.009}$ |
| | $k_{E_V}$ (min$^{-1}$) | $0.039 \pm 0.003$ | $0.043 \pm 0.004$ | $0.049 \pm 0.007$ | $0.052 \pm 0.007$ |
| | $k_{VB}$ (min$^{-1}$) | $0.049 \pm 0.005$ | $0.047 \pm 0.004$ | $0.053 \pm 0.005$ | $0.052 \pm 0.005$ |
| | $k_{E_B}$ (min$^{-1}$) | N/A | $-0.006 \pm 0.003$ | N/A | $-0.005 \pm 0.003$ |
| | $k_{DV}$ (min$^{-1}$) | N/A | N/A | $0.086 \pm 0.047$ | $0.78 \pm 0.043$ |
| | $k_{VD}$ (min$^{-1}$) | N/A | N/A | $0.125 \pm 0.06$ | $0.114 \pm 0.057$ |
| | BIC | 10782 | 10776 | 10708 | 10705 |
| | Brain RMS residuals (mM) | 10.78 | 10.74 | 10.63 | 10.59 |
| | Vein RMS residuals (mM) | 17.34 | 17.21 | 16.45 | 16.37 |
| | | | | | |
| **Animal 3** | $V_{Dis}$ (L) | $0.091^{+0.05}_{-0.04}$ | $0.093^{+0.005}_{-0.004}$ | $0.081 \pm 0.005$ | $0.079^{+0.005}_{-0.004}$ |
| | $k_{E_V}$ (min$^{-1}$) | $0.057 \pm 0.002$ | $0.052 \pm 0.004$ | $0.065 \pm 0.004$ | $0.05 \pm 0.004$ |
| | $k_{VB}$ (min$^{-1}$) | $0.006 \pm 0.001$ | $0.005 \pm 0.001$ | $0.006 \pm 0.004$ | $0.006 \pm 0.001$ |
| | $k_{E_B}$ (min$^{-1}$) | N/A | $0.001 \pm 0.001$ | N/A | $0.004 \pm 0.001$ |
| | $k_{DV}$ (min$^{-1}$) | N/A | N/A | $0.023 \pm 0.011$ | $0.039 \pm 0.009$ |
| | $k_{VD}$ (min$^{-1}$) | N/A | N/A | $0.077 \pm 0.029$ | $0.044 \pm 0.011$ |
| | BIC | 6470 | 6467 | 6447 | 6354 |
| | Brain RMS residuals (mM) | 0.85 | 0.84 | 0.85 | 0.83 |
| | Vein RMS residuals (mM) | 9.14 | 9.13 | 8.91 | 8.45 |

The additional data provided by simultaneous in-brain and in-vein measurements provide an opportunity to "relax" the various reasonable, though rarely tested, assumptions usually employed to fit intercranial pharmacokinetics that we described above. Here we have done so. Specifically, we first relaxed assumption 1, that the drug is only removed from the brain via the blood, while retaining assumption 2, that drug transport into the brain does not significantly alter the concentration found in the vein. We then reversed this to test assumption 2 before finally relaxing both assumptions.

The first assumption, that rate constant for elimination within the brain, $k_{E_B}$, is zero. That is, that drug is lost from the brain only via passive diffusion back into the blood stream, with no degradation of the drug occurring in the brain and no significant loss of drug via the bulk transport of CSF into the dural venous sinuses. Relaxation of this assumption leads to a model in which the in-vein and in-brain dynamics are described by equations 5 and 4, respectively. When we simultaneously fit in-brain and in-vein data from our animals to these equations (Fig. 4, orange curves) we find that the root mean squared residuals improve slightly relative to the model in which assumptions 1 and 2 both remain in place (Fig. 4, blue curves; Table 3). This, however, is not surprising as this new model is more complex (has more fitted parameters) than the prior model. Thus, to more rigorously compare the performance of our models (i.e., taking into account model complexity) we have employed the Bayesian Information Criteria (BIC). This uses the log-likelihood of the candidate model as a goodness-of-fit measure, while simultaneously penalizing for model complexity (Schwarz, 1978). Simply put, the candidate model with the lowest BIC is the preferred model, albeit models within two units of the lowest BIC are generally considered to be

indistinguishably good descriptions of the system (Fabozzi, 2014). Using this criterion, we see that, despite the greater complexity of the model in which assumption 1 is relaxed, it is preferred relative to the model that includes both assumptions 1 and 2 for all of our study animals (Table 3).

The relaxation of assumption 1 does not alter the estimated distribution volumes, as this parameter is defined predominantly by the maximum concentration, $C_{max}$. Likewise, relaxing assumption 1 produces a best fit estimate for the in-brain elimination rate, $k_{E_B}$, that is within error of zero for animal 3, suggesting that, despite the improved fit, we see no evidence for anything but passive diffusion of the drug into and out of the brain for this animal. For both animals 1 and 2, in contrast, the estimate for $k_{E_B}$ is slightly, but statistically significantly, smaller than 0. This implies that drug continues to move from the plasma to the CSF even after the concentration in the former drops below that in the latter. A possible explanation for this is that there is an intermediate compartment that the drug enters from the plasma before it moves into the CSF. As drug generally reaches the CSF after transiting from the blood through solid brain tissue, this is perhaps not an unreasonable hypothesis. Conversely, however, we also note that deviations from zero could also arise due to other failed assumptions, such as failure of the various rate constants to remain *constant* in the face of metabolic fluctuations (i.e., changes in kidney function causing $k_{E_V}$ to change (Dauphin-Ducharme et al., 2019)).

We next tested assumption 2, the assumption that the concentration of drug found in the blood is not significantly affected by the transport of drugs out of the vein

compartment (defined here to include both the blood and the solid tissues that are in rapid equilibration with it). To test this, we introduced a single additional compartment to our model, which models the summed impact of all other bodily compartments. We call this compartment the distribution compartment, which we denote with a subscript D. We assume that this compartment (a) passively exchanges drug with the vein, (b) is not the site of drug metabolism, and (c) does not exchange drug directly with the brain. Fortunately, each of these simplifying assumptions are thought to hold in the case of vancomycin, as the venous pharmacokinetics of this drug are well-described by a two-compartment model (Matzke et al., 1986), it is not actively transported, and it is excreted unmetabolized via the kidneys (Matzke et al., 1986). The resulting three-compartment model uses equation 4 (repeated here as equation 8 for convenience) to describe the observed in-brain concentrations.

$$\frac{dC_V(t)}{dt} = \frac{1}{V_{Dis}}u(\mathrm{t}) + k_{D_V}\big(C_V(t) - C_D(t)\big) - k_{E_V}C_V(t) \tag{7}$$

$$\frac{dC_B(t)}{dt} = k_{V_B}\big(C_V(t) - C_B(t)\big) - k_{E_B}C_B(t) \tag{8}$$

$$\frac{dC_D(t)}{dt} = k_{V_D}\big(C_V(t) - C_D(t)\big) \tag{9}$$

The rate constants newly introduced here, $k_{V_D}$ and $k_{D_V}$, describe the impact of transfer from the vein to the distribution compartments on the concentration in the latter compartments and vice versa, respectively.

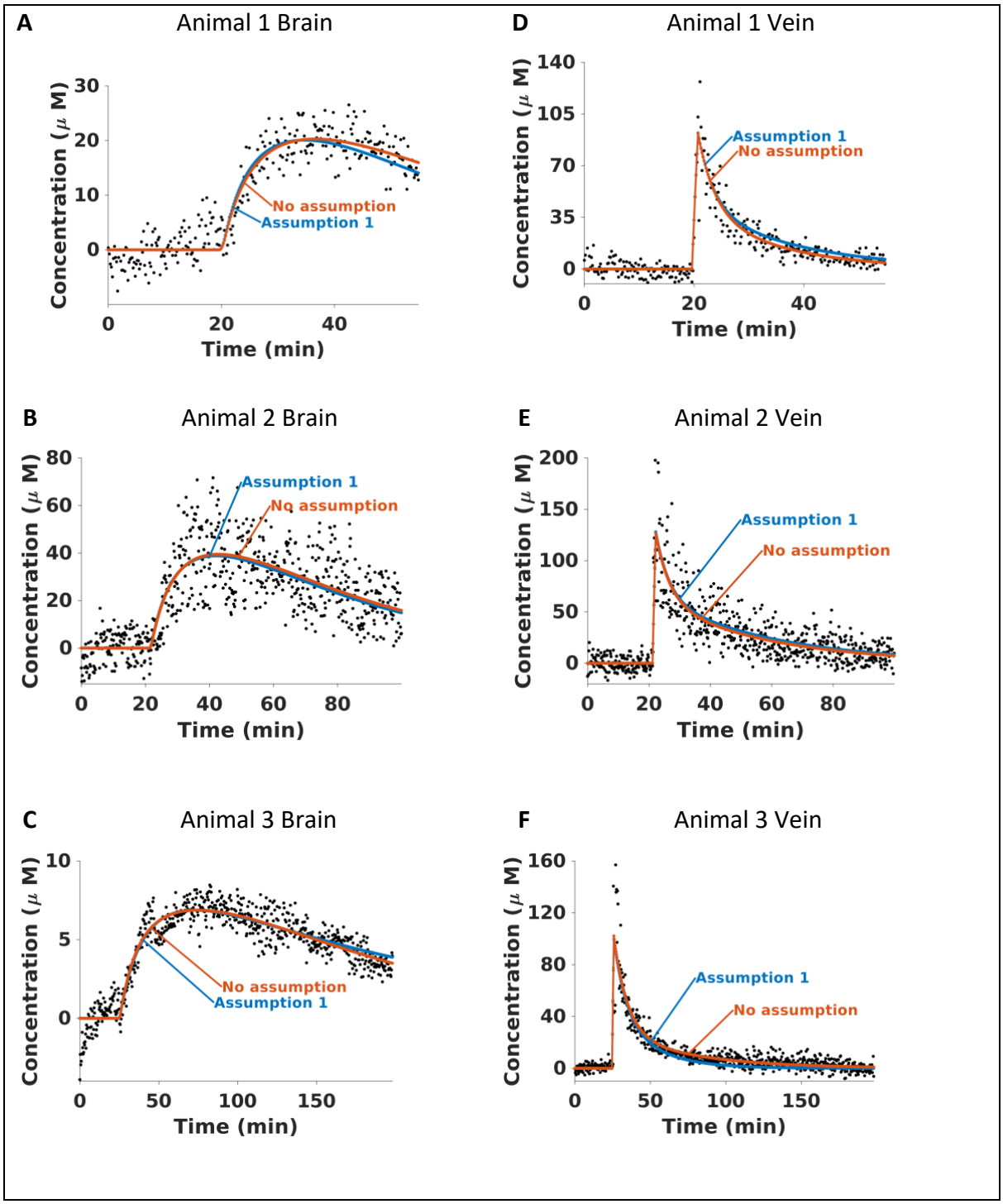


**Figure 5.** The availability of simultaneous measurements in the two compartments provides an opportunity to fit three compartment models, in which the body is modeled as the brain, the peripheral tissues, and the circulatory system, with transport between the brain and the peripheral tissues occurring only via the blood. The blue lines indicate the best fits to 3-compartment models in which assumption 1 holds and the orange lines indicate the best fits to 3-compartment models in which both assumption 1 and 2 are relaxed.

Relaxing assumption 2 while retaining assumption 1 (Fig. 5, blue curves) provides a statistically significantly improved fit relative to the model in which we retained assumption 2 but relaxed assumption 1 (Table 3). Specifically, while we see little if any improvement in the residuals for the in-brain measurements, both the in-vein residuals, and the BIC criterion improves significantly for all three animals. Consistent with this, this model produces statistically significant rate constants for diffusion into and out of the non-brain tissues that are consistent with previous estimates of the distribution rate of this drug in rats (Dauphin-Ducharme et al., 2019). Under this model the distribution volume is also reduced (by 10 to 30%), presumably due to the drug's distribution being divided between the vein compartment (which includes rapidly infused solid tissues) and the tissues into which drug distributes more slowly.

We next examined the effects of simultaneously relaxing both assumptions 1 and 2 (Fig. 5, orange curves). Doing so we found that, by the BIC criterion, this model is preferred over models that employ either assumption (Table 3). This means we see statistically significant evidence of a bi-exponential process occurring in the plasma and that the in-brain data support a statistically significant, nonzero (if small) rate of elimination from the brain ($k_{E_B}$). As discussed above, the small, but statistically significantly negative value for $k_{E_B}$ seen under this model for animal 1 and 2 can be attributed to an unmodeled transport compartment (e.g., the solid brain tissue). Conversely, for animal 3 $k_{E_B}$ is now slightly, but statistically significantly, positive, suggesting that there may be an alternative mechanism by which drug is lost from the CSF in this animal, perhaps due to drainage of CSF into the circulatory system via the dural venous sinuses. Alternatively, however, we again note that deviations of $k_{E_B}$

from zero could be attributed to unmodeled dynamics (e.g., a changing excretion rate constant driven by changes in kidney function).

As our final study we attempted to distinguish the contributions of the brain compartment from those of the distribution compartment in defining the pharmacokinetics seen in the plasma. We were motivated to do this because the most complicated model we considered, in which all assumptions were relaxed, was chosen by the BIC as the being the preferred model, suggesting that still more detailed models may be justified by our data. Thus motivated, we have also explored a third assumption:

**Assumption 3:** The impact of the brain on the vein is either trivial or is indistinguishable from the impact of the distribution compartment on the vein.

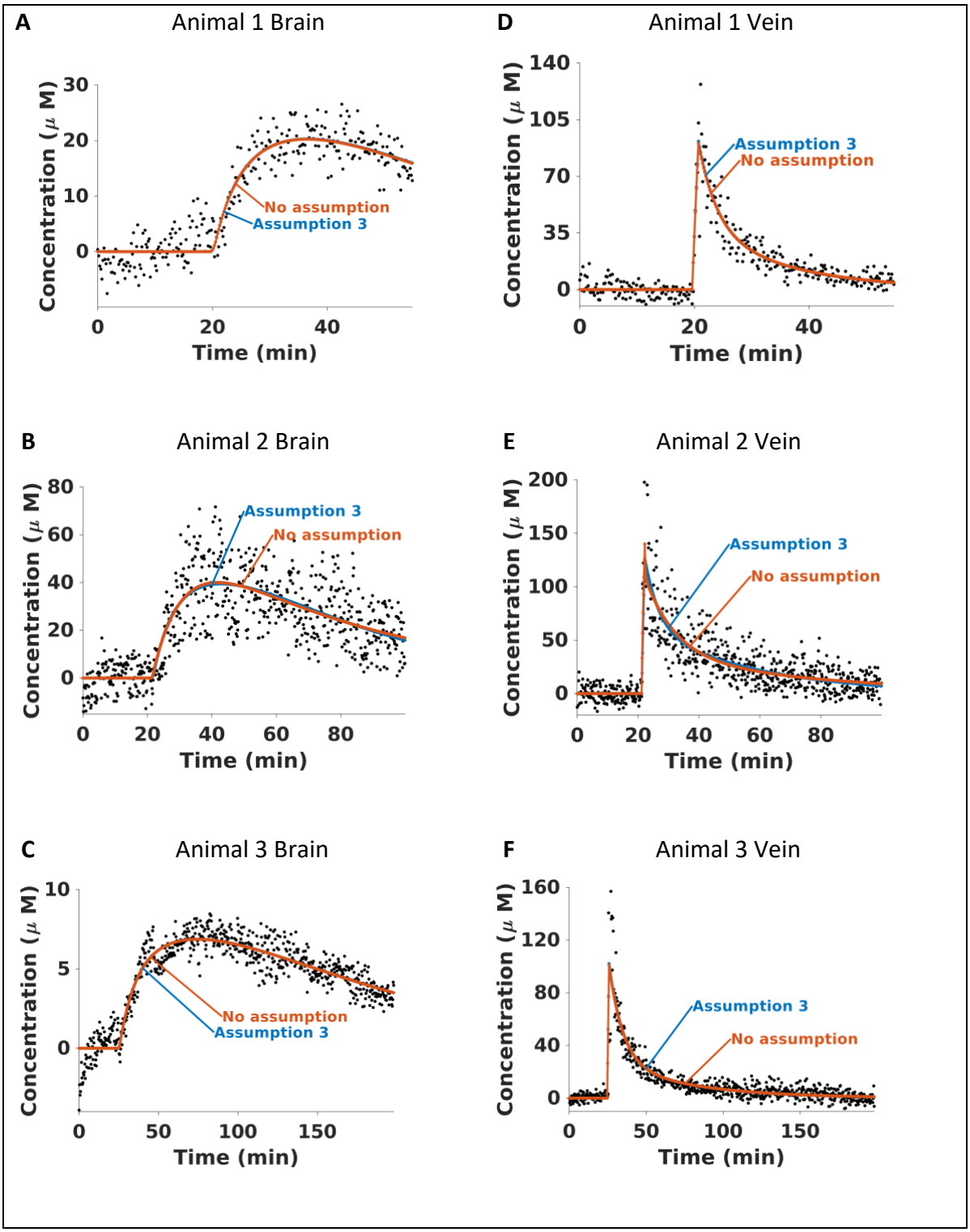


**Figure 6.** In our final study we attempted to distinguish the impact the brain has on the pharmacokinetics observed in the plasma from the impact that the rest of the body (the distribution compartment) has on that pharmacokinetics. The blue lines indicate the best fits to 3-compartment models in which assumption 3 is held and the orange lines indicate the best fits to 3-compartment models in which both assumptions 1 and 3 are relaxed.

| Table 4. Attempting to distinguish the impact of the brain from the rest of the body | | | | |
|---|---|---|---|---|
| | Assumptions applied | 3* | 1 | none |
| | Compartments | Three | | |
| | Plasma pharmacokinetics | Bi-exponential | Tri-exponential | Tri-exponential |
| Animal 1 | $V_{Dis}$ (L) | $0.119^{+0.001}_{-0.009}$ | $0.120^{+0.007}_{-0.007}$ | $0.121^{+0.007}_{-0.006}$ |
| | $k_{E_V}$ (min$^{-1}$) | $0.13 \pm 0.02$ | $0.11 \pm 0.02$ | $0.12 \pm 0.01$ |
| | $k_{VB}$ (min$^{-1}$) | $0.048 \pm 0.003$ | $0.053 \pm 0.003$ | $0.048 \pm 0.002$ |
| | $k_{E_B}$ (min$^{-1}$) | $-0.014 \pm 0.004$ | N/A | $-0.014 \pm 0.002$ |
| | $k_{DV}$ (min$^{-1}$) | $0.1 \pm 0.4$ | $0.12 \pm 0.06$ | $0.09 \pm 0.05$ |
| | $k_{VD}$ (min$^{-1}$) | $0.2 \pm 0.1$ | $0.2 \pm 0.1$ | $0.2 \pm 0.1$ |
| | $k_{BV}$ (min$^{-1}$) | N/A | $0^{\dagger}$ | $0^{\dagger}$ |
| | BIC | 3601 | 3650 | 3608 |
| | Brain RMS residuals (mM) | 3.03 | 3.13 | 3.03 |
| | Vein RMS residuals (mM) | 7.35 | 7.71 | 7.35 |
| | | | | |
| Animal 2 | $V_{Dis}$ (L) | $0.096^{+0.011}_{-0.009}$ | $0.045^{+0.009}_{-0.007}$ | $0.045^{+0.009}_{-0.007}$ |
| | $k_{E_V}$ (min$^{-1}$) | $0.052 \pm 0.007$ | $0.09 \pm 0.02$ | $0.11 \pm 0.02$ |
| | $k_{VB}$ (min$^{-1}$) | $0.052 \pm 0.005$ | $0.053 \pm 0.004$ | $0.051 \pm 0.003$ |
| | $k_{E_B}$ (min$^{-1}$) | $-0.005 \pm 0.003$ | N/A | $-0.005 \pm 0.002$ |
| | $k_{DV}$ (min$^{-1}$) | $0.78 \pm 0.04$ | $3.1 \pm 1.0$ | $3.1 \pm 1.0$ |
| | $k_{VD}$ (min$^{-1}$) | $0.11 \pm 0.06$ | $2.2 \pm 0.6$ | $2.2 \pm 0.6$ |
| | $k_{BV}$ (min$^{-1}$) | N/A | $0.09 \pm 0.02$ | $0.08 \pm 0.02$ |
| | BIC | 10705 | 10703 | 10699 |
| | Brain RMS residuals (mM) | 10.59 | 10.62 | 10.58 |
| | Vein RMS residuals (mM) | 16.37 | 16.30 | 16.23 |
| | | | | |
| Animal 3 | $V_{Dis}$ (L) | $0.079^{+0.005}_{-0.004}$ | $0.082^{+0.004}_{-0.003}$ | $0.080 \pm 0.003$ |
| | $k_{E_V}$ (min$^{-1}$) | $0.05 \pm 0.004$ | $0.065 \pm 0.004$ | $0.05 \pm 0.01$ |
| | $k_{VB}$ (min$^{-1}$) | $0.006 \pm 0.001$ | $0.006 \pm 0.0002$ | $0.006 \pm 0.001$ |
| | $k_{E_B}$ (min$^{-1}$) | $0.004 \pm 0.001$ | N/A | $0.004 \pm 0.001$ |
| | $k_{DV}$ (min$^{-1}$) | $0.039 \pm 0.009$ | $0.022 \pm 0.008$ | $0.038 \pm 0.008$ |
| | $k_{VD}$ (min$^{-1}$) | $0.04 \pm 0.01$ | $0.08 \pm 0.02$ | $0.04 \pm 0.01$ |
| | $k_{BV}$ (min$^{-1}$) | N/A | $0 \pm N/A^{\dagger}$ | $0 \pm N/A^{\dagger}$ |
| | BIC | 6354 | 6454 | 6361 |
| | Brain RMS residuals (mM) | 0.83 | 0.85 | 0.82 |
| | Vein RMS residuals (mM) | 8.45 | 8.92 | 8.45 |

*This is the model presented in Table 3, rightmost column. It is repeated here to ease comparison.

† We cannot meaningfully estimate the confidence intervals since the values estimated are at the lower constraints we impose, $k_{BV} > 0$.

To test assumption 3 we add to our model an additional term, $k_{B_V}$, reflecting the impact of the brain on the vein. This expands equation 7, now updated as equation 10.

$$\frac{dC_V(t)}{dt} = \frac{1}{V_{Dis}}u(\mathrm{t}) + k_{D_V}\big(C_V(t) - C_D(t)\big) + k_{B_V}\big(C_V(t) - C_B(t)\big) - k_{E_V}C_V(t) \qquad (10)$$

This models the plasma pharmacokinetics as a tri-exponential decay, and thus has the potential to improve the fit to the plasma measurements. For completeness we have tested this new model with and without relaxing assumption 1, though we expect the impact of assumption 1 to be similar to our previous results.

The relaxation of assumption 3 does not systematically improve our fitting (Fig. 6), suggesting we have surpassed the point at which further increases in model complexity are justified for even our unprecedentedly highly-resolved data. Specifically, the relaxation of assumption 3 leads to an improved fit for only one of our three animals, and even then, relaxation of this assumption significantly degrades the precision with which the rate constants for transport into and out of the distribution compartment are defined (Table 4). It likewise estimates for this animal that the rate constant of transfer from the brain to the plasma is larger than that for transport in the opposite direction (i.e., $k_{BV} > k_{VB}$), suggesting - improbably- that the brain is the larger of the two compartments. These observations lead us to suspect that, for the only animal for which the BIC suggests the relaxation of assumption 3 is warranted, the model is trying to fit the noise rather than any meaningful trend. Consistent with these arguments, use of this more complex model also reduces the root-mean-squared residuals by less than 1% (Table 4).

## 4.5 Discussion

Here we have employed EAB sensors to monitor the transport of a drug from the blood into the CSF with few-second time resolution. The hundreds of measurements this approach affords over the course of a single drug lifetime is sufficient to produce high-precision estimates of the rate constants for transport into the CSF and for the elimination of the drug from the kidneys. Confidence in these values, however, is reduced by a mathematical ambiguity fundamental to any attempt to fit a two-compartment pharmacokinetic model using data collected in only a single compartment to which the drug is not directly injected. The collection of simultaneous measurements in both the CSF and plasma, in contrast, resolves this ambiguity, leading to high precision (precision of 5 to 20% at the 95% confidence level) estimates of the relevant pharmacokinetic parameters at levels of model complexity up to three compartments (i.e., the addition of a peripheral compartment).

The simultaneous, seconds-resolved dual measurements presented here provide sufficient constraints to relax the major assumptions that have historically been employed in the multi-compartment models used to characterize molecular transport from the blood to other bodily compartments. These include assumptions such as a lack of active transport to or from the tissues, the bulk flow of tissue fluids (e.g., CSF or lymph draining), and in-tissue drug metabolism. Indeed, for all of our animals we see small, but statistically significant effects from such previously unmodeled (unmodellable) processes. This said, even the most sophisticated model we have explored still retains several potentially significant assumptions, including some that are likely “untrue” given the precision afforded us by the

large amount of data in-vivo EAB sensors provide. Key among these, we believe, is the assumption that the various rate constants are constants; prior studies employing intravenous EAB sensors in live rats have shown that drug elimination rates, for example, can change several-fold over the course of a few hours (Arroyo-Currás et al., 2017; Arroyo-Currás, Ortega, et al., 2018), including studies of vancomycin (Dauphin-Ducharme et al., 2019). Likewise, without experimental observations in the peripheral compartment, we cannot uniquely constrain models allowing for still more compartments (beyond the 3 employed in our most complex models), the metabolism of the target molecule in the peripheral compartment, or the target molecule's active transport into or out of it. This said, the extremely large quantity of data provided by EAB sensor measurements, and the relative ease with which EAB sensors can be inserted into multiple compartments simultaneously, suggests that, moving forward, the platform will provide opportunities to surmount even these issues.

We close by noting that, although this study focused on vancomycin as a test-bed molecular target, the EAB platform is modular, and thus can be adapted to new molecular targets via the simple expedient of changing the recognition aptamer. Our group alone, for example, has already demonstrated in-vivo EAB sensors against a range of antibiotics (aminoglycosides (Arroyo-Currás, Dauphin-Ducharme, et al., 2018; Arroyo-Currás et al., 2017; Arroyo-Currás, Ortega, et al., 2018) and vancomycin (Dauphin-Ducharme et al., 2019)), chemotherapeutics (doxorubicin (Arroyo-Currás et al., 2017; Ferguson et al., 2013; Mage et al., 2017), and irinotecan (Idili, Arroyo-Currás, et al., 2019), psychoactive drugs (Taylor et al., 2017), and metabolites (Idili et al., 2021). Taken with the work presented here,

these examples highlight the potential of EAB sensors in the tracking intercompartmental molecular transport in the living body, which would not only increase our ability to understand -and therefore modulate- such transport but could be used as a powerful preclinical tool during drug development to screen drug candidates more effectively in vivo. Such an advance would allow swifter, more accurate, exploration of the clinical impact of novel drug candidates, opening the door for better dosing regimens, as well as potentially saving millions of dollars by rejecting candidates at an earlier stage in their development.

# Chapter 5

## Real-time, seconds-resolved drug concentration monitoring in situ in the brains of free-moving rats provide high-precision, subject-specific pharmacokinetics.

## 5.1 Abstract

Existing methods for measuring drug concentrations in the brains of live subjects have historically been constrained on a number of dimensions, including poor temporal resolution, significant time lags, and in many cases, the need for restrained or anesthetized subjects. Here, however, we describe the adaptation of electrochemical aptamer-based (EAB) sensors – a versatile, receptor-based technology that is independent of the reactivity of its target – to the problem of performing seconds-resolved, real-time, multi-hour measurements of absolute drug concentrations in situ in the brains of freely-moving animals. Specifically, using 76 μm-diameter, 3 mm-long "intracranial" EAB sensors, we have measured procaine in the ventricles of behaving, freely moving rats. The resulting multi-hour, real-time measurements achieve precision of better than 4 mM and time resolution as good as 10 s, with the latter being an order of magnitude better than that of the best prior microdialysis studies of intracranial drug levels and two orders of magnitude better than typical studies. This enormous increase in time resolution enables the collection of hundreds of data points per animal, permitting the observation of statistically significant correlations between in-vivo drug levels and the behavioral responses of individual subjects (e.g., $R^2$ ~ 0.67) for intracranial procaine concentration versus overall locomotion). These high-volume data sets similarly permit the comparison of pharmacokinetic differences between individuals. The initial results presented here thus showcase the utility of EAB molecular measurements in the determination of the site-specific, seconds-resolved neuropharmacokinetics of individual subjects, and the correlation of these with drug-induced changes in individual behavior.

## 5.2 Introduction

The impact of drugs on brain function depends critically on drug brain pharmacokinetics and, thus, accurate and highly time-resolved concentration measurements are necessary to achieve a detailed understanding of drug-brain interactions. The greater abuse potential of injecting rather than oral ingestion or "snorting" of psychotropic drugs, for example, is thought to occur because in-brain drug levels peak a few tens of seconds faster in the former (Javaid et al., 1978; Jeffcoat et al., 1989; Melichar et al., 2001). The induction of anesthesia likewise typically requires just seconds (e.g., the time required to count backwards from 100 to 90).

In contrast to the few tens of seconds time course of anesthesia, the best-resolved prior studies of the pharmacokinetics of psychoactive substances only achieved time resolutions of minutes (Minogianis et al., 2019; Usubiaga et al., 1967). For example, procaine, a compound that has local, general,and epidural anesthetic properties (Azimi, 1994; Tu et al., 1998; Veneziano & Tobias, 2017; Winter, 1950), has only ever been measured with ~5 min temporal resolution. A time frame far too slow to accurately resolve its pharmacokinetics. This is because current methods of measuring drugs in the brain are limited to post-mortem sample collection, positron emission tomography (PET), or microdialysis (Kitamura et al., 2016; Reiter & Stimpfl, 2015) , all of which fail to achieve the performance necessary to address key questions in behavioral neuropharmacology. Post-mortem measurements, for example, provide only a single time point and typically lack spatial resolution (specimens are often homogenized). PET, in contrast, supports the measurement of drug time courses, but is limited to those molecules for which high-speed

isotopic labeling protocols are available, requires constrained subjects, and suffers from poor (typically minutes) resolution (Garg et al., 2017; Moses, 2011; Rose, 2010). Microdialysis, which also supports the collection of multiple, time-resolved meaurements, provides exceptional versatility in molecular detection and supports studies of freely moving subjects (M. Wang et al., 2011; Zestos & Kennedy, 2017) but also suffers from generally poor temporal resolution. Specifically, while a single study (Su et al., 2014) once achieved 2 s resolution (a feat that does not appear to have ever been repeated) and a small number have achieved tens of seconds resolution (Gowers, 2018b; Harstad & Bowser, 2016; Saylor & Lunte, 2015; H. Yang et al., 2013), such studies remain far from common, much less "turn key." A recent survey of an unbiased, representative set of 64 in-brain microdialysis studies found the *best* resolved study used 5 min sampling, and most (82%) employed sampling times of 20 min or greater (H. Yang et al., 2013). Moreover, although numerous authors have described "on-line" set-ups in which dialysate is delivered directly to analytical instrumentation (Gowers, 2018a), long sample transport times mean that the approach is not meaningfully real-time, precluding its application to emerging engineering approaches, such as feedback-controlled drug delivery (Arroyo-Currás, Ortega, et al., 2018; Dauphin-Ducharme et al., 2019) or closed-loop optogenetics (Newman, 2015; Prsa et al., 2017).

In contrast to in-brain *drug* measurements, current methods of measuring *neurotransmitters* in the brain sometimes achieve far superior temporal resolution. Specifically, the direct electrochemical detection of monoamines and the enzymatic electrochemical detection of glutamate and acetylcholine commonly achieve resolution of ~1 s (Shin et al., 2019). (Note: the interrogation frequency of such sensors, which is often >>

1 Hz, is not synonymous with their time resolution as the latter is limited by the slow diffusion of target to the sensor surface; see, e.g., figure 1 of ref. (Keithley et al., 2011), table 1 of ref. (Hoeben & Gunneweg, 2015), and table 2 of ref. (Ngernsutivorakul et al., 2018a)). These approaches, however, depend on the electrochemical or enzymatic reactivity of their targets, and thus cannot be generally adapted to the measurement of, for example, psychoactive drugs. Here, however, we describe the adaptation of electrochemical aptamer-based (EAB) sensors (Fig. 1), a versatile, receptor-based, electrochemical detection approach that is independent of the reactivity of its targets e.g. (Arroyo-Currás et al., 2017; Idili, Arroyo-Currás, et al., 2019), to the problem of performing seconds-resolved, real-time, multi-hour measurements of procaine concentrations in situ in the brains of freely behaving rats.

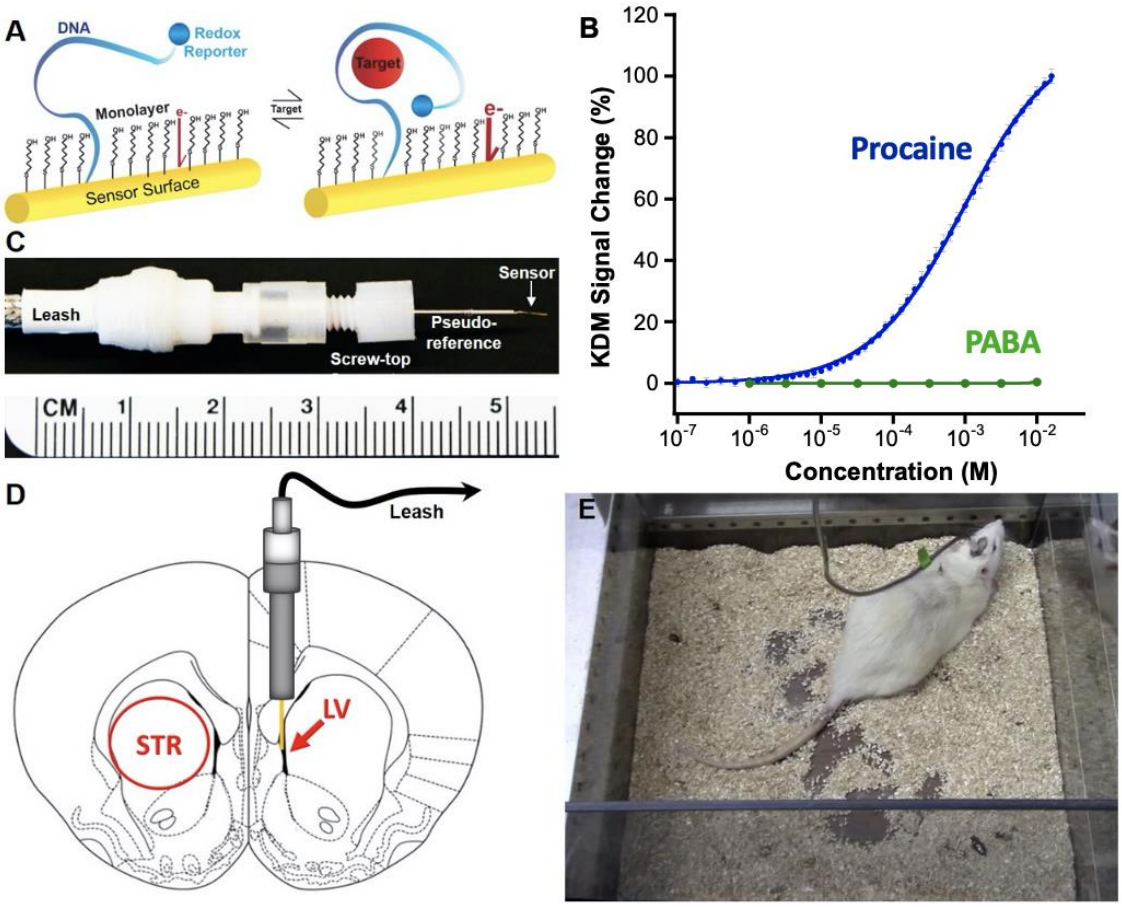


**Figure 1.** (**A**) Electrochemical Aptamer-Based (EAB) sensors are comprised of a redox-reporter-modified, drug-binding aptamer covalently attached to a gold electrode (via the formation of a self-assembled monolayer). Binding-induced folding of the aptamer leads to an easily measured change in electron transfer that is monotonically related to target concentration. (**B**) The sensors we have employed here respond to procaine, and not the drug's primary metabolite, para-amino benzoic acid (PABA). The calibration curve presented were collected in vitro in undiluted bovine CSF. (**C**) For in-brain studies we fabricated EAB sensors on a 75 □m-diameter, 3-mm-long gold electrode extending from the end of a 22-gauge stainless steel cannula that acts as both a guide and a counter/pseudo-reference electrode. Shown is a fully assembled "probe" with its attached leash. (**D**) This is inserted into the brain region of interest using an 18-gauge guide cannula that was stereotaxically introduced a week prior to the measurements. (**E**) After insertion of the sensor (under light anesthesia), the animals were allowed to recover and to move freely about the locomotor apparatus during measurements. LV = lateral ventricle

## 5.3 Materials and Methods

### Chemical Reagents and Materials

All reagents were purchased from Sigma-Aldrich (St. Louis, MO) and used as received. The synthesis of the HPLC-purified, reporter-and-thiol-modified, procaine-binding aptamer was obtained from Biosearch Technologies (Novato, CA), dissolved in deionized water (18.2 MΩ) to 100 µM, aliquoted into separate tubes, and stored at -20ºC until used.

The in-brain "probes" we employ consist of three parts: the sensor itself (Fig. 1C), an indwelling cannula (Fig. 1D), and a flexible leash (Fig. 1E), all of which were custom constructed based on our design by Plastics One (Roanoke, VA). The indwelling cannula, which also served as the counter electrode and a pseudo-reference, was constructed from an 18-gauge stainless steel cannula (2 mm length below pedestal) with a plastic screw-top connector (total length 13 mm). The sensor was constructed from a 22-gauge threaded stainless steel cannula (15 mm length below pedestal) filled with Teflon-coated gold wire (76 µm diameter, 3 mm exposed, active sensor length, 19 mm total length), and surrounded by a plastic screw-top connector with 2 ports for electrode pins. The electrode leash (50 cm) was built to contain male and female ends for electrode pins on opposite sides and is protected with a stainless-steel mesh exterior.

To allow rapid drug delivery we employed chronic, indwelling jugular catheters (see refs (Ploense, 2018a, 2018b)). In brief, these are constructed using a 22-gauge bent steel guide cannula with a plastic connector (Plastics One, Roanoke, VA), silastic tubing (11 cm long, 0.64 mm internal diameter, 1.19 mm external diameter; Dow Corning, Midland, MI),

prolite polypropylene monofilament mesh (Atrium Medical Corporation, Hudson, NH), methyl methacrylate cement, and a silicon ball 2.5 cm from the terminal end of the tubing.

**Sensor Fabrication and Measurements**

We first validated the EAB sensor in vitro using devices fabricated on 2 mm diameter gold disk electrodes (CH Instruments, Austin, TX), which we tested in undiluted bovine cerebral spinal fluid (CSF) (BioIVT, Westbury, NY) to ensure they achieved physiologically relevant detection limits and selectivity (i.e., that they reject any endogenous molecules in the CSF). To fabricate sensors on these electrodes we first cleaned them by repeated electrochemical cycling (see supplemental information for details). To prepare the aptamer for attachment to the gold surface we first reduced 4 µL of a 100 µM solution of the appropriate thiol-and-methylene-blue-modified oligonucleotide (5'– thiol– C6 –$PO_4$–GAC AAG GAA AAT CCT TCA ACG AAG TGG GTC–$PO_4$–methylene blue–3') using 4 µL of 10 mM of Tris(2-carboxyethyl) phosphine hydrochloride (TCEP) for 1 h at 25 ºC. We then diluted the solution to 500 nM with 1X PBS. We then submerged freshly cleaned electrodes in this solution for 1 h before moving them to a 10 mM 6-mercaptohexanol solution for 12 h to form a self-assembled monolayer.

Our custom in-brain probes consist of two major parts - an electrode leash and an implantable gold/stainless-steel electrode pair (Plastics One, Roanoke, VA). The former (50 cm length) is comprised of two copper wires encased in a braided stainless-steel mesh leash. At each end of the leash, are two gold-coated copper pins (1 mm apart) that emerge from a plastic casing and a screw-on plastic collar (8 mm length). One end of this is attached to the

implanted electrodes and the other to a 2-channel swivel commutator (Fig. 1E). Before using the electrode pair, we cleaned the gold electrode and applied the DNA aptamer and self-assembling monolayer to it as described above (and in detail in the supplemental information).

To optimize the electrochemical parameters employed in sensor interrogation, we conducted a 50-point titration of our sensors at 8 different square wave frequencies in vitro in undiluted bovine CSF at 37 ºC and determined the "signal-on" (150 Hz) and "signal-off" (10 Hz) frequencies with the largest relative changes in current. Using serial voltammetric measurements performed at 10 and 150 Hz, we corrected the baseline drift seen in vivo using "kinetic differential measurements" (KDM; detailed in ref[31] and below). To convert KDM signals into drug concentrations we fitted the in-vitro titration data to the equation: $y = B_{MAX} \times \frac{[target]}{K_D + [target]}$, where y is the KDM signal, $B_{MAX}$ is the signal change seen at saturating target concentrations, [target] is drug concentration, and $K_D$ is the dissociation constant of the aptamer.

**Animal Housing and Care**

Adult male Sprague-Dawley rats (350-600 g) were pair-housed in a standard light cycle room (08:00 on, 20:00 off) and allotted ad-libitum access to food and water. The housing and care of all rats were conducted in accordance with the guidelines set forth by the "Guide for the Care and Use of Laboratory Rats, 8th edition" (*IACUC, Guide for the Care and Use of Laboratory Animals: Eighth Edition*, 2011). Temperature, heart rate, SPO2 (specific peripheral oxygen concentration), and respiration rate were recorded and maintained within veterinary recommended levels during surgical procedures.

**Surgery**

We induced anesthesia prior to surgery using 4% isoflurane gas (Medline, Northfield, IL) and maintained it using 2-3% for the remainder of surgical procedures. After inducing anesthesia, we shaved the head, back, and chest of the rats, and disinfected the surgical sites with 10% betadine solution and 70% isopropanol before injecting the local anesthetic Lidocaine (2 mg/kg subcutaneous) into each incision site. Briefly, we first inserted the silastic catheter into the jugular vein and the catheter port into a 3 mm hole on the dorsal side of the rat. Following jugular implantation, we inserted a 19-gauge stainless-steel guide cannula (Plastics One, Roanoke, VA) and 22-gauge stainless-steel obturator into either the lateral ventricle or the dorsal striatum. After surgery, we allowed the rats to recover for at least seven days before experimentation. Our initial trials to test the electrode efficacy were conducted in the cerebrospinal fluid of the lateral ventricle, as this region better mimics our prior in vivo work with sensors in this class, all of which was performed in plasma. After successfully measuring drugs in the lateral ventricle, we then tested sensors within the solid tissues of the dorsal striatum, an area of the brain that plays a central role in locomotor function. Following the experiment, we removed the brains from the rats and performed histology to confirm sensor placement (complete details are provided in the supplemental information).

**In Vivo Measurements**

Before commencing measurements, we weighed each rat and tested the patency of its catheter by injecting 0.1 mg of the fast-acting anesthetic methohexital sodium (Covetrus, Chicago, IL). One hour after recovery from the patency test, we induced anesthesia using 3%

isoflurane gas, quickly flushed and then withdrew 50 µL of 0.9% saline solution in the top of the cannula with a 30 G needle, and maintained anesthesia as we inserted the sensor through the cannula and then affixed the sensor in place by the screw fittings on the surgically implanted 19-gauge guide cannula. We then placed the rat into a Kinder Scientific Motor Monitor system (Fig. 1E), allowed them to recover from anesthesia, and began recording locomotion via the supplied Motor Monitor software. We commenced EAB measurements using square-wave voltammetry on a CH1208C mini-potentiostat, alternating between square-wave frequencies of 30 Hz (swept at 0.02 V/s) and 150 Hz (swept at 0.15 V/s), both at an amplitude of 25 mV and over a voltage window of approximately 0 to -0.45 V (relative to the stainless-steel pseudo-reference). To visualize our measurements in real time we used SACMES, an open-source Python script previously reported by our laboratories (Curtis et al., 2019). Briefly, SACMES loads voltammograms corresponding to the two frequency measurements and performs a polynomial fit to each voltammogram to calculate peak current. The raw peak currents resulting from this analysis are normalized relative to a peak current corresponding to the measurement baseline (with [procaine] = 0 M). . Following these data processing steps, SACMES performs KDM by subtracting the 30 Hz data from that obtained at 150 Hz. Doing so results in drift-corrected signals which can be directly used to calculate target concentration from the sensor's calibration curves obtained in vitro. We varied the width of the voltage window to optimize voltammetric peak placement, which shifted occasionally because our measurements relied on a pseudo-reference electrode. This, in turn, altered the time required to collect the two sequential voltammograms and thus time resolution, which varied between 10 and 11 s. In all studies, we collected baseline

measurements for 20 min before any drug infusion to determine confidence intervals. We then commenced infusion of the drug (0.1 M procaine at 5 mg/ kg/ min) via the jugular catheter and continued both locomotor and EAB measurements.

**Histology**

To ensure proper sensor placement, we euthanized the rats with an intravenous injection of 0.1 mL of Somnasol (Covetrus, Chicago, Il) following our measurements and performed histology on their brains. To do so, we decapitated the animals with a guillotine (Braintree Scientific, Braintree, MA), collected their brains in 10% formalin, and incubated them in this for 1 week. Brains were then transferred to ___% sucrose solution for 3 days Following formalin treatment, we blocked the brains at the cerebellum, flash froze them over dry ice for 1 min, mounted them on a stand, and sliced them into 40 µm sections. These were then loaded into a slide holder and stained and analyzed as described in the supplemental information.

**Statistical Analyses**

The high-frequency measurements provided by EAB sensors vastly increases the number of concentration measurements (by two orders of magnitude over typical microdialysis studies) of in-brain drug concentrations in individual animals. Given the size of the resulting data sets we can perform within-subject statistical analyses on individual animals, which is effectively unprecedented. Thus motivated, we evaluated the relationship between drugs and locomotor behavior by running linear regressions on locomotor data separated into bins for different concentrations of drug present in the tissue with the Graphpad Prism 9 Software (San Diego, CA). Data were averaged over bins consisting of

baseline, 0 μM measurements (pre-injection) and linearly increasing concentration ranges incrementing by 5 μM bins (e.g., 0 – 5 μM, 5 – 10 μM). The concentration of each bin was assigned to its mid-point value. Bins containing fewer than a half-dozen data points, which only occurred at the one or two highest measured concentrations, were excluded from the analysis.

**5.4 Results**

EAB sensors are comprised of a redox-reporter-modified aptamer (nucleic acid-based receptors selected in vitro to bind specific molecular targets) that is covalently attached to the surface of a gold electrode via an alkane thiol chain (Fig. 1A). Upon the aptamer undergoing a binding-induced conformational change, electron transfer from the redox reporter is altered, changing in turn the peak current observed when the sensors are interrogated using square-wave voltammetry (Fig. S1). Fabricating such sensors using a modified version of a previously developed aptamer (Shoara, 2018) that binds the anesthetic procaine, we were able to monitor this target with pharmacologically-relevant sensitivity, specificity, and time resolution. For example, when challenged in vitro with 200 □M procaine in undiluted CSF, the sensor responds with a 30% change in signaling current (Fig. 1B). In contrast, the sensor does not measurably respond to para-amino benzoic acid, one of the two primary procaine metabolites. Finally, the sensor is rapid; its equilibration is effectively complete within the 10 to 11 s required to perform the pair of voltammetric scans required for in-vivo sensing, and thus the sensor's scan repetition rate defines its time resolution.

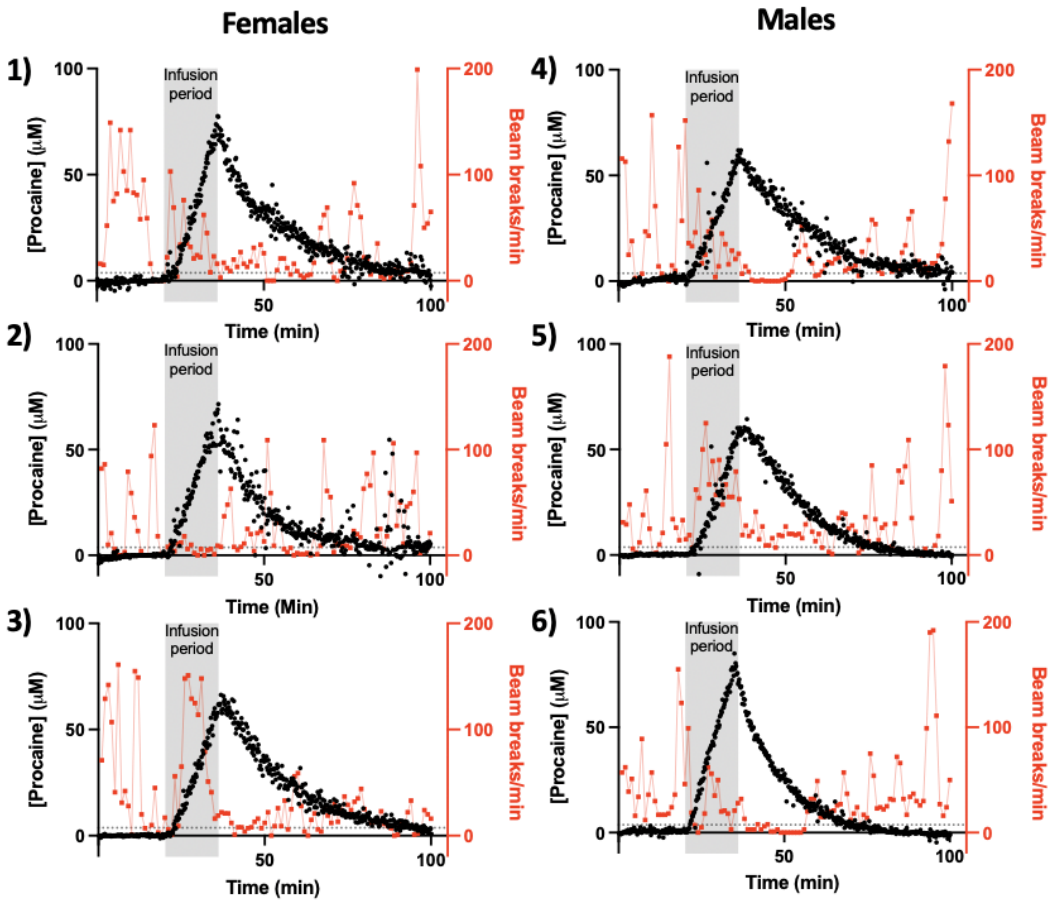


**Figure 2**. Employing EAB sensors we have measured procaine levels (black) in the lateral ventricles of freely moving rats while simultaneously monitoring their behavior (in red is beam breaks/min). Male and female are given an 80 mg/kg continuous IV infusion at a rate of 5 mg/kg/min (the resulting 16 min infusion periods are denoted by the vertical grey bars). We first detected the drug (at the 3-standard deviation confidence level; denoted by dashed, horizontal lines) in the ventricle within 71 to 175 s of the initiation of the infusion. The level of the drug in the ventricles then rises monotonically for the duration of the infusion. NB: animal number is provided next to each panel and is consistent between figures and tables.

When placed in the lateral ventricles of freely moving, normally behaving rats, EAB sensors support seconds-resolved, real-time measurements of absolute (not relative) drug concentrations (Fig. 2). To see this, we placed intracranial sensors in the left lateral ventricles of six animals (See Fig. S2 for histology) and used them to monitor levels of the drug in the CSF before, during, and after a constant IV infusion (5 mg/kg/min) while simultaneously recording the animals' locomotor responses. Based on noise measurements collected over the pre-infusion baseline, we estimate that the sensor's limit of detection for procaine is 3.7 □M (this represents 3 standard deviations above zero for the noisiest sensor), a value that is defined by the affinity of the aptamer and the conservative statistical threshold we have employed, and that is not a fundamental limitation of the EAB approach.

Procaine first reaches the 3.7 mM detection threshold in the ventricles of our animals some 71 to 220 s after the initiation of infusion. When we dose at 80 mg/kg (i.e., 16 min at 5 mg/kg/min) (Fig. 2) these rise to peak concentrations of 58 to 80 □M shortly after the end of the infusion. In contrast, when we dose at 160 mg/kg (i.e., 32 min at 5 mg/kg/min) (Fig. 3) the corresponding peak concentrations range from 122 to 197 □M. After reaching these maximum values, the rapid metabolism of procaine (Azimi, 1994; Qin, 2010; Seifen et al., 1979) causes its concentration to fall with the concomitant recovery of locomotor behavior. In contrast (and as expected), in-vivo control experiments in which we injected only the drug vehicle (1X PBS) failed to produce any significant change in sensor output (Fig. S3).

The enormously improved time resolution of EAB sensors provides hundreds of drug measurements during a single, ~100-150 min period following drug exposure, in turn rendering it possible to identify relations between drug-induced changes in behavior (i.e.

pharmacodynamics) and drug time-concentration profiles (i.e. pharmacokinetics) at the level of *individual animals* with generally good statistical confidence. For example, the correlation between intracranial procaine concentrations and basic locomotion (beambreaks/min), which is, as expected, negative for all animals, is statistically significant for 7 of the 9 animals we investigated (Fig. 4 $R^2 > 0.44$).

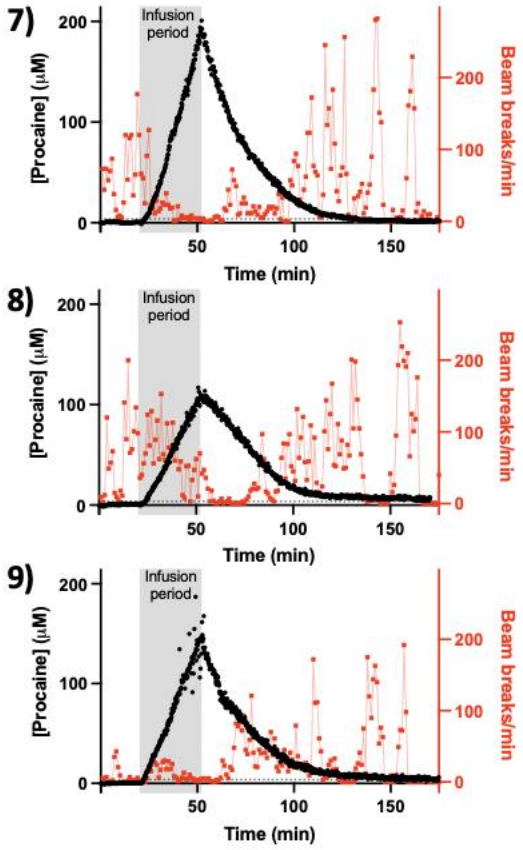


**Figure 3.** E-AB sensors perform well over multiple hours and successfully measure procaine, administered with long infusion times (32 min). Procaine levels (black) in the lateral ventricles of awake, freely behaving rats while simultaneously monitoring their behavior (in red is beam breaks/min), are shown above. Male rats receive a 160 mg/kg continuous IV infusion at rate of 5 mg/kg/min (the infusion period is denoted by the vertical grey bars). In these studies, we first detected the drug (at the 3-standard deviation confidence level; denoted with dashed lines) in within 174 to 220 s of the initiation of the infusion. NB: animal number is provided next to each panel and is consistent between figures.

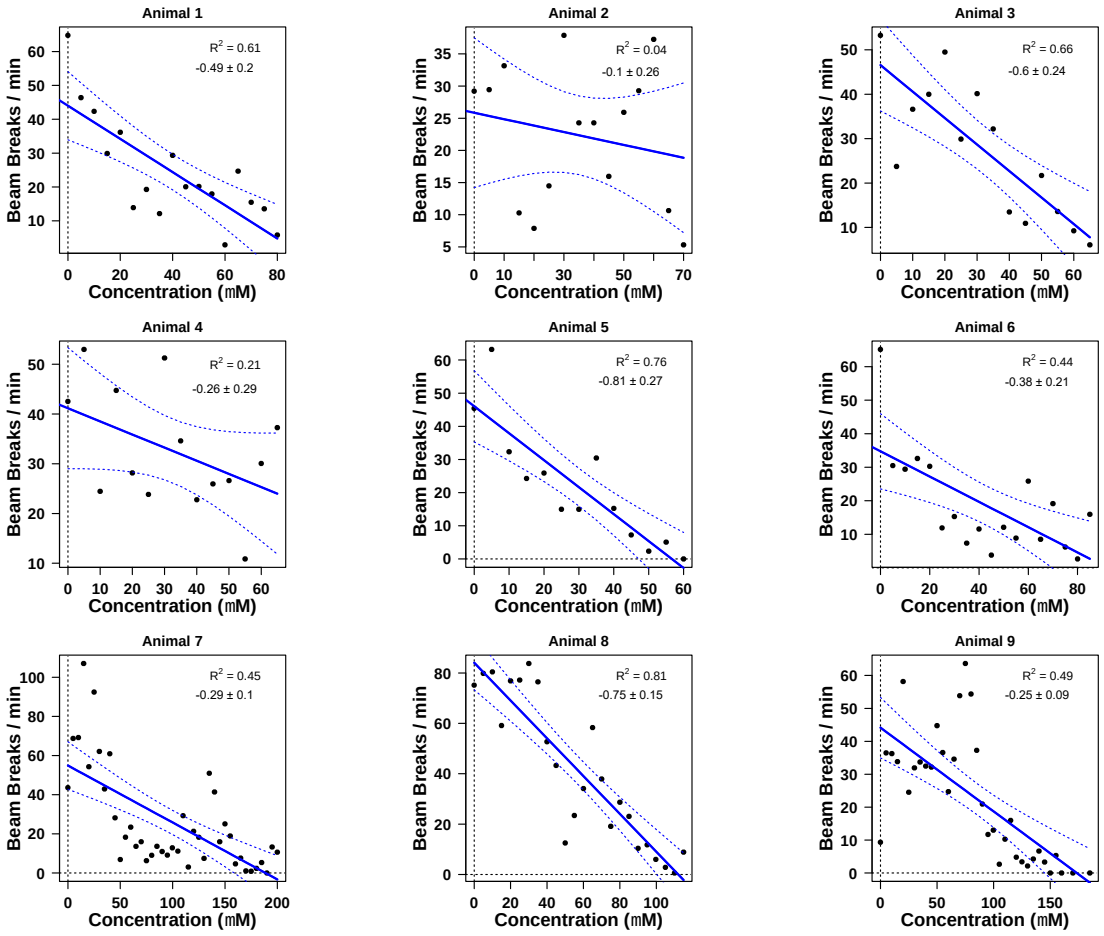


**Figure 4. Correlations between procaine concentration and basic locomotion** For each rat, data is binned by concentration in 5μM increments. Each bin sums the number of beambreaks and divides by the amount of time spent in that concentration bin, resulting in beam breaks/min for each concentration bin. Data is fitted with a simple linear regression model where the bin value is the regressor and beam breaks/min is the response. $R^2$ and 95% CI are included for each animal. Corresponding ρ estimates and 95% asymptotic confidence intervals are seen in Table 1. For animals 2 and, the asymptotic CI's cover 0, implying we fail to reject the null hypothesis that ρ = 0 in these two rats. In the other seven rats, however, the CI do not cover 0 and the ρ estimates vary between -0.66 and -0.90; showing moderate to strong, negative linear correlation in these data.

| **Table 1.** Animal-specific pharmacokinetics and pharmacodynamics | | | | | | |
|---|---|---|---|---|---|---|
| | **pharmacokinetics** | | | **pharmacodynamics** | | |
| Animal | Time to first detection (min) | $C_{max}$ (μM) | $t_{1/2}$ (min) | $R^2$ | Intercept (beam breaks/min) | Slope (beam breaks/min/μM) |
| 80 mg/kg dosing | | | | | | |
| **1** | 1.18 | 66.4 ±0.3 | 13.8 ±0.1 | 0.61* | 44.01 ±9.25 | -0.49 ±0.20 |
| **2** | 1.98 | 57.9 ±0.3 | 11.2 ±0.1 | 0.04 | 25.86 ±10.56 | -0.10 ±0.26 |
| **3** | 2.72 | 66.3 ±0.3 | 14.3 ±0.1 | 0.66* | 46.57 ±9.30 | -0.60 ±0.24 |
| **4** | 2.92 | 61.2 ±0.3 | 15.3 ±0.1 | 0.21 | 40.69 ±10.95 | -0.25 ±0.29 |
| **5** | 1.23 | 65.7 ±0.3 | 10.9 ±0.1 | 0.76* | 46.04 ±9.56 | -0.81 ±0.27 |
| **6** | 1.60 | 79.5 ±0.3 | 8.6 ± 0.1 | 0.44* | 34.77 ±10.37 | -0.38 ±0.21 |
| 160 mg/kg dosing | | | | | | |
| **7** | 2.90 | 197.2 ±0.3 | 15.9 ±0.1 | 0.45* | 54.91 ±11.77 | -0.29 ±0.10 |
| **8** | 3.67 | 122.2 ±0.2 | 19.6 ±0.1 | 0.81* | 84.07 ±10.18 | -0.75 ±0.15 |
| **9** | 2.17 | 137.4 ±0.2 | 17.7 ±0.1 | 0.49* | 44.15 ±8.86 | -0.25 ±0.09 |
| *denotes results are significant at $p < 0.05$ level | | | | | | |

## 5.5 Discussion

Here we have adapted EAB sensors to the problem of monitoring psychoactive drug concentrations in situ in the brains and ventricles of freely moving rats. These measurements, which were collected in real time, were performed in parallel with simultaneous observations of the animals' behavioral (locomotor) responses. The resulting real-time, single-animal, pharmacokinetic profiles for procaine achieved time resolution of 10 to 11 s in experiments that spanned up to multiple hours. The large data volumes this unprecedented time resolution provides enabled the identification of strong correlations ($R^2$ as great as 0.81) between intracranial drug levels and behavior (locomotor function) within individual animals.

The EAB approach described here represents a significant advance in our ability to monitor brain chemistry. Indeed, we are aware of only 3 prior reports of drug measurements being performed in situ in the brains of live animals *at all*, all of which required averaging over multiple animals to achieve statistical significance. In two, Rocchitta et al. employed an enzymatic sensor specific for alcohols to measure ethanol in the brains of awake, behaving rats, albeit with averaging over multiple animals (Rocchitta et al., 2012, 2019). In the third, Taylor et al. employed a sensor similar to that described here to monitor cocaine in the brains of anesthetized rats after 2 mg/kg IV dosing, but they had to average over four sensors placed in the brains of two animals (Taylor et al., 2017). For example, the study reports peak in-brain cocaine concentrations of 15 □M, a value exceeding by many-fold the peak levels measured in prior microdialysis studies employing similar drug doses (S. H. Ahmed et al.,

2003; Bradberry et al., 1993; Hurd et al., 1988; Minogianis et al., 2019; H.-T. Pan et al., 1991; Pettit & Pettit, 1994; Rocchitta et al., 2012, 2019).

Although the measurements presented here are of significantly improved resolution relative to prior microdialysis studies, the peak concentrations and pharmacokinetic timescales we observe are consistent with those seen previously. The only prior measurements of intracranial procaine levels that we are aware of employed the removal of CSF from anesthetized dogs with a sampling interval of 3 min (or greater), saw peak concentrations of 150 □M some 12 min after a 50 mg/kg infusion (Usubiaga et al., 1967), values reasonably close to those we report here for the rat. In contrast, microdialysis studies of intracranial cocaine levels are relatively plentiful, including many studies that, like the procaine studies described here, were performed in rats, proving an opportunity to compare state-of-the-art time resolution on in-brain drug measurements and the consequences poor resolution has on our understanding of pharmacokinetics (S. H. Ahmed et al., 2003; Bradberry et al., 1993; Hurd et al., 1988; Minogianis et al., 2019; H.-T. Pan et al., 1991; Pettit & Pettit, 1994; Rocchitta et al., 2012, 2019). Prior microdialysis studies typically employed sampling intervals of between 4 and 20 min. Due to the poor match between such sampling rates and the timescale of cocaine pharmacokinetics, the large majority of these studies observed peak concentrations in their first sample, implying their time resolution was too poor to accurately capture either the height or the timing of the peak. In contrast, a recent study by Minogianis and co-workers that employed microdialysis to achieve 2 min time resolution (although their sampling rate was 1 min, their system required 2 min to equilibrate; see figure 2 of ref. (Minogianis et al., 2019)) was able to capture peak drug

concentrations, as the authors typically collected at least 2 data points (samples) prior to observing the peak, highlighting the value of improved time resolution in the study of psychoactive drugs and their behavioral effects.

Both the order of magnitude improvement in time resolution over the *best* microdialysis-derived intracranial drug measurements (which represents a two orders of magnitude improvement over *typical* microdialysis studies) and the real-time capabilities of EAB sensors should enable a better understanding of pharmacology and its effects on behavior. For example, the improved temporal resolution of EAB sensors provided unique opportunities to identify both inter-subject differences (e.g., the animal-specific drug half-lives we observed) and inter-subject similarities (such as the pharmacodynamic effects of procaine on relative locomotion) between individual animals with good statistical significance. Finally, moving forward the real-time capabilities of EAB measurements should enable powerful new feedback-controlled approaches to studying pharmacology, including closed-loop feedback control (Arroyo-Currás, Ortega, et al., 2018; Dauphin-Ducharme et al., 2019) over in-brain drug levels and the drug-level-driven optogenetic manipulation of neural circuits (Newman, 2015). Overall, such approaches will evolve the study of neuropsychopharmacology by allowing detailed elucidation of in-brain concentration to response analyses necessary to improve our understanding of the impact of drug levels on behavioral and neural outcomes.

# Chapter 6

# General Discussion

## 6.1 Summary

The findings presented in this dissertation demonstrate the potential of E-AB sensors to be applied to the field of neuropsychopharmacology. Although further improvements to the E-AB platform are necessary for more generalized employment in pharmacology and neuroscience, my thesis has developed and/or modified EAB sensors to enable the monitoring of endogenous molecules in blood, the tracking of molecules as they move from vein to brain, and the monitoring of molecules in the brains of freely-moving subjects. Overall, the thesis represents the achievement of several milestones in the development of a potentially generalizable approach to monitoring molecules in vivo.

In the first study (described in Chapter 2), I focused on development of a novel EAB against an endogenous target. As a proof of principle, point of care (POC) diagnostic tool, I developed an EAB for the measurement of tryptophan. By using an inorganic receptor-Tryptophan complex I was successful in generating an ex-vivo E-AB sensor that responds across the entire physiologically relevant tryptophan concentration ranges observed in healthy individuals, as well as patients suffering from metabolic disorders such as Tryptophaneuria. While this proof of principle study has important clinical applications as a POC device, this particular E-AB sensor is not suitable for in-vivo applications as it is not reagentless. Specifically, the reliance of the E-AB sensor on the target-inorganic receptor complex for aptamer binding precludes this sensor from being deployed directly in-vivo as it would require the addition of the inorganic receptor to the animal. As such, this sensor fails one of the five key requirements outlined in the introduction of this dissertation. In response

to this my focus shifted towards the development of a sensor for a similar target that did not require the addition of any exogenous agent in order to function.

In Chapter 3 of this dissertation, I described an E-AB sensor specific to the amino acid phenylalanine and its subsequent deployment in the circulatory system of a rat model to enable monitoring in a living subject. The resulting, seconds-resolved, real-time measurements of this endogenous metabolite represent the first such data collected using an enzyme-free biosensor, that is, a sensor independent of the target's chemical reactivity. In doing so I was able to monitor the plasma phenylalanine levels, in real-time, directly in the veins of live rats with low-micromolar concentration sensitivity and 12 s temporal resolution. The orders-of-magnitude improved time resolution enabled the high-precision determination of physiological phases that are too rapid to capture using traditional approaches which rely on blood draws or microdialysis. It also produces sufficient numbers and quality of data to characterize the kinetics of individual animals with excellent statistical significance, thus providing an unprecedented tool with which to study inter-subject disposition kinetics variability.

Critically, the monitoring of Phe represents the first ever real-time monitoring of any endogenous target in situ within a living subject using an E-AB. Other approaches (electrochemical enzyme-based sensors) have performed similar monitoring for glucose, lactate, and the amino acid, glutamate, however, this approach has extremely limited generalizability due to the need for a highly specific enzyme that produces a redox reactive product (i.e., H2O2). Importantly, we developed a unique calibration procedure that enabled not only the quantification of relative changes in PHE concentrations, but also the

determination of the basal levels present at the time of sensor insertion. In-vivo E-AB measurements of Phe directly in the jugular veins of rats revealed similar peak concentrations, distribution rates, and elimination rates for all animals. Moreover, my sensor was also sensitive to subtle differences in physiological state of the subjects. For fasted animals, plasma phenylalanine levels returned to within 20% of the pre-dosing baseline over the course of approximately 20 min. In contrast to the situation with fasted animals, however, the plasma phenylalanine levels of non-fasted animals remained elevated by ~50% above pre-challenge baseline levels over the course of these experiments. The high-precision, data rich, measurement generated by in-vivo E-AB recordings rendered it possible to discern metabolic differences between animals of different (i.e. fed vs food restricted) as well as inter-subject metabolic variabiltiy.

In general, the ability to measure endogenous targets is an important aspect in the study of neuropsychopharmacology as the behavioral effects of psychoactive drugs are often driven by altering endogenous molecules in the brain. The specific mechanisms of action of psychoactive drugs in the brain are extremely complex, involving connections between multiple brain regions and a variety of chemical and electrical signaling mechanisms. At its core, however, one fundamental mechanism governing psychoactive drugs (in particular, for example, most psychostimulants and antidepressants) actions is altering neural activity and behavior by *indirectly* changing levels of chemical messengers in the brain. Conversely, even direct agonists are known to produce a variety of downstream neurochemical alterations important to their behavioral effects. While this perspective is extremely reductionist, it highlights that in order to fully understand drug action in the

brain, we must be able to measure drugs themselves, the chemical messengers they act upon, as well as the associated behaviors. No prior sensing platform is capable of detection of both drugs and endogenous molecules, such as neurotransmitters, on biologically relevant timescales. As such, the E-AB platform has the potential to fill this gap.

The fourth chapter of this thesis shows the adaptation of the E-AB sensor platform to make in brain measurements possible and its application to the study of drug transport between two compartments. Moving from a three-electrode set up to a two-electrode set up I was able to monitor the antibiotic vancomycin directly in the brain of an awake, ambulatory rat, again, these measurements are performed in real-time at high temporal resolution in an unprecedented fashion for any drug. Next, I coupled the novel in-brain platform with the established in-vein platform to perform simultaneous measurements of the drug in both the CSF and the circulatory system, following intravenous administration i.e., monitoring the drug as it moves from vein to brain. The hundreds of paired data points generated in these experiments allowed for the determination of high-precision estimates of the rate constants for transport into the CSF as well as drug elimination via the kidneys. To build on this further I, in conjunction with collaborators in computational modeling, compared the estimates generated using one compartment data (CSF only) vs both data sets (CSF and plasma). Although the collection of hundreds of concentration values in one compartment over a single drug lifetime enables high-precision estimates of the parameters describing intracranial transport, due to a mathematical equivalence the data produced two divergent descriptions of the drug's pharmacokinetics that fit the data equally well. Conversely, the simultaneous collection of intravenous measurements, however, resolved

this ambiguity, enabling high precision (<10% at the 95% confidence level estimates of the key pharmacokinetic parameters describing transport from the blood to the cerebrospinal fluid in individual animals. The availability of such simultaneous, high-density “in-vein” (plasma) and “in-brain” (cerebrospinal fluid) measurements also provides an opportunity to explore the assumptions almost universally employed in prior compartmental models of drug/molecule transport, allowing us to quantitatively address (rather than simply assume), for example, whether the targeted drug is subject to bulk transport out of the central nervous system via the lymphatic system or other route.

This study highlights the potential of EAB sensors in the tracking intercompartmental molecular transport in the living body and has research implications that extend beyond the study of just vancomycin. For example, while this study focused on the blood/CSF barrier, the same technique could be applied to study the blood-brain barrier. The blood-brain barrier (BBB) is a significant obstacle in the development of therapeutic drugs that target the brain, and, as such, a significant amount of research is devoted to this subject. E-AB sensors could be used to increase our understanding of the BBB itself, as well as assessing strategies to modulate the penetration of therapeutics through it.

The final experimental portion of this thesis in Chapter 5 applied the E-AB platform directly to the study of neuropsychopharmacology. Using the in-brain E-AB platform the resulting multi-hour, real-time measurements achieving ultra-high temporal resolution of a drug in brain as good as 10 s and with precision lower than 4 μM (as defined by the 99% CI of the sensor baseline). This time resolution represents an order of magnitude improvement over the best prior microdialysis studies of intracranial drug levels and two orders of

magnitude better than typical studies. Equally, the sensitivity is sufficient to establish complete pharmacokinetic analyses at levels relevant to the behavioral effects of the drug. These high-volume data sets similarly permit the comparison of pharmacokinetic differences between individuals. One-compartment fits of the data revealed unprecedentedly precise pharmacokinetic estimates with an average 95% confidence intervals of 6s for estimated half-life and 0.3 μM for estimates of $C_{max}$.

The hundreds of paired data points collected per animal likewise permitted establishing the relation between dynamic in-brain drug concentrations with behavioral effects of the drug. Namely, I observed statistically significant correlations between in-vivo drug concentrations and the behavioral responses of individual subjects with an average $R^2$ = 0.67 for intracranial procaine concentration versus overall locomotion. These initial results thus showcase the utility of EAB molecular measurements in the determination of the site-specific, seconds-resolved neuropharmacokinetics of individual subjects which can be correlated to drug-induced changes in individual behavior. Thus, allowing determination of concentration-behavior response relations as opposed to mere dose-response relation (that are agnostic to concentration of pharmacological agent at site of action) using conventional techniques.

**6.2 Limitations of these studies**

One limitation of the study performed in chapter 3 pertains to the calibration curves generated for this experiment. These in vitro calibrations were performed at room temperature, significantly lower than the temperature of the environment when the E-AB

sensor is deployed in-vivo. Differing temperatures could alter the rate of electron transfer of the aptamers covalently attached redox reporter and thus alter the signal gain of the sensor at each frequency for a given frequency, ultimately changing calibration curve. Any differences between the calibration curves would be reflected in the in-vivo data generated, leading to incorrectly reported concentration values. In order to determine, and solve, this potential issue, the calibrations should be repeated at body temperature and applied to the in-vivo data to update the pharmacokinetic parameters; this is being performed in on-going projects aimed at tracking Phe in multiple compartments of the body.

Another general limitation, particularly as it relates to the employment of EAB sensors to further our understanding of neural and pharmacological determinants of behavior, is the currently available aptamer-based sensors employed in my studies. Although the EAB platform is generalizable to multiple targets, the realization of this potential is only beginning. Our group (including myself) is actively engaged in the development of sensors that are relevant to understanding addiction neurobiology. For instance, we have long sought a sensor to monitor cocaine levels in the brain, however, to date this effort is still in progress. In fact, the EAB that I employed to monitor procaine is also responsive to cocaine but the sensitivity is not optimal for behavioral studies. Not included in the present thesis, I have performed preliminary assessment of the same sensor for monitoring in-brain cocaine and while it does “work”, robust signal detection has only been observed following bolus dosing with 15 mg/kg IV—dosing much higher than normally employed in behavioral paradigms. Similarly, our group is developing an EAB against serotonin (based on a previously reported serotonin aptamer (Nakatsuka, 2018)) but we, to date, we have not found reliable

responses in this sensor. As such, a significant area of critical need for progress in order to apply EAB sensors to generally study neuropsychopharmacology is creation of novel EABs.

## 6.3 Opportunities for improved adaptation of the E-AB platform to neuropsychopharmacology

**6.3.1** ***Improvements to SELEX.*** The E-AB platform is only as powerful as the aptamers they employ as their recognition elements. As such, advances and modifications in the selection process of aptamers presents an avenue to improve E-AB sensors. In order to improve aptamer selection, specifically for E-AB sensing, the SELEX process could be tweaked to better reflect the target environment. Aptamers could be selected for in physiologically relevant buffers (e.g., neurotransmitter targeting aptamers could be selected for in, ideally cerebral spinal fluid, or minimally artificial CSF), and at body temperature, in order to better mimic the environment in which the aptamer-based sensors will be employed. Furthermore, SELEX is performed in solution phase, whereas E-AB sensors use surface bound aptamers. Anchoring of the aptamer often producing large shifts in affinity of the aptamer for a target (Watkins et al., 2012) and, thus, modifying the SELEX protocol with surface adherence may lead to aptamers that have better affinities for specific targets when used in the E-AB platform.

**6.3.2** ***Sensor lifetime.*** The ability to perform longer duration measurements over multiple days, or even weeks, would expand the uses of the EAB platform drastically. It could for example, be used for continuous tracking of a neurotransmitter for the entire duration of a behavioral study, as opposed to simply during a particular trial of the study. Beyond

neuroscience, improved sensor lifetime would open the door for wearable technology, like the continuous glucose monitor. To date, E-AB sensors have successfully been deployed for up to 12 hours in the veins of awake, ambulatory rats (Arroyo-Currás, Ortega, et al., 2018). While the time course of this particular study is impressive, it must be noted that the precision of the measurements decreases significantly after the 6-hour mark (Arroyo-Currás et al., 2017). This loss of precision of E-AB sensors over time is driven by sensor degradation that is hypothesized to stem from two major sources. The first, and most significant is biofouling (Leung et al., 2021). When challenged in biological media, or in-vivo, aggregation occurs on the surface of the sensor over time, causing a reduction in the relative signal gain resulting in sensor drift. While the drift caused by fouling appears to saturate after around 90 minutes in whole blood, the relative signal loss during that period is usually around 50-60% (Leung et al., 2021). The second contributor to sensor signal decay is due to loss of the reporter-modified DNA via electrochemistry-driven desorption of the monolayer (Leung et al., 2021). While this contribution to signal decay is relatively minor in comparison to fouling over a short period, there is no saturation point for this cause of signal loss as it is caused by the interrogation of the sensor itself. Thus, as observed in Arroyo-Currás et al (2017) current versions of EAB sensors have a finite employment.

In order to correct for signal drift, Kinetic differential measurements (KDM; described in chapters 3-5) is employed. This loss in relative signal gain, due to fouling and sensor interrogation, however, still leads to a decrease in the overall signal to noise ratio of the sensor. Thus, ultimately sensor longevity is defined by inability to overcome noise due to loss

of signal. In order to increase the durability of E-AB sensors the impact of these two sources of sensor degradation must be reduced.

To target signal decay associated with fouling agents specifically, surface membranes and coatings, could provide a good approach by limiting access to the sensor surface. Hydrogel coatings have been shown to reduce fouling by blocking the access of potential fouling agents above a certain size. The pore size of the membrane can be changed to alter the size limit cut off point, however the sensing target must be smaller than the pore size in order to gain access. Even if the target of interest is small enough to access the sensor surface the membrane can reduce the response time of the sensor and therefore a tradeoff between sensor lifetime and meaningful temporal resolution of the sensor, particularly if real-time data is required, may arise. That is the employment of protective coatings can result in delays in between changes in concentration and response of the sensor.

Loss of signal associated with voltametric scanning of the sensor has been shown to be greatly reduced by simply altering the scanning window of the sensor to minimize oxidative/reductive loss of the monolayer. A recent paper from the Plaxco group demonstrates simply narrowing the potential window of an E-AB sensor to between -0.2 to -0.4 V versus Ag/AgCl significantly diminishes the loss of signal resulting from sensor scanning (Leung et al., 2021). Thus, measurement parameters of the voltammetry can be optimized to increase their longevity. Although this provides increased duration, it does not eliminate sensor signal degradation.

Altering the composition of the surface assembled monolayer (SAM) may provide an avenue to minimize the contributions of both fouling and voltametric scanning to signal loss and improve sensor stability over time. For example, antifouling monolayer head-groups can reduce fouling induced signal decay (44/23 Downs). Alternatively, use of a 1-hexanethiol monolayer has been shown to be more resistant to desorption from the surface even when deployed in blood serum for up to 60 hours. While the 1-hexanethiol monolayer can alter an aptamers response to target, combining both mercaptohexanol and 1-hexanethiol monolayers results in improved sensor stability, without affecting the aptamers response to target.

**6.3.3** ***Miniaturizing the in-brain E-AB platform.*** The in-brain E-AB platform presented in this dissertation employs a working electrode that is 76 µm in diameter and 3 mm in length. This sensor architecture is well suited to making ventricular measurements and could even be used to target brain structures with large enough dorsal/ventral coverage (e.g., hippocampus). While the diameter of this E-AB sensor poses few spatial constraints in the rat brain, the length of 3 mm precludes the sensor from being able to measure in many regions, let alone, functionally-distinct subregions of the brain. For example, while these dimensions are suitable for making hippocampal measurements, the sensor cannot, in its current form, specifically target any of the hippocampal subregions (e.g., CA1-4/dentate gyrus/subiculum). These subregions have been shown to have distinct functional differences (Lepage et al., 1998; Moser & Moser, 1998; Schacter & Wagner, 1999; Zeineh et al., 2001, 2003). Miniaturization of the platform would allow for more precise spatial resolution to further elucidate the specific functionalization of these, and

other, neural subregions in the brain. Smaller sensors would also allow for the expansion of the in-brain E-AB platform to smaller animal models, such as mice. Mice models have advantages over rat models for certain research topics (e.g., certain transgenic models have been more established in mice) and the ability to use E-AB technology in mice would expand the ability to coordinate with recent and emerging research technologies.

A recent approach toward miniaturizing the size of E-AB sensors focuses on increasing the microscopic surface area of the working electrode. By increasing the surface area, more aptamers can be attached to surface to generate a higher baseline current and significantly improve the signal to noise ratio. As detailed in Chapters 3-5 of this dissertation, this has largely been done, to date, by electrochemically roughening the electrode surface using chronoamperometry. Recently, however, nanoporous gold substrates, capable of increasing surface area significantly more than chronoamperometric methods, have been employed that have resulted in a 6-fold reduction in the necessary probe size without decrement in signal-to-noise during measurements in blood (Downs et al., 2021). Further exploration of nanoporous gold substrates and applying this to the in-brain E-AB platform could pave the way for even finer probe dimensions to enable highly-localized, subregion specific in-brain measurements. Assuming both the geometric and nanoporous strategies work and are mutually compatible, we could develop probes that are in the range of 200 μm diameter and about 150 μm (i.e., 1 mm divided by 6) in length which would, for instance, well match, subregions of the rat nucleus accumbens or even the mouse nucleus accumbens. Thus, there are existing avenues to enhancing the physical

parameters of EAB probes to make them more compatible with monitoring molecules in brain.

Another, relatively simple, approach to better matching sensor dimensions to brain region size is to produce a more proportional sensor. To this end, we have started to assess the use of thicker wire (200 μm) that, while still implantable in the brain, might allow for reduction in sensor length. Again, a tradeoff is involved wherein the thicker probe may produce greater tissue disruption when placed into brain; however, it is worth pointing out that traditional (e.g., microdialysis) and recent (e.g., optic sensors monitored by fiberphotometry) strategies employ probes that are of similar thickness. Mathematically, the increased diameter would permit sensor length to be reduced to ~ 1 mm without loss of surface area and presumably without loss of total signal; this length would approximate the dorsal-ventral boundaries of many more brain regions, for instance, the rat nucleus accumbens. Thus, one general approach to better matching EABs to brain region targets is the geometric reconfiguration of the probe.

Assuming both the geometric and nanoporous strategies work and are mutually compatible, we could develop probes that are in the range of 200 μm diameter and about 150 μm (i.e., 1 mm divided by 6) in length which would, for instance, well match, subregions of the rat nucleus accumbens or even the mouse nucleus accumbens. Thus, there are existing avenues to enhancing the physical parameters of EAB probes to make them more compatible with monitoring molecules in brain.

**6.4 Future directions in neuropsychopharmacology**

**6.4.1** ***Validation of EAB platform for in-brain monitoring.*** Before this technology can be widely adopted by the neuroscience community, it is essential that the platform is validated using the current gold standard technique, microdialysis. While my observed levels of procaine in brain do match fairly well to previously reported data, in order to further validate the sensor, the study in Chapter 5 could be repeated using concurrent microdialysis. An E-AB sensor and a microdialysis probe could be inserted simultaneously, and contralaterally into the lateral ventricle (or in brain tissue) and the resulting pharmacokinetic profiles and parameters using each technique could be compared to demonstrate the accuracy of the E-AB platform. While a comparison could be done by using each technique in an independent animal, performing both techniques in a single animal would remove inter-animal differences in drug pharmacokinetics as a potential confounding variable.

**6.4.2** ***Expansion of targets.*** In this dissertation I have successfully adapted the E-AB platform to measure two drugs in the brain, one of which is psychoactive. While this is a significant step forward, in order to better support neuropsychopharmacological research, the number of targets that can be measured, in-brain, using the E-AB platform must be expanded. Prior electrochemical techniques are incapable of measuring several important neurotransmitters such as GABA, Glycine and acetylcholine, as well as most neuropeptides, as well as all psychoactive drugs, except alcohol. The amino acid neurotransmitter GABA, for example, is the primary inhibitory neurotransmitter in the central nervous system and has been heavily implicated in the stimulant and opiate drug use. Neuropeptide Y is also implicated in the neuromodulation of responses to drugs of abuse, such as psychostimulants. Microdialysis, with its unsuitable temporal resolution, is currently our only method of

detection of these important molecules and therefore our understanding of their dynamics is limited. As such, I believe these endogenous targets that cannot be measured by prior electrochemical methods should be prioritized in conjunction with psychoactive drugs in the expansion of E-AB in-brain targets, so as their relationship can be better understood.

***6.4.3 Simultaneous measurement of related targets.*** One of the major advantages of E-AB sensors is that they are generalizable to multiple targets by incorporation of appropriate aptamers indicating that they have to potential to monitor multiple molecular targets with the possibility of multiplexing the sensor for simultaneous monitoring. For instance, simultaneous real-time monitoring of the psychoactive drug cocaine and serotonin (5-HT). 5-HT is a critical neuromodulator that has been described as "involved in everything" (Muller & Homberg, 2015), and cocaine has been shown to modulate its levels, however the relationship is much less understood than cocaine and dopamine. Prior theories propose that the primary function of 5-HT in the brain is to modulate anxiety and stress (Wise et al., 1970). Therefore, it follows that 5-HT should be involved, at least indirectly, in addiction. Cocaine shows both anxiolytic and anxiogenic properties and 5-HT has been implicated in the latter (Klein et al., 2017). Recent studies involving Serotonin Reuptake Transporter (SERT) KO rats, however, show that 5-HT may actually be more directly involved in an inhibitory role in the establishment of addiction and the motivational/reinforcing aspect of psychostimulants such as cocaine (Homberg et al., 2008; Sora et al., 2001). SERT KO rats show higher cocaine self-administration in short access as well as larger escalation in long access conditions (Sora et al., 2001) and show increased drug seeking behavior during extinction. SERT KO show higher levels of extracellular 5-HT, in general, compared to

wildtypes due to the removal of transporters that sequester free 5-HT in synapses, however, tissue levels of 5-HT are lower in the dorsal striatum and hippocampus (Homberg et al., 2007). As such, it is possible that the reduction in 5-HT in these regions could decrease the inhibitory role of 5-HT on the motivational/reinforcing nature of psychostimulants. To further build upon these findings, levels of cocaine and 5-HT could be monitored simultaneously using addiction operant models.

**6.4.4** ***Concentration controlled neuropsychopharmacology.*** Current experimental approaches in neuropsychopharmacology focus on dose-controlled experiments in which animals receive the same cumulative drug dose as each other and resulting perturbations in behavior are observed. While this approach can highlight individual differences in animals' behavioral responses, it cannot consider, nor can it reveal, individual differences in animal neuropharmacokinetics. In light of this shortcoming, E-AB sensors are capable of altering, and precisely controlling the pharmacokinetic profiles of drugs in the circulatory systems of rats, through feedback-controlled drug delivery. Applying this technique to the brain could prove a powerful tool. It would allow researchers to control and manipulate the neuropharmacokinetic profile of a particular drug across various animals in a study. Simultaneously measuring behavioral responses could elucidate the relationship between pharmacokinetics and behavior. As an example, this tool could be applied to the field of addiction research by allowing us to investigate, in an entirely controlled manner, the role that individual pharmacokinetics play in the manifestation and maintenance of addiction. For instance, one could employ feedback control to achieve the same pharmacokinetic profile (i.e., time-dependent changes in concentration) in a group of subjects regardless of

individual differences (Vieira et al., 2019) or one could achieve static concentrations of a drug at any desired level to examine individual responses upon initial exposure as well as hold the concentration for prolonged periods to examine neuroadaptive and behavioral responses.

***6.4.5 Closed loop feedback-controlled optogenetics.*** Because E-AB sensors easily achieve high temporal resolution (here in the few seconds but up to 100s of msec) and, more importantly, they function in real-time with essentially zero-time lag, they could be used in closed-loop engineering approaches to drive effectors of neural response, such as optogenetics. The concept of closed-loop "neuroengineering" has the potential to dramatically reshape our understanding of the brain and behavior (Potter et al., 2014) due to its ability to link specific quantitative events (e.g. a level of a drug or neurotransmitter in a specific brain region) to an immediate modulation of neural response. Researchers have demonstrated that, real-time measurements of neuronal outputs (e.g., dopamine levels (McCutcheon et al., 2014)) can be coupled with the optical manipulation of neuronal activity (via neurons transfected with light-sensitive ion channels) to achieve closed-loop feedback control of neural circuits. Here, the response of a neuronal system to a perturbation can be quantified and communicated back to the circuit on physiologically relevant timescales. This approach provides compelling tests of models of neuronal dynamics, connectivity, and causation [e.g., (Edward & Kouzani, 2020; Grosenick et al., 2015)], and is proving a powerful tool for under-standing neural circuits and their dynamics. Such tools are also likely to have clinical applications, for instance, in the management of epilepsy in which detection of epileptiform discharges can be used to drive inhibition of an identified epileptic foci to prevent full-blown seizures (Stieve et al., In Press). However, the necessary "detectors"

available to provide the real-time by monitoring of molecular events remain a crucial limitation in closed-loop neuroengineering. Given that E-AB sensors are likewise real-time, and have been shown to support feedback control of drug delivery (Arroyo-Currás, Ortega, et al., 2018; Dauphin-Ducharme et al., 2019), they are ideally positioned for incorporation into other closed-loop strategies. For instance, EAB for psychoactive drugs or neurotransmitters could be integrated into closed-loop neural circuits. For example, we could optogenetically inhibit serotonin transmission from the dorsal Raphe into the prelimbic cortex following detection of a precise level of cocaine to infer the importance of this neural process in the drug-driven control of reward/reinforcement-seeking behavior.

**6.6 Conclusions**

In conclusion, this dissertation contributes to both the field of neuroscience and E-AB sensing. The ability to measure endogenous targets drastically expands the list of potential targets in the brain, and body. Using multiple compartment measurements with E-AB sensing, we can study the transport of these targets within the body with a level of precision previously unattainable. Finally, simultaneous high precision measurements of psychoactive drugs, in conjunction with behavior, allows us to explore how drug concentration, as well as individual pharmacokinetics, influence behavior. Together, I believe these milestones lay the foundation for a powerful new technique for studying neuropsychopharmacology.

**References**


1. Addy, N. A., Daberkow, D. P., Ford, J. N., Garris, P. A., & Wightman, R. M. (2010). Sensitization of Rapid Dopamine Signaling in the Nucleus Accumbens Core and Shell After Repeated Cocaine in Rats. *Journal of Neurophysiology*, *104*(2), 922–931. https://doi.org/10.1152/jn.00413.2010

2. Ahmed, M. U., Saaem, I., Wu, P. C., & Brown, A. S. (2014). Personalized diagnostics and biosensors: A review of the biology and technology needed for personalized medicine. *CRITICAL REVIEWS IN BIOTECHNOLOGY*, *34*(2), 180–196. https://doi.org/10.3109/07388551.2013.778228

3. Ahmed, S. H., Lin, D., Koob, G. F., & Parsons, L. H. (2003). Escalation of cocaine self-administration does not depend on altered cocaine-induced nucleus accumbens dopamine levels. *Journal of Neurochemistry*, *86*(1), 102–113. https://doi.org/10.1046/j.1471-4159.2003.01833.x

4. Al Hafid, N., & Christodoulou, J. (2015). Phenylketonuria: A review of current and future treatments. *TRANSLATIONAL PEDIATRICS*, *4*(4), 304–317. https://doi.org/10.3978/j.issn.2224-4336.2015.10.07

5. Albrecht, L. M., Rybak, M. J., Warbasse, L. H., & Edwards, D. J. (1991). Vancomycin Protein Binding in Patients with Infections Caused by Staphylococcus Aureus. *DICP*, *25*(7–8), 713–715. https://doi.org/10.1177/106002809102500701

6. Anderzhanova, E., & Wotjak, C. T. (2013). Brain microdialysis and its applications in experimental neurochemistry. *Cell and Tissue Research*, *354*(1), 27–39. https://doi.org/10.1007/s00441-013-1709-4

7. Ariansen, J., Heien, M. L. A. V., Hermans, A., Phillips, P. E. M., Hernadi, I., Bermudez, M., Schultz, W., & Wightman, R. M. (2012). Monitoring extracellular pH, oxygen, and dopamine during reward delivery in the striatum of primates. *Frontiers in Behavioral Neuroscience*, *6*. https://www.frontiersin.org/article/10.3389/fnbeh.2012.00036

8. Arroyo-Currás, N., Dauphin-Ducharme, P., Ortega, G., Ploense, K. L., Kippin, T. E., & Plaxco, K. W. (2018). Subsecond-Resolved Molecular Measurements in the Living Body Using Chronoamperometrically Interrogated Aptamer-Based Sensors. *ACS Sensors*, *3*(2), 360–366. https://doi.org/10.1021/acssensors.7b00787

9. Arroyo-Currás, N., Ortega, G., Copp, D. A., Ploense, K. L., Plaxco, Z. A., Kippin, T. E., Hespanha, J. P., & Plaxco, K. W. (2018). High-Precision Control of Plasma Drug Levels Using Feedback-Controlled Dosing. *ACS Pharmacology & Translational Science*, *1*(2), 110–118. https://doi.org/10.1021/acsptsci.8b00033

10. Arroyo-Currás, N., Somerson, J., Vieira, P. A., Ploense, K. L., Kippin, T. E., & Plaxco, K. W. (2017). Real-time measurement of small molecules directly in awake, ambulatory animals. *Proceedings of the National Academy of Sciences of the United States of America*, *114*(4), 645–650. https://doi.org/10.1073/pnas.1613458114

11. Aucella, F., Lauriola, V., Vecchione, G., Tiscia, G. L., & Grandone, E. (2013). Liquid chromatography–tandem mass spectrometry method as the golden standard for therapeutic drug monitoring in renal transplant. *Journal of Pharmaceutical and Biomedical Analysis*, *86*, 123–126. https://doi.org/10.1016/j.jpba.2013.08.001

12. Azimi, P. H. (1994). Concentrations of procaine and aqueous penicillin in the cerebrospinal fluid of infants treated for congenital syphilis. *The Journal of Pediatrics*, *124*, 649–653.

13. Baker, B., Lai, R., Wood, M., Doctor, E., Heeger, A., & Plaxco, K. (2006). An electronic, aptamer-based small-molecule sensor for the rapid, label-free detection of cocaine in adulterated samples and biological fluids. *JOURNAL OF THE AMERICAN CHEMICAL SOCIETY*, *128*(10), 3138–3139. https://doi.org/10.1021/ja056957p

14. Baker, K. L., Bolger, F. B., & Lowry, J. P. (2015). A microelectrochemical biosensor for real-time in vivo monitoring of brain extracellular choline. *The Analyst*, *140*(11), 3738–3745. https://doi.org/10.1039/C4AN02027H

15. Bard, A. J., & Faulkner, L. R. (2002). *Student Solutions Manual to accompany Electrochemical Methods: Fundamentals and Applicaitons, 2e*. John Wiley & Sons.

16. Beach, J. E., Perrott, J., Turgeon, R. D., & Ensom, M. H. H. (2017). Penetration of Vancomycin into the Cerebrospinal Fluid: A Systematic Review. *Clinical Pharmacokinetics*, *56*(12), 1479–1490. https://doi.org/10.1007/s40262-017-0548-y

17. Beitollahi, H., Karimi-Maleh, H., & Khabazzadeh, H. (2008). Nanomolar and Selective Determination of Epinephrine in the Presence of Norepinephrine Using Carbon Paste Electrode Modified with Carbon Nanotubes and Novel 2-(4-Oxo-3-phenyl-3,4-dihydro-quinazolinyl)- *N* ′-phenyl-hydrazinecarbothioamide. *Analytical Chemistry*, *80*(24), 9848–9851. https://doi.org/10.1021/ac801854j

18. Bik-Multanowski, M., & Pietrzyk, J. J. (2011). Blood phenylalanine clearance and BH4-responsiveness in classic phenylketonuria. *MOLECULAR GENETICS AND METABOLISM*, *103*(4), 399–400. https://doi.org/10.1016/j.ymgme.2011.04.014

19. Blau, N., van Spronsen, F. J., & Levy, H. L. (2010). Phenylketonuria. *LANCET*, *376*(9750), 1417–1427. https://doi.org/10.1016/S0140-6736(10)60961-0

20. BOURGET, L., & CHANG, T. (1986). PHENYLALANINE AMMONIA-LYASE IMMOBILIZED IN MICROCAPSULES FOR THE DEPLETION OF PHENYLALANINE IN PLASMA IN

PHENYLKETONURIC RAT MODEL. *BIOCHIMICA ET BIOPHYSICA ACTA*, *883*(3), 432–438. https://doi.org/10.1016/0304-4165(86)90281-3

21. Bradberry, C. W., Nobiletti, J. B., Elsworth, J. D., Murphy, B., Jatlow, P., & Roth, R. H. (1993). Cocaine and cocaethylene: Microdialysis comparison of brain drug levels and effects on dopamine and serotonin. *Journal of Neurochemistry*, *60*(4), 1429–1435. https://doi.org/10.1111/j.1471-4159.1993.tb03305.x

22. Brandhorst, G., Oellerich, M., Maine, G., Taylor, P., Veen, G., & Wallemacq, P. (2012). Liquid chromatography-tandem mass spectrometry or automated immunoassays: What are the future trends in therapeutic drug monitoring? *Clinical Chemistry*, *58*(5), 821–825. https://doi.org/10.1373/clinchem.2011.167189

23. Brunner, M., & Langer, O. (2006). Microdialysis versus other techniques for the clinical assessment of in vivo tissue drug distribution. *The AAPS Journal*, *8*(2), 263–271. https://doi.org/10.1007/BF02854896

24. Bucher, E. S., & Wightman, R. M. (2015). Electrochemical Analysis of Neurotransmitters. *Annual Review of Analytical Chemistry*, *8*(1), 239–261. https://doi.org/10.1146/annurev-anchem-071114-040426

25. Burmeister, J. J., Moxon, K., & Gerhardt, G. A. (2000). Ceramic-Based Multisite Microelectrodes for Electrochemical Recordings. *Analytical Chemistry*, *72*(1), 187–192. https://doi.org/10.1021/ac9907991

26. Cakir, B., Xiang, Y., Tanaka, Y., Kural, M. H., Parent, M., Kang, Y. J., Chapeton, K., Patterson, B., Yuan, Y., & He, C. S. (2019). Engineering of human brain organoids with a functional vascular-like system. *Nat Methods*, *16*(11), 1169–1175.

27. Camp, K. M., Lloyd-Puryear, M. A., & Huntington, K. L. (2012). Nutritional treatment for inborn errors of metabolism: Indications, regulations, and availability of medical foods and dietary supplements using phenylketonuria as an example. *MOLECULAR GENETICS AND METABOLISM*, *107*(1–2, SI), 3–9. https://doi.org/10.1016/j.ymgme.2012.07.005

28. CAMPISTRON, G., GUIRAUD, R., CROS, J., & MOSSER, J. (1982). PHARMACOKINETICS OF ARGININE AND ASPARTIC-ACID ADMINISTERED SIMULTANEOUSLY IN THE RAT .1. PLASMA KINETICS. *EUROPEAN JOURNAL OF DRUG METABOLISM AND PHARMACOKINETICS*, *7*(4), 307–313. https://doi.org/10.1007/BF03189634

29. Carelli, R. M. (2004). Nucleus accumbens cell firing and rapid dopamine signaling during goal-directed behaviors in rats. *Neuropharmacology*, *47*, 180–189. https://doi.org/10.1016/j.neuropharm.2004.07.017

30. CASTELLS, S., & SHIRALI, S. (1971). DAILY RHYTHMIC CHANGES IN HEPATIC PHENYLALANINE HYDROXYLASE ACTIVITY - ROLE OF DIETARY PHENYLALANINE. *LIFE*

*SCIENCES PT-2 BIOCHEMISTRY GENERAL AND MOLECULAR BIOLOGY*, *10*(4), 233-. https://doi.org/10.1016/0024-3205(71)90023-3

31. CHAMI, J., REIDENBERG, M., WELLNER, D., DAVID, D., RUBIN, A., & STENZEL, K. (1978). PHARMACOKINETICS OF ESSENTIAL AMINO-ACIDS IN CHRONIC DIALYSIS PATIENTS. *AMERICAN JOURNAL OF CLINICAL NUTRITION*, *31*(9), 1652–1659. https://doi.org/10.1093/ajcn/31.9.1652

32. Chefer, V. I., Thompson, A. C., Zapata, A., & Shippenberg, T. S. (2009). Overview of Brain Microdialysis. *Current Protocols in Neuroscience / Editorial Board, Jacqueline N. Crawley ... [et Al.]*, *CHAPTER*, Unit7.1. https://doi.org/10.1002/0471142301.ns0701s47

33. Cheung, K. M., Yang, K.-A., Nakatsuka, N., Zhao, C., Ye, M., Jung, M. E., Yang, H., Weiss, P. S., Stojanovic, M. N., & Andrews, A. M. (2019). Phenylalanine Monitoring via Aptamer-Field-Effect Transistor Sensors. *ACS SENSORS*, *4*(12), 3308–3317. https://doi.org/10.1021/acssensors.9b01963

34. Clarke, S. E., & Foster, J. R. (2012). A history of blood glucose meters and their role in self-monitoring of diabetes mellitus. *BRITISH JOURNAL OF BIOMEDICAL SCIENCE*, *69*(2), 83–93.

35. Cleary, M., Trefz, F., Muntau, A. C., Feillet, F., van Spronsen, F. J., Burlina, A., Belanger-Quintana, A., Gizewska, M., Gasteyger, C., Bettiol, E., Blau, N., & MacDonald, A. (2013). Fluctuations in phenylalanine concentrations in phenylketonuria: A review of possible relationships with outcomes. *MOLECULAR GENETICS AND METABOLISM*, *110*(4), 418–423. https://doi.org/10.1016/j.ymgme.2013.09.001

36. Cordeiro, C. A., de Vries, M. G., Ngabi, W., Oomen, P. E., Cremers, T. I. F. H., & Westerink, B. H. C. (2015). In vivo continuous and simultaneous monitoring of brain energy substrates with a multiplex amperometric enzyme-based biosensor device. *Biosensors and Bioelectronics*, *67*, 677–686. https://doi.org/10.1016/j.bios.2014.09.101

37. Cordeiro, C. A., Sias, A., Koster, T., Westerink, B. H. C., & Cremers, T. I. F. H. (2018). In vivo “real-time” monitoring of glucose in the brain with an amperometric enzyme-based biosensor based on gold coated tungsten (W-Au) microelectrodes. *Sensors and Actuators B: Chemical*, *263*, 605–613. https://doi.org/10.1016/j.snb.2018.02.116

38. Cornford, E. M., Young, D., Paxton, J. W., & Sofia, R. D. (1992). Blood-brain barrier penetration of felbamate. *Epilepsia*, *33*(944).

39. Curtis, S. D., Ploense, K. L., Kurnik, M., Ortega, G., Parolo, C., Kippin, T. E., Plaxco, K. W., & Arroyo-Curras, N. (2019). Open Source Software for the Real-Time Control,

Processing, and Visualization of High-Volume Electrochemical Data. *ANALYTICAL CHEMISTRY*, *91*(19), 12321–12328. https://doi.org/10.1021/acs.analchem.9b02553

40. Dankoski, E. C., Agster, K. L., Fox, M. E., Moy, S. S., & Wightman, R. M. (2014). Facilitation of serotonin signaling by SSRIs is attenuated by social isolation. *Neuropsychopharmacology: Official Publication of the American College of Neuropsychopharmacology*, *39*(13), 2928–2937. https://doi.org/10.1038/npp.2014.162

41. Dasgupta, A. (2016). Limitations of immunoassays used for therapeutic drug monitoring of immunosuppressants. In *Personalized Immunosuppression in Transplantation* (pp. 29–56). Elsevier. https://doi.org/10.1016/B978-0-12-800885-0.00002-3

42. Dauphin-Ducharme, P., Ploense, K. L., Arroyo-Currás, N., Kippin, T. E., & Plaxco, K. W. (2022). Electrochemical Aptamer-Based Sensors: A Platform Approach to High-Frequency Molecular Monitoring In Situ in the Living Body. In M. R. Ossandon, H. Baker, & A. Rasooly (Eds.), *Biomedical Engineering Technologies: Volume 1* (pp. 479–492). Springer US. https://doi.org/10.1007/978-1-0716-1803-5_25

43. Dauphin-Ducharme, P., Yang, K., Arroyo-Currás, N., Ploense, K. L., Zhang, Y., Gerson, J., Kurnik, M., Kippin, T. E., Stojanovic, M. N., & Plaxco, K. W. (2019). Electrochemical Aptamer-Based Sensors for Improved Therapeutic Drug Monitoring and High-Precision, Feedback-Controlled Drug Delivery. *ACS Sensors*, *4*(10), 2832–2837. https://doi.org/10.1021/acssensors.9b01616

44. Dengler, A. K., & McCarty, G. S. (2013). Microfabricated microelectrode sensor for measuring background and slowly changing dopamine concentrations. *Journal of Electroanalytical Chemistry*, *693*, 28–33. https://doi.org/10.1016/j.jelechem.2013.01.022

45. DUNLOP, D., YANG, X., & LAJTHA, A. (1994). THE EFFECT OF ELEVATED PLASMA PHENYLALANINE LEVELS ON PROTEIN-SYNTHESIS RATES IN ADULT-RAT BRAIN. *BIOCHEMICAL JOURNAL*, *302*(2), 601–610. https://doi.org/10.1042/bj3020601

46. EC, L., BA, B., & DD, B. (1999). Microdialysis for pharmacokinetic analysis of drug transport to the brain. *Adv Drug Deliv Rev*, *36*(211).

47. Edward, E. S., & Kouzani, A. Z. (2020). A Closed-Loop Optogenetic Stimulation Device. *Electronics*, *9*(1), 96. https://doi.org/10.3390/electronics9010096

48. Egbers, N., Schwenke, C., Maxeiner, A., Teichgräber, U., & Franiel, T. (2015). MRI-guided core needle biopsy of the prostate: Acceptance and side effects. *Diagnostic and Interventional Radiology (Ankara, Turkey)*, *21*(3), 215–221. https://doi.org/10.5152/dir.2014.14372

49. Ehrich, J. M., Phillips, P. E. M., & Chavkin, C. (2014). Kappa opioid receptor activation potentiates the cocaine-induced increase in evoked dopamine release recorded in vivo in the mouse nucleus accumbens. *Neuropsychopharmacology: Official Publication of the American College of Neuropsychopharmacology*, *39*(13), 3036–3048. https://doi.org/10.1038/npp.2014.157

50. Elsinga, P. H., Hendrikse, N. H., Bart, J., Vaalburg, W., & Waarde, A. (2004). PET Studies on P-glycoprotein function in the blood-brain barrier: How it affects uptake and binding of drugs within the CNS. *Curr Pharm Des*, *10*(1493).

51. Fabozzi, F. J. (2014). *The Basics of Financial Econometrics*.

52. Farin, D., Piva, G. A., Gozlan, I., & Kitzes-Cohen, R. (1998). A modified HPLC method for the determination of vancomycin in plasma and tissues and comparison to FPIA (TDX). *Journal of Pharmaceutical and Biomedical Analysis*, *18*(3), 367–372. https://doi.org/10.1016/S0731-7085(98)00095-8

53. Ferguson, B. S., Hoggarth, D. A., Maliniak, D., Ploense, K., White, R. J., Woodward, N., Hsieh, K., Bonham, A. J., Eisenstein, M., Kippin, T. E., Plaxco, K. W., & Soh, H. T. (2013). Real-time, aptamer-based tracking of circulating therapeutic agents in living animals. *Science Translational Medicine*, *5*(213), 213ra165. https://doi.org/10.1126/scitranslmed.3007095

54. Figueiredo-Filho, L. C. S., Silva, T. A., Vicentini, F. C., & Fatibello-Filho, O. (2014). Simultaneous voltammetric determination of dopamine and epinephrine in human body fluid samples using a glassy carbon electrode modified with nickel oxide nanoparticles and carbon nanotubes within a dihexadecylphosphate film. *Analyst*, *139*(11), 2842–2849. https://doi.org/10.1039/C4AN00229F

55. Fournier, A., Eggimann, P., Pantet, O., Pagani, J. L., Dupuis-Lozeron, E., Pannatier, A., Sadeghipour, F., Voirol, P., & Que, Y.-A. (2018). Impact of Real-Time Therapeutic Drug Monitoring on the Prescription of Antibiotics in Burn Patients Requiring Admission to the Intensive Care Unit. *Antimicrobial Agents and Chemotherapy*, *62*(3), e01818-17. https://doi.org/10.1128/AAC.01818-17

56. Fox, M. E., & Wightman, R. M. (2017). Contrasting Regulation of Catecholamine Neurotransmission in the Behaving Brain: Pharmacological Insights from an Electrochemical Perspective. *Pharmacological Reviews*, *69*(1), 12–32. https://doi.org/10.1124/pr.116.012948

57. Garg, P. K., Lokitz, S. J., Nazih, R., & Garg, S. (2017). Biodistribution and Radiation Dosimetry of (11)C-Nicotine from Whole-Body PET Imaging in Humans. *Journal of Nuclear Medicine : Official Publication, Society of Nuclear Medicine*, *58*, 473–478.

58. Giuliano, C., Parikh, V., Ward, J. R., Chiamulera, C., & Sarter, M. (2008). Increases in cholinergic neurotransmission measured by using choline-sensitive microelectrodes: Enhanced detection by hydrolysis of acetylcholine on recording sites? *Neurochemistry International*, *52*(7), 1343–1350. https://doi.org/10.1016/j.neuint.2008.02.002

59. Goldstein, A., & Vockley, J. (2017). Clinical trials examining treatments for inborn errors of amino acid metabolism. *EXPERT OPINION ON ORPHAN DRUGS*, *5*(2), 153–164. https://doi.org/10.1080/21678707.2017.1275565

60. Gowers, S. A. N. (2018a). An improved rapid sampling microdialysis system for human and porcine organ monitoring in a hospital setting. *Analytical Methods : Advancing Methods and Applications*, *10*, 5273–5281.

61. Gowers, S. A. N. (2018b). High temporal resolution delayed analysis of clinical microdialysate streams. *The Analyst*, *143*, 715–724.

62. Grabowska, I., Sharma, N., Vasilescu, A., Iancu, M., Badea, G., Boukherroub, R., Ogale, S., & Szunerits, S. (2018). Electrochemical Aptamer-Based Biosensors for the Detection of Cardiac Biomarkers. *ACS OMEGA*, *3*(9), 12010–12018. https://doi.org/10.1021/acsomega.8b01558

63. Grosenick, L., Marshel, J. H., & Deisseroth, K. (2015). Closed-Loop and Activity-Guided Optogenetic Control. *Neuron*, *86*(1), 106–139. https://doi.org/10.1016/j.neuron.2015.03.034

64. HAMDAN, S. K., & MOHD ZAIN, ainiharyati. (2014). In vivo Electrochemical Biosensor for Brain Glutamate Detection: A Mini Review. *The Malaysian Journal of Medical Sciences : MJMS*, *21*(Spec Issue), 12–26.

65. Harstad, R. K., & Bowser, M. T. (2016). High-Speed Microdialysis-Capillary Electrophoresis Assays for Measuring Branched Chain Amino Acid Uptake in 3T3-L1 cells. *Analytical Chemistry*, *88*, 8115–8122.

66. Hashemi, P., Dankoski, E. C., Petrovic, J., Keithley, R. B., & Wightman, R. M. (2009). Voltammetric Detection of 5-Hydroxytryptamine Release in the Rat Brain. *Analytical Chemistry*, *81*(22), 9462–9471. https://doi.org/10.1021/ac9018846

67. HJELLE, J., DUDLEY, R., MARIETTA, M., SANDERS, P., DICKIE, B., BRISSON, J., & KOTSONIS, F. (1992). PLASMA-CONCENTRATIONS AND PHARMACOKINETICS OF PHENYLALANINE IN RATS AND MICE ADMINISTERED ASPARTAME. *PHARMACOLOGY*, *44*(1), 48–60. https://doi.org/10.1159/000138873

68. Hoeben, B., & Gunneweg, F. (2015). *A critical review on glutamate sensing* (p. 10 13140 2 1 2450 7360).

69. Hoedemaekers, C. W. E., Gunnewiek, J. M. T. K., Prinsen, M. A., Willems, J. L., & Van der Hoeven, J. G. (2008). Accuracy of bedside glucose measurement from three glucometers in critically ill patients. *CRITICAL CARE MEDICINE*, *36*(11), 3062–3066. https://doi.org/10.1097/CCM.0b013e318186ffe6

70. Homberg, J. R., De Boer, S. F., Raaso, H. S., Olivier, J. D., Verheul, M., Ronken, E., & Cuppen, E. (2008). Adaptations in pre- and postsynaptic 5-HT1A receptor function and cocaine supersensitivity in serotonin transporter knockout rats. *Psychopharmacology*, *200*(3), 367–380. https://doi.org/10.1007/s00213-008-1212-x

71. Homberg, J. R., Olivier, J. D., Smits, B. M., Mul, J. D., Mudde, J., Verheul, M., & Cuppen, E. (2007). Characterization of the serotonin transporter knockout rat: A selective change in the functioning of the serotonergic system. *Neuroscience*, *146*(4), 1662–1676. https://doi.org/10.1016/j.neuroscience.2007.03.030

72. Hurd, Y. L., Kehr, J., & Ungerstedt, U. (1988). In Vivo Microdialysis as a Technique to Monitor Drug Transport: Correlation of Extracellular Cocaine Levels and Dopamine Overflow in the Rat Brain. *Journal of Neurochemistry*, *51*(4), 1314–1316. https://doi.org/10.1111/j.1471-4159.1988.tb03103.x

73. *IACUC, Guide for the Care and Use of Laboratory Animals: Eighth Edition*. (2011). The National Academies Press.

74. Idili, A., Arroyo-Currás, N., Ploense, K. L., Csordas, A. T., Kuwahara, M., Kippin, T. E., & Plaxco, K. W. (2019). Seconds-resolved pharmacokinetic measurements of the chemotherapeutic irinotecan in situ in the living body. *Chemical Science*, *10*(35), 8164–8170. https://doi.org/10.1039/C9SC01495K

75. Idili, A., Gerson, J., Kippin, T., & Plaxco, K. W. (2021). Seconds-Resolved, In Situ Measurements of Plasma Phenylalanine Disposition Kinetics in Living Rats. *Analytical Chemistry*, *93*(8), 4023–4032. https://doi.org/10.1021/acs.analchem.0c05024

76. Idili, A., Gerson, J., Parolo, C., Kippin, T., & Plaxco, K. W. (2019). An electrochemical aptamer-based sensor for the rapid and convenient measurement of L-tryptophan. *Analytical and Bioanalytical Chemistry*, *411*(19), 4629–4635. https://doi.org/10.1007/s00216-019-01645-0

77. Idili, A., Parolo, C., Ortega, G., & Plaxco, K. W. (2019). Calibration-Free Measurement of Phenylalanine Levels in the Blood Using an Electrochemical Aptamer-Based Sensor Suitable for Point-of-Care Applications. *ACS SENSORS*, *4*(12), 3227–3233. https://doi.org/10.1021/acssensors.9b01703

78. Isherwood, S. N., Robbins, T. W., Dalley, J. W., & Pekcec, A. (2018). Bidirectional variation in glutamate efflux in the medial prefrontal cortex induced by selective

positive and negative allosteric mGluR5 modulators. *Journal of Neurochemistry*, *145*(2), 111–124. https://doi.org/10.1111/jnc.14290

79. JAGENBURG, R., OLSSON, R., REGARDH, C., & RODJER, S. (1977). KINETICS OF INTRAVENOUS ADMINISTERED L-PHENYLALANINE IN PATIENTS WITH CIRRHOSIS OF LIVER. *CLINICA CHIMICA ACTA*, *78*(3), 453–463. https://doi.org/10.1016/0009-8981(77)90078-X

80. Javaid, J. I., Fischman, M. W., Schuster, C. R., Dekirmenjian, H., & Davis, J. M. (1978). Cocaine plasma concentration: Relation to physiological and subjective effects in humans. *Science*, *202*, 227–228. https://doi.org/10.1126/science.694530

81. Javorska, L., Krcmova, L. K., Solichova, D., Solich, P., & Kaska, M. (2016). Modern methods for vancomycin determination in biological fluids by methods based on high-performance liquid chromatography—A review. *Journal of Separation Science*, *39*(1), 6–20. https://doi.org/10.1002/jssc.201500600

82. Jeffcoat, A. R., Perez-Reyes, M., Hill, J. M., Sadler, B. M., & Cook, C. E. (1989). Cocaine disposition in humans after intravenous injection, nasal insufflation (snorting), or smoking. *Drug Metabolism and Disposition: The Biological Fate of Chemicals*, *17*, 153–159.

83. Jesús Valle, M. J. de, López, F. G., & Navarro, A. S. (2008). Development and validation of an HPLC method for vancomycin and its application to a pharmacokinetic study. *Journal of Pharmaceutical and Biomedical Analysis*, *48*(3), 835–839. https://doi.org/10.1016/j.jpba.2008.05.040

84. Kaluzna-Czaplinska, J., Gatarek, P., Chirumbolo, S., Chartrand, M. S., & Bjorklund, G. (2019). How important is tryptophan in human health? *CRITICAL REVIEWS IN FOOD SCIENCE AND NUTRITION*, *59*(1), 72–88. https://doi.org/10.1080/10408398.2017.1357534

85. Kaluzna-Czaplinska, J., Michalska, M., & Rynkowski, J. (2010). Determination of tryptophan in urine of autistic and healthy children by gas chromatography/mass spectrometry. *MEDICAL SCIENCE MONITOR*, *16*(10), CR488–CR492.

86. Kaufman, S. (1999). A model of human phenylalanine metabolism in normal subjects and in phenylketonuric patients. *PROCEEDINGS OF THE NATIONAL ACADEMY OF SCIENCES OF THE UNITED STATES OF AMERICA*, *96*(6), 3160–3164. https://doi.org/10.1073/pnas.96.6.3160

87. Keithley, R. B., Takmakov, P., Bucher, E. S., Belle, A. M., Owesson-White, C. A., Park, J., & Wightman, R. M. (2011). Higher Sensitivity Dopamine Measurements with Faster-Scan Cyclic Voltammetry. *Analytical Chemistry*, *83*(9), 3563–3571. https://doi.org/10.1021/ac200143v

88. Kennedy, R. T., Watson, C. J., Haskins, W. E., Powell, D. H., & Strecker, R. E. (n.d.). *In vivo neurochemical monitoring by microdialysis and capillary separations*. 7.

89. Kennedy, R. T., Watson, C. J., Haskins, W. E., Powell, D. H., & Strecker, R. E. (2002). In vivo neurochemical monitoring by microdialysis and capil- lary separations. *Curr Opin Chem Biol*, *6*, 659–665.

90. Kitamura, A., Okura, T., Higuchi, K., & Deguchi, Y. (2016). Cocktail-Dosing Microdialysis Study to Simultaneously Assess Delivery of Multiple Organic-Cationic Drugs to the Brain. *J Pharm Sci*, *105*, 935–940.

91. Klein, A. K., Brito, M. A., Akhavan, S., Flanagan, D. R., Le, N., Ohana, T., & Ettenberg, A. (2017). Attenuation of the anxiogenic effects of cocaine by 5-HT1B autoreceptor stimulation in the bed nucleus of the stria terminalis of rats. *Psychopharmacology*, *234*(3), 485–495. https://doi.org/10.1007/s00213-016-4479-3

92. Kozai, T. D. Y., Langhals, N. B., Patel, P. R., Deng, X., Zhang, H., Smith, K. L., Lahann, J., Kotov, N. A., & Kipke, D. R. (2012). Ultrasmall implantable composite microelectrodes with bioactive surfaces for chronic neural interfaces. *Nature Materials*, *11*(12), 1065–1073. https://doi.org/10.1038/nmat3468

93. Kucherenko, I. S., Topolnikova, Ya. V., & Soldatkin, O. O. (2019). Advances in the biosensors for lactate and pyruvate detection for medical applications: A review. *TRAC-TRENDS IN ANALYTICAL CHEMISTRY*, *110*, 160–172. https://doi.org/10.1016/j.trac.2018.11.004

94. Lada, M. W., Vickroy, T. W., & Kennedy, R. T. (1997). High Temporal Resolution Monitoring of Glutamate and Aspartate in Vivo Using Microdialysis On-Line with Capillary Electrophoresis with Laser-Induced Fluorescence Detection. *Analytical Chemistry*, *69*(22), 4560–4565. https://doi.org/10.1021/ac970518u

95. Lai, R. Y., Plaxco, K. W., & Heeger, A. J. (2007). Aptamer-based electrochemical detection of picomolar platelet-derived growth factor directly in blood serum. *ANALYTICAL CHEMISTRY*, *79*(1), 229–233. https://doi.org/10.1021/ac061592s

96. LEE, H., & BLAUFOX, M. (1985). BLOOD-VOLUME IN THE RAT. *JOURNAL OF NUCLEAR MEDICINE*, *26*(1), 72–76.

97. Lepage, M., Habib, R., & Tulving, E. (1998). Hippocampal PET activations of memory encoding and retrieval: The HIPER model. *Hippocampus*, *8*(4), 313–322. https://doi.org/10.1002/(SICI)1098-1063(1998)8:4<313::AID-HIPO1>3.0.CO;2-I

98. Leung, K. K., Downs, A. M., Ortega, G., Kurnik, M., & Plaxco, K. W. (2021). Elucidating the Mechanisms Underlying the Signal Drift of Electrochemical Aptamer-Based Sensors in Whole Blood. *ACS Sensors*, *6*(9), 3340–3347. https://doi.org/10.1021/acssensors.1c01183

99. Li, H., Li, S., Dai, J., Li, C., Zhu, M., Li, H., Lou, X., Xia, F., & Plaxco, K. W. (2019). High frequency, calibration-free molecular measurements *in situ* in the living body. *Chemical Science*, *10*(47), 10843–10848. https://doi.org/10.1039/C9SC04434E

100. Lin, Y., Yu, P., Hao, J., Wang, Y., Ohsaka, T., & Mao, L. (2014). Continuous and Simultaneous Electrochemical Measurements of Glucose, Lactate, and Ascorbate in Rat Brain Following Brain Ischemia. *Analytical Chemistry*, *86*(8), 3895–3901. https://doi.org/10.1021/ac4042087

101. Lindseth, G., Helland, B., & Caspers, J. (2015). The Effects of Dietary Tryptophan on Affective Disorders. *ARCHIVES OF PSYCHIATRIC NURSING*, *29*(2), 102–107. https://doi.org/10.1016/j.apnu.2014.11.008

102. Lubin, A. A., & Plaxco, K. W. (2010). Folding-Based Electrochemical Biosensors: The Case for Responsive Nucleic Acid Architectures. *ACCOUNTS OF CHEMICAL RESEARCH*, *43*(4), 496–505. https://doi.org/10.1021/ar900165x

103. Lutz, J. D., Fujioka, Y., & Isoherranen, N. (2010). Rationalization and prediction of in vivo metabolite exposures: The role of metabolite kinetics, clearance predictions and in vitro parameters. *EXPERT OPINION ON DRUG METABOLISM & TOXICOLOGY*, *6*(9), 1095–1109. https://doi.org/10.1517/17425255.2010.497487

104. Mage, P. L., Ferguson, B. S., Maliniak, D., Ploense, K. L., Kippin, T. E., & Soh, H. T. (2017). Closed-loop control of circulating drug levels in live animals. *Nature Biomedical Engineering*, *1*(5), 0070. https://doi.org/10.1038/s41551-017-0070

105. MARTIN, J., MELLOR, C., & FRASER, F. (1995). FAMILIAL HYPERTRYPTOPHANEMIA IN 2 SIBLINGS. *CLINICAL GENETICS*, *47*(4), 180–183.

106. Matzke, G. R., Zhanel, G. G., & Guay, D. R. (1986). Clinical pharmacokinetics of vancomycin. *Clinical pharmacokinetics*, *Oct;11(4):257-82*.

107. McCutcheon, J. E., Cone, J. J., Sinon, C. G., Fortin, S. M., Kantak, P. A., Witten, I. B., Deisseroth, K., Stuber, G. D., & Roitman, M. F. (2014). Optical suppression of drug-evoked phasic dopamine release. *Frontiers in Neural Circuits*, *8*, 114. https://doi.org/10.3389/fncir.2014.00114

108. Melichar, J. K., Daglish, M. R., & Nutt, D. J. (2001). Addiction and withdrawal–current views. *Current Opinion in Pharmacology*, *1*, 84–90.

109. Metallo, C. M., & Vander Heiden, M. G. (2013). Understanding Metabolic Regulation and Its Influence on Cell Physiology. *MOLECULAR CELL*, *49*(3), 388–398. https://doi.org/10.1016/j.molcel.2013.01.018

110. Minogianis, E.-A., Shams, W. M., Mabrouk, O. S., Wong, J.-M. T., Brake, W. G., Kennedy, R. T., du Souich, P., & Samaha, A.-N. (2019). Varying the rate of

intravenous cocaine infusion influences the temporal dynamics of both drug and dopamine concentrations in the striatum. *The European Journal of Neuroscience*, *50*(3), 2054–2064. https://doi.org/10.1111/ejn.13941

111. Miranda, A. (2019). PET imaging of freely moving interacting rats. *Neuroimage*, *191*, 560-567,.

112. Moraldo, C., Vuille-dit-Bille, E., Shkodra, B., Kloter, T., & Nakatsuka, N. (2022). Aptamer-modified biosensors to visualize neurotransmitter flux. *Journal of Neuroscience Methods*, *365*, 109386. https://doi.org/10.1016/j.jneumeth.2021.109386

113. Moran, R. J., Kishida, K. T., Lohrenz, T., Saez, I., Laxton, A. W., Witcher, M. R., Tatter, S. B., Ellis, T. L., Phillips, P. E., Dayan, P., & Montague, P. R. (2018). The Protective Action Encoding of Serotonin Transients in the Human Brain. *Neuropsychopharmacology: Official Publication of the American College of Neuropsychopharmacology*, *43*(6), 1425–1435. https://doi.org/10.1038/npp.2017.304

114. Moser, M.-B., & Moser, E. I. (1998). Functional differentiation in the hippocampus. *Hippocampus*, *8*(6), 608–619. https://doi.org/10.1002/(SICI)1098-1063(1998)8:6<608::AID-HIPO3>3.0.CO;2-7

115. Moses, W. W. (2011). Fundamental Limits of Spatial Resolution in PET. *Nucl Instrum Methods Phys Res A*, *648 Supplement 1*, 236–240.

116. Motallebnejad, P., Thomas, A., Swisher, S. L., & Azarin, S. M. (2019). An isogenic hiPSC-derived BBB-on-a-chip. *Biomicrofluidics*, *13*(6).

117. Muller, C. P., & Homberg, J. (2015). Serotonin revisited. *Behav Brain Res*, *277*, 1–2.

118. Nakatsuka, N. (2018). Aptamer-field-effect transistors overcome Debye length limitations for small-molecule sensing. *Science*. https://doi.org/10.1126/science.aao6750

119. Nayak, S., Blumenfeld, N. R., Laksanasopin, T., & Sia, S. K. (2017). Point-of-Care Diagnostics: Recent Developments in a Connected Age. *ANALYTICAL CHEMISTRY*, *89*(1), 102–123. https://doi.org/10.1021/acs.analchem.6b04630

120. Newman, J. P. (2015). Optogenetic feedback control of neural activity. *ELife*, *4, e07192*. https://doi.org/10.7554/eLife.07192.001

121. Ngernsutivorakul, T., White, T. S., & Kennedy, R. T. (2018a). Microfabricated Probes for Studying Brain Chemistry: A Review. *ChemPhysChem*, *19*(10), 1128–1142. https://doi.org/10.1002/cphc.201701180

122. Ngernsutivorakul, T., White, T. S., & Kennedy, R. T. (2018b). Review: Microfabricated Probes for Studying Brain Chemistry. *Chemphyschem : A European Journal of Chemical Physics and Physical Chemistry*, *19*(10), 1128–1142. https://doi.org/10.1002/cphc.201701180

123. Nicolazzo, J. A., Charman, S. A., & Charman, W. N. (2006). Methods to assess drug permeability across the blood- brain barrier. *J Pharm Pharmacol*, *58*(281).

124. Oakes, R. S., Polei, M. D., Skousen, J. L., & Tresco, P. A. (2018). An astrocyte derived extracellular matrix coating reduces astrogliosis surrounding chronically implanted microelectrode arrays in rat cortex. *Biomaterials*, *154*, 1–11. https://doi.org/10.1016/j.biomaterials.2017.10.001

125. Owesson-White, C. A., Ariansen, J., Stuber, G. D., Cleaveland, N. A., Cheer, J. F., Wightman, R. M., & Carelli, R. M. (2009). Neural Encoding of Cocaine Seeking Behavior is Coincident with Phasic Dopamine Release in the Accumbens Core and Shell. *The European Journal of Neuroscience*, *30*(6), 1117–1127. https://doi.org/10.1111/j.1460-9568.2009.06916.x

126. Owesson-White, C. A., Cheer, J. F., Beyene, M., Carelli, R. M., & Wightman, R. M. (2008). Dynamic changes in accumbens dopamine correlate with learning during intracranial self-stimulation. *Proceedings of the National Academy of Sciences of the United States of America*, *105*(33), 11957–11962. https://doi.org/10.1073/pnas.0803896105

127. Oyaert, M., Peersman, N., Kieffer, D., Deiteren, K., Smits, A., Allegaert, K., Spriet, I., Van Eldere, J., Verhaegen, J., Vermeersch, P., & Pauwels, S. (2015). Novel LC-MS/MS method for plasma vancomycin: Comparison with immunoassays and clinical impact. *Clinica Chimica Acta; International Journal of Clinical Chemistry*, *441*, 63–70. https://doi.org/10.1016/j.cca.2014.12.012

128. Palego, L., Betti, L., & Giannaccini, G. (2016). *Tryptophan Biochemistry: Structural, Nutritional, Metabolic, and Medical Aspects in Humans*. SAGE-Hindawi Access to Research.

129. Pan, H.-T., Menacherry, S., & Justice Jr., J. B. (1991). Differences in the Pharmacokinetics of Cocaine in Naive and Cocaine-Experienced Rats. *Journal of Neurochemistry*, *56*(4), 1299–1306. https://doi.org/10.1111/j.1471-4159.1991.tb11425.x

130. Pan, W. H. T., Lim, L.-H., & Shiau, M.-R. (1994). Difference in extracellular cocaine concentration between the ventral tegmental area and the medial prefrontal cortex following intravenous administration as revealed by quantitative microdialysis coupled with in vivo calibration. *Journal of Neuroscience Methods*, *53*(1), 65–71. https://doi.org/10.1016/0165-0270(94)90145-7

131. Papamichael, K., & Cheifetz, A. S. (2017). Therapeutic Drug Monitoring in IBD: The New Standard-of-Care for Anti-TNF Therapy. *The American Journal of Gastroenterology*, *112*(5), 673–676. https://doi.org/10.1038/ajg.2017.21

132. Park, J., Kile, B. M., & Wightman, R. M. (2009). In vivo voltammetric monitoring of norepinephrine release in the rat ventral bed nucleus of the stria terminalis and anteroventral thalamic nucleus. *The European Journal of Neuroscience*, *30*(11), 2121–2133. https://doi.org/10.1111/j.1460-9568.2009.07005.x

133. Park, J., Takmakov, P., & Wightman, R. M. (2011). In vivo comparison of norepinephrine and dopamine release in rat brain by simultaneous measurements with fast-scan cyclic voltammetry. *Journal of Neurochemistry*, *119*(5), 932–944. https://doi.org/10.1111/j.1471-4159.2011.07494.x

134. Park, T.-E., Mustafaoglu, N., Herland, A., Hasselkus, R., Mannix, R., FitzGerald, E. A., Prantil-Baun, R., Watters, A., Henry, O., Benz, M., Sanchez, H., McCrea, H. J., Goumnerova, L. C., Song, H. W., Palecek, S. P., Shusta, E., & Ingber, D. E. (2019). Hypoxia-enhanced Blood-Brain Barrier Chip recapitulates human barrier function and shuttling of drugs and antibodies. *Nature Communications*, *10*(1), 2621. https://doi.org/10.1038/s41467-019-10588-0

135. Parolo, C., Idili, A., Ortega, G., Csordas, A., Hsu, A., Arroyo-Curras, N., Yang, Q., Ferguson, B. S., Wang, J., & Plaxco, K. W. (2020). Real-Time Monitoring of a Protein Biomarker. *ACS SENSORS*, *5*(7), 1877–1881. https://doi.org/10.1021/acssensors.0c01085

136. Patsalos, P. N., Spencer, E. P., & Berry, D. J. (2018). Therapeutic Drug Monitoring of Antiepileptic Drugs in Epilepsy: A 2018 Update. *Therapeutic Drug Monitoring*, *40*(5), 526–548. https://doi.org/10.1097/FTD.0000000000000546

137. Pattison, L. P., McIntosh, S., Budygin, E. A., & Hemby, S. E. (2012). Differential regulation of accumbal dopamine transmission in rats following cocaine, heroin and speedball self-administration. *Journal of Neurochemistry*, *122*(1), 138–146. https://doi.org/10.1111/j.1471-4159.2012.07738.x

138. Pepe, P., & Aragona, F. (2013). Morbidity After Transperineal Prostate Biopsy in 3000 Patients Undergoing 12 vs 18 vs More Than 24 Needle Cores. *Urology*, *81*(6), 1142–1146. https://doi.org/10.1016/j.urology.2013.02.019

139. Pettit, H. O., & Pettit, A. J. (1994). Disposition of cocaine in blood and brain after a single pretreatment. *Brain Research*, *651*(1–2), 261–268. https://doi.org/10.1016/0006-8993(94)90705-6

140. Plaxco, K. W., & Soh, H. T. (2011). Switch-based biosensors: A new approach towards real-time, in vivo molecular detection. *TRENDS IN BIOTECHNOLOGY*, *29*(1), 1–5. https://doi.org/10.1016/j.tibtech.2010.10.005

141. Ploense, K. L. (2018a). Contributions of prolonged contingent and non-contingent cocaine exposure to escalation of cocaine intake and glutamatergic gene expression. *Psychopharmacology (Berl*, *235*, 1347–1359.

142. Ploense, K. L. (2018b). Prolonged-access to cocaine induces distinct Homer2 DNA methylation, hydroxymethylation, and transcriptional profiles in the dorsomedial prefrontal cortex of Male Sprague-Dawley rats. *Neuropharmacology*, *143*, 299–305.

143. Potter, S. M., El Hady, A., & Fetz, E. E. (2014). Closed-loop neuroscience and neuroengineering. *Frontiers in Neural Circuits*, *8*. https://doi.org/10.3389/fncir.2014.00115

144. Prsa, M., Galinanes, G. L., & Huber, D. (2017). Rapid Integration of Artificial Sensory Feedback during Operant Conditioning of Motor Cortex Neurons. *Neuron*, *93*, 929-939 926.

145. Qin, W. W. (2010). Simultaneous determination of procaine, lidocaine, ropivacaine, tetracaine and bupivacaine in human plasma by high-performance liquid chromatography. *Journal of Chromatography. B, Analytical Technologies in the Biomedical and Life Sciences*, *878*, 1185–1189.

146. Quintero, J. E., Day, B. K., Zhang, Z., Grondin, R., Stephens, M. L., Huettl, P., Pomerleau, F., Gash, D. M., & Gerhardt, G. A. (2007). Amperometric mea- sures of age-related changes in glutamate regulation in the cortex of rhesus monkeys. *Exp Neurol*, *208*, 238–246.

147. Rathee, K., Dhull, V., Dhull, R., & Singh, S. (2016). Biosensors based on electrochemical lactate detection: A comprehensive review. *Biochemistry and Biophysics Reports*, *5*, 35–54. https://doi.org/10.1016/j.bbrep.2015.11.010

148. Regev, A., Berho, M., Jeffers, L. J., Milikowski, C., Molina, E. G., Pyrsopoulos, N. T., Feng, Z.-Z., Reddy, K. R., & Schiff, E. R. (2002). Sampling error and intraobserver variation in liver biopsy in patients with chronic HCV infection. *The American Journal of Gastroenterology*, *97*(10), 2614–2618. https://doi.org/10.1111/j.1572-0241.2002.06038.x

149. Reiter, B., & Stimpfl, T. (2015). Quantification of Drugs in Brain Samples. *Journal of Analytical Toxicology*, *39*, 702–706.

150. Roberts, J. G., & Sombers, L. A. (2018). Fast-Scan Cyclic Voltammetry: Chemical Sensing in the Brain and Beyond. *Analytical Chemistry*, *90*(1), 490–504. https://doi.org/10.1021/acs.analchem.7b04732

151. Robinson, D. L., Hermans, A., Seipel, A. T., & Wightman, R. M. (2008). Monitoring Rapid Chemical Communication in the Brain. *Chemical Reviews*, *108*(7), 2554–2584. https://doi.org/10.1021/cr068081q

152. Rocchitta, G., Peana, A. T., Bazzu, G., Cossu, A., Carta, S., Arrigo, P., Bacciu, A., Migheli, R., Farina, D., Zinellu, M., Acquas, E., & Serra, P. A. (2019). Simultaneous wireless and high-resolution detection of nucleus accumbens shell ethanol concentrations and free motion of rats upon voluntary ethanol intake. *Alcohol*, *78*, 69–78. https://doi.org/10.1016/j.alcohol.2019.04.002

153. Rocchitta, G., Secchi, O., Alvau, M. D., Migheli, R., Calia, G., Bazzu, G., Farina, D., Desole, M. S., O'Neill, R. D., & Serra, P. A. (2012). Development and Characterization of an Implantable Biosensor for Telemetric Monitoring of Ethanol in the Brain of Freely Moving Rats. *Analytical Chemistry*, *84*(16), 7072–7079. https://doi.org/10.1021/ac301253h

154. Rodbard, D. (2016). Continuous Glucose Monitoring: A Review of Successes, Challenges, and Opportunities. *DIABETES TECHNOLOGY & THERAPEUTICS*, *18*(2), 3–13. https://doi.org/10.1089/dia.2015.0417

155. Rose, J. E. (2010). Kinetics of brain nicotine accumulation in dependent and nondependent smokers assessed with PET and cigarettes containing 11C-nicotine. *Proceedings of the National Academy of Sciences of the United States of America*, *107*, 5190–5195.

156. Rowe, A. A., Miller, E. A., & Plaxco, K. W. (2010). Reagent less Measurement of Aminoglycoside Antibiotics in Blood Serum via an Electrochemical, Ribonucleic Acid Aptamer-Based Biosensor. *ANALYTICAL CHEMISTRY*, *82*(17), 7090–7095. https://doi.org/10.1021/ac101491d

157. Sarter, M., & Kim, Y. (2015). Interpreting Chemical Neurotransmission in Vivo: Techniques, Time Scales, and Theories. *ACS Chemical Neuroscience*, *6*(1), 8–10. https://doi.org/10.1021/cn500319m

158. Saudubray, J., Sedel, F., & Walter, J. (2006). Clinical approach to treatable inborn metabolic diseases: An introduction. *JOURNAL OF INHERITED METABOLIC DISEASE*, *29*(2–3), 261–274. https://doi.org/10.1007/s10545-006-0358-0

159. Saylor, R. A., & Lunte, S. M. (2015). A review of microdialysis coupled to microchip electrophoresis for monitoring biological events. *Journal of Chromatography. A*, *1382*, 48–64. https://doi.org/10.1016/j.chroma.2014.12.086

160. Schacter, D. L., & Wagner, A. D. (1999). Medial temporal lobe activations in fMRI and PET studies of episodic encoding and retrieval. *Hippocampus*, *9*(1), 7–24. https://doi.org/10.1002/(SICI)1098-1063(1999)9:1<7::AID-HIPO2>3.0.CO;2-K

161. Schork, N. J. (2015). Time for one-person trials. *NATURE*, *520*(7549), 609–611. https://doi.org/10.1038/520609a

162. Schoukroun-Barnes, L. R., Macazo, F. C., Gutierrez, B., Lottermoser, J., Liu, J., & White, R. J. (2016). Reagentless, Structure-Switching, Electrochemical Aptamer-Based Sensors. *Annual Review of Analytical Chemistry (Palo Alto, Calif.)*, *9*(1), 163–181. https://doi.org/10.1146/annurev-anchem-071015-041446

163. Schwarz, G. (1978). Estimating the Dimension of a Model. *The Annals of Statistics*, *6*(2), 461–464. https://doi.org/10.1214/aos/1176344136

164. Seifen, A. B., Ferrari, A. A., Seifen, E. E., Thompson, D. S., & Chapman, J. (1979). Pharmacokinetics of intravenous procaine infusion in humans. *Anesthesia and Analgesia*, *58*, 382–386.

165. Seo, J.-W., Fu, K., Correa, S., Eisenstein, M., Appel, E. A., & Soh, H. T. (2022). Real-time monitoring of drug pharmacokinetics within tumor tissue in live animals. *Science Advances*. https://doi.org/10.1126/sciadv.abk2901

166. Seymour, J. P., Wu, F., Wise, K. D., & Yoon, E. (2017). State-of-the-art MEMS and microsystem tools for brain research. *Microsystems & Nanoengineering*, *3*(1), 16066. https://doi.org/10.1038/micronano.2016.66

167. Shaver, A., Curtis, S. D., & Arroyo-Curras, N. (2020). Alkanethiol Monolayer End Groups Affect the Long-Term Operational Stability and Signaling of Electrochemical, Aptamer-Based Sensors in Biological Fluids. *ACS APPLIED MATERIALS & INTERFACES*, *12*(9), 11214–11223. https://doi.org/10.1021/acsami.9b22385

168. Shin, M., Wang, Y., Borgus, J. R., & Venton, B. J. (2019). Electrochemistry at the Synapse. Annual review of analytical chemistry (Palo Alto. *Calif*, *12*, 297–321.

169. Shoara, A. A. (2018). Development of a thermal-stable structure-switching cocaine-binding aptamer. *Biochimie*, *145*, 137–144.

170. Shyamala, K., Girish, H. C., & Murgod, S. (2014). Risk of tumor cell seeding through biopsy and aspiration cytology. *Journal of International Society of Preventive & Community Dentistry*, *4*(1), 5–11. https://doi.org/10.4103/2231-0762.129446

171. SNEDDEN, W., MELLOR, C., & MARTIN, J. (1983). FAMILIAL HYPERTRYPTOPHANEMIA, TRYPTOPHANURIA AND INDOLEKETONURIA. *CLINICA CHIMICA ACTA*, *131*(3), 247–256. https://doi.org/10.1016/0009-8981(83)90094-3

172. Solnica, B., Naskalski, J., & Sieradzki, J. (2003). Analytical performance of glucometers used for routine glucose self-monitoring of diabetic patients. *CLINICA CHIMICA ACTA*, *331*(1–2), 29–35. https://doi.org/10.1016/S0009-8981(03)00079-2

173. Sora, I., Hall, F. S., Andrews, A. M., Itokawa, M., Li, X. F., Wei, H. B., & Uhl, G. R. (2001). Molecular mechanisms of cocaine reward: Combined dopamine and serotonin transporter knockouts eliminate cocaine place preference. *Proceedings of the National Academy of Sciences of the United States of America*, *98*(9), 5300–5305. https://doi.org/10.1073/pnas.091039298

174. Stieve, B. J., Richner, T. J., Krook-Magnuson, C., & Netoff, T. I. (In Press). *Cerebellar-directed seizure control*. 44.

175. Stott, K. E., & Hope, W. W. (2017). Therapeutic drug monitoring for invasive mould infections and disease: Pharmacokinetic and pharmacodynamic considerations. *The Journal of Antimicrobial Chemotherapy*, *72*(suppl_1), i12–i18. https://doi.org/10.1093/jac/dkx029

176. Su, C. K., Hsia, S. C., & Sun, Y. C. (2014). A high-throughput microdialysis-parallel solid phase extraction-inductively coupled plasma mass spectrometry hyphenated system for continuous monitoring of extracellular metal ions in living rat brain. *Journal of Chromatography. A*, *1326*, 73–79.

177. Taylor, I. M., Du, Z., Bigelow, E. T., Eles, J. R., Horner, A. R., Catt, K. A., Weber, S. G., Jamieson, B. G., & Cui, X. T. (2017). Aptamer-functionalized neural recording electrodes for the direct measurement of cocaine in vivo. *Journal of Materials Chemistry B*, *5*(13), 2445–2458. https://doi.org/10.1039/C7TB00095B

178. TENGAMNUAY, P., SHAO, Z., & MITRA, A. (1991). SYSTEMIC ABSORPTION OF L-PHENYLALANINE AND D-PHENYLALANINE ACROSS THE RAT NASAL-MUCOSA. *LIFE SCIENCES*, *48*(15), 1477–1481. https://doi.org/10.1016/0024-3205(91)90185-E

179. TESSARI, P., INCHIOSTRO, S., BARAZZONI, R., ZANETTI, M., ORLANDO, R., BIOLO, G., SERGI, G., PINO, A., & TIENGO, A. (1994). FASTING AND POSTPRANDIAL PHENYLALANINE AND LEUCINE KINETICS IN LIVER-CIRRHOSIS. *AMERICAN JOURNAL OF PHYSIOLOGY*, *267*(1, 1), E140–E149. https://doi.org/10.1152/ajpendo.1994.267.1.E140

180. Tessari, P., Kiwanuka, E., Vettore, M., Barazzoni, R., Zanetti, M., Cecchet, D., & Orlando, R. (2008). Phenylalanine and tyrosine kinetics in compensated liver cirrhosis: Effects of meal ingestion. *AMERICAN JOURNAL OF PHYSIOLOGY-GASTROINTESTINAL AND LIVER PHYSIOLOGY*, *295*(3), G598–G604. https://doi.org/10.1152/ajpgi.00355.2007

181. Tu, W. F., Lin, G. F., Shen, J. F., & Xu, J. G. (1998). Changes in erythrocyte membrane ATPases and plasma lipid peroxides in upper abdominal surgery under intravenous procaine-balanced anesthesia. *World Journal of Gastroenterology*, *4*, 430–433. https://doi.org/10.3748/wjg.v4.i5.430

182. Tugtekin, I., Wachter, U., Barth, E., Weidenbach, H., Wagner, D., Adler, G., Georgieff, M., Radermacher, P., & Vogt, J. (2002). Phenylalanine kinetics in healthy volunteers and liver cirrhotics: Implications for the phenylalanine breath test. *AMERICAN JOURNAL OF PHYSIOLOGY-ENDOCRINOLOGY AND METABOLISM*, *283*(6), E1223–E1231. https://doi.org/10.1152/ajpendo.0311.2001

183. Uitert, R., JI, S., DE, L., & TE, D. (1981). Comparison of radio-labeled butanol and iodoantipyrine as cerebral blood flow markers. *Brain Res*, *222*(365).

184. Usubiaga, J. E., Moya, F., Wikinski, J. A., Wikinski, R., & Usubiaga, L. E. (1967). Relationship between the passage of local anaesthetics across the blood-brain barrier and their effects on the central nervous system. *Br J Anaesth*, *39*, 943–947.

185. Vander Weele, C. M., Porter-Stransky, K. A., Mabrouk, O. S., Lovic, V., Singer, B. F., Kennedy, R. T., & Aragona, B. J. (2014). Rapid dopamine transmission within the nucleus accumbens: Dramatic difference between morphine and oxycodone delivery. *The European Journal of Neuroscience*, *40*(7), 3041–3054. https://doi.org/10.1111/ejn.12709

186. Vatine, G. D., Barrile, R., Workman, M. J., Sances, S., Barriga, B. K., Rahnama, M., Barthakur, S., Kasendra, M., Lucchesi, C., & Kerns, J. (2019). Human iPSC-derived blood–brain barrier chips enable disease modeling and personalized medicine applications. *Cell Stem Cell*, *24*(6), 995–1005.

187. Veneziano, G., & Tobias, J. D. (2017). Chloroprocaine for epidural anesthesia in infants and children. *Pediatric Anesthesia*, *27*, 581–590.

188. Vieira, P. A., Shin, C. B., Arroyo-Currás, N., Ortega, G., Li, W., Keller, A. A., Plaxco, K. W., & Kippin, T. E. (2019). Ultra-High-Precision, in-vivo Pharmacokinetic Measurements Highlight the Need for and a Route Toward More Highly Personalized Medicine. *Frontiers in Molecular Biosciences*, *6*, 69. https://doi.org/10.3389/fmolb.2019.00069

189. Waisbren, S. E., Noel, K., Fahrbach, K., Cella, C., Frame, D., Dorenbaum, A., & Levy, H. (2007). Phenylalanine blood levels and clinical outcomes in phenylketonuria: A systematic literature review and meta-analysis. *MOLECULAR GENETICS AND METABOLISM*, *92*(1–2), 63–70. https://doi.org/10.1016/j.ymgme.2007.05.006

190. Walter, J., White, F., Hall, S., MacDonald, A., Rylance, G., Boneh, A., Francis, D., Shortland, G., Schmidt, M., & Vail, A. (2002). How practical are recommendations for dietary control in phenylketonuria? *LANCET*, *360*(9326), 55–57. https://doi.org/10.1016/S0140-6736(02)09334-0

191. Wang, M., Hershey, N. D., Mabrouk, O. S., & Kennedy, R. T. (2011). Collection, storage, and electrophoretic analysis of nanoliter microdialysis samples collected from

awake animals in vivo. *Analytical and Bioanalytical Chemistry*, *400*(7), 2013–2023. https://doi.org/10.1007/s00216-011-4956-9

192. Wang, R., Ashwal, S., Tone, B., Tian, H. R., Badaut, J., Rasmussen, A., & Obenaus, A. (2007). Albumin reduces blood-brain barrier permeability but does not alter infarct size in a rat model of neonatal stroke. *Pediatr Res*, *62*(261).

193. Watkins, H. M., Vallée-Bélisle, A., Ricci, F., Makarov, D. E., & Plaxco, K. W. (2012). Entropic and Electrostatic Effects on the Folding Free Energy of a Surface-Attached Biomolecule: An Experimental and Theoretical Study. *Journal of the American Chemical Society*, *134*(4), 2120–2126. https://doi.org/10.1021/ja208436p

194. Wegner, A., Meiser, J., Weindl, D., & Hiller, K. (2015). How metabolites modulate metabolic flux. *CURRENT OPINION IN BIOTECHNOLOGY*, *34*, 16–22. https://doi.org/10.1016/j.copbio.2014.11.008

195. Wei, C., Han, X., Weng, D., Feng, Q., Qi, X., Li, J., & Luo, M. (2018). Response dynamics of midbrain dopamine neurons and serotonin neurons to heroin, nicotine, cocaine, and MDMA. *Cell Discovery*, *4*(1), 60. https://doi.org/10.1038/s41421-018-0060-z

196. White, R. J., & Plaxco, K. W. (2010). Exploiting Binding-Induced Changes in Probe Flexibility for the Optimization of Electrochemical Biosensors. *Analytical Chemistry*, *82*(1), 73–76. https://doi.org/10.1021/ac902595f

197. White, R. J., Rowe, A. A., & Plaxco, K. W. (2010). Re-engineering aptamers to support reagentless, self-reporting electrochemical sensors. *ANALYST*, *135*(3), 589–594. https://doi.org/10.1039/b921253a

198. Wickham, R. J., Solecki, W., Rathbun, L. R., Neugebauer, N. M., Wightman, R. M., & Addy, N. A. (2013). Advances in studying phasic dopamine signaling in brain reward mechanisms. *Frontiers in Bioscience (Elite Edition)*, *0*, 982–999.

199. WILCKEN, B., YU, J., & BROWN, D. (1977). NATURAL-HISTORY OF HARTNUP DISEASE. *ARCHIVES OF DISEASE IN CHILDHOOD*, *52*(1), 38–40. https://doi.org/10.1136/adc.52.1.38

200. Wilson, G., & Gifford, R. (2005). Biosensors for real-time in vivo measurements. *BIOSENSORS & BIOELECTRONICS*, *20*(12), 2388–2403. https://doi.org/10.1016/j.bios.2004.12.003

201. Wilson, G., & Hu, Y. (2000). Enzyme based biosensors for in vivo measurements. *CHEMICAL REVIEWS*, *100*(7), 2693–2704. https://doi.org/10.1021/cr990003y

202. Winter, L. (1950). Intravenous procaine infusions in the postoperative period. *Annals of Surgery*, *132*, 143–146.

203. Wise, C. D., Berger, B. D., & Stein, L. (1970). Serotonin: A possible mediator of behavioral suppression induced by anxiety. *Dis Nerv Syst*, *31*. Suppl:34

204. Xiao, G., Song, Y., Zhang, S., Yang, L., Xu, S., Zhang, Y., Xu, H., Gao, F., Li, Z., & Cai, X. (2017). A high-sensitive nano-modified biosensor for dynamic monitoring of glutamate and neural spike covariation from rat cortex to hippocampal sub-regions. *Journal of Neuroscience Methods*, *291*, 122–130. https://doi.org/10.1016/j.jneumeth.2017.08.015

205. Xiao, Y., Lai, R. Y., & Plaxco, K. W. (2007). Preparation of electrode-immobilized, redox-modified oligonucleotides for electrochemical DNA and aptamer-based sensing. *NATURE PROTOCOLS*, *2*(11), 2875–2880. https://doi.org/10.1038/nprot.2007.413

206. Xiao, Y., Lubin, A. A., Heeger, A. J., & Plaxco, K. W. (2005). Label-Free Electronic Detection of Thrombin in Blood Serum by Using an Aptamer-Based Sensor. *Angewandte Chemie*, *117*(34), 5592–5595. https://doi.org/10.1002/ange.200500989

207. Xiao, Y., Piorek, B., Plaxco, K., & Heeger, A. (2005). A reagentless signal-on architecture for electronic, aptamer-based sensors via target-induced strand displacement. *JOURNAL OF THE AMERICAN CHEMICAL SOCIETY*, *127*(51), 17990–17991. https://doi.org/10.1021/ja056555h

208. Yang, H., Thompson, A. B., McIntosh, B. J., Altieri, S. C., & Andrews, A. M. (2013). Physiologically Relevant Changes in Serotonin Resolved by Fast Microdialysis. *ACS Chemical Neuroscience*, *4*(5), 790–798. https://doi.org/10.1021/cn400072f

209. Yang, K.-A., Barbu, M., Halim, M., Pallavi, P., Kim, B., Kolpashchikov, D. M., Pecic, S., Taylor, S., Worgall, T. S., & Stojanovic, M. N. (2014). Recognition and sensing of low-epitope targets via ternary complexes with oligonucleotides and synthetic receptors. *NATURE CHEMISTRY*, *6*(11), 1003–1008. https://doi.org/10.1038/NCHEM.2058

210. Yoo, E.-H., & Lee, S.-Y. (2010). Glucose Biosensors: An Overview of Use in Clinical Practice. *SENSORS*, *10*(5), 4558–4576. https://doi.org/10.3390/s100504558

211. Yuan, W., Lv, Y., Zeng, M., & Fu, B. M. (2009). Non-invasive measurement of solute permeability in cerebral microvessels of the rat. *Microvasc Res*, *77*(166).

212. Zeineh, M. M., Engel, S. A., Thompson, P. M., & Bookheimer, S. Y. (2001). Unfolding the human hippocampus with high resolution structural and functional MRI. *The Anatomical Record*, *265*(2), 111–120. https://doi.org/10.1002/ar.1061

213. Zeineh, M. M., Engel, S. A., Thompson, P. M., & Bookheimer, S. Y. (2003). Dynamics of the hippocampus during encoding and retrieval of face-name pairs. *Science (New York, N.Y.)*, *299*(5606), 577–580. https://doi.org/10.1126/science.1077775

214. Zestos, A. G., & Kennedy, R. T. (2017). Microdialysis Coupled with LC-MS/MS for In Vivo Neurochemical Monitoring. *The AAPS Journal*, *19*, 1284–1293.

215. Zhang, H., Lin, S.-C., & Nicolelis, M. A. L. (2010). Spatiotemporal Coupling between Hippocampal Acetylcholine Release and Theta Oscillations In Vivo. *The Journal of Neuroscience*, *30*(40), 13431–13440. https://doi.org/10.1523/JNEUROSCI.1144-10.2010

216. Zlokovic, B. V., Begley, D. J., Djuricic, B. M., & Mitrovic, D. M. (1986). Measurement of solute transport across the blood-brain barrier in the perfused guinea pig brain: Method and application to N-methyl-alpha- aminoisobutyric acid. *J Neurochem*, *46*(1444).